RIEMANNIAN LOW-RANK ADAPTATION FOR FEDERATED FINE-TUNING OF FOUNDATION MODELS

Anonymous authors
Paper under double-blind review

ABSTRACT

Rank-adaptive low-rank adaptation (LoRA), a parameter-efficient fine-tuning (PEFT) technology, has achieved state-of-the-art performance in fine-tuning foundation models (FM). Directly transplanting the rank-adaptive LoRA methods from centralized learning to federated learning raises two critical issues: client drift and rank drift. This paper presents a Riemannian LoRA algorithm with adaptive rank for federated fine-tuning of foundation models (FFT-FM), RAFFT, which solves the client-drift and rank-drift issues, and significantly improves the computational cost. First, by utilizing Riemannian Procrustes analysis, we propose a Riemannian parameter matching method to avoid the client-drift issue for ensuring the effectiveness of FFT-FM with rank-adaptive LoRA, and to reduce the cost of matrix decomposition by transforming the singular value decomposition (SVD) of high-dimensional full parameter matrices into the SVD of low-dimensional $r \times r$ matrices, where r is the rank parameter in the LoRA. We theoretically derive the equivalence between our RAFFT algorithm with rank-adaptive LoRA for the FFT-FM and the standard FFT-FM on the full parameter matrices based on FedAvg and verify the bounded error introduced by approximation. Second, by leveraging Riemannian manifold theory, we develop a Riemannian gradient descent (RGD) method to guarantee the local full parameter matrices on clients in the form of low-rank ones with fixed rank optimized by the server in each FFT-FM round, for alleviating the rank-drift issue to speed up the convergence of RAFFT. We theoretically demonstrate that the RGD optimization on the Riemannian manifold ensures the rank invariance during the local update process and the RGD optimization can converge in the FFT-FM context.

1 INTRODUCTION

Parameter-efficient fine-tuning (PEFT) for fine-tuning of foundation models (FT-FM) has attracted active research in recent years, such as adapter tuning (Houlsby et al., 2019; Lin et al., 2020; Pfeiffer et al., 2021; Rücklé et al., 2021; He et al., 2022), prefix tuning (Li & Liang, 2021), P-Tuning (Liu et al., 2021b), P-Tuning V2 (Liu et al., 2021a), low-rank adaptation (LoRA) (Hu et al., 2022), and prompt tuning (Lester et al., 2021; Li & Liang, 2021). These methods freeze the backbone parameters (i.e., original weights of pre-trained FMs) and adjust only a small portion of parameters (i.e., adapter weights during the FT phase), to improve the efficiency. Among the above PEFT approaches, LoRA has achieved the state-of-the-art FT performance (Wu et al., 2024). The idea of the LoRA method can be illustrated as follows: $\mathbf{W} = \mathbf{W}_0 + \Delta\mathbf{W} = \mathbf{W}_0 + \mathbf{B}\mathbf{A}$, where $\mathbf{W} \in \mathbb{R}^{m\times n}$ is the complete parameter of a FM. $\mathbf{W}_0$ and $\Delta\mathbf{W}$ are the backbone (pre-trained FM parameters) and adapter parameters respectively. A low-rank decomposition $\Delta\mathbf{W} = \mathbf{B}\mathbf{A}$ where $\mathbf{B} \in \mathbb{R}^{m\times r}$, $\mathbf{A} \in \mathbb{R}^{r\times n}$, and rank $r << \min(m, n)$. During the FT phase, only $\mathbf{B}$ and $\mathbf{A}$ are trained while freezing $\mathbf{W}_0$ on the clients. Notice that in the LoRA-style methods, rank r is often user-defined and keeps unchanged during the entire FT process.

In order to further enhance the performance of the LoRA-style methods, various rank-adaptive LoRA methods have been recently proposed to dynamically allocate the ranks among parameter matrices based on their importance: assigning more/less trainable parameters with higher/lower ranks to the critical/insignificant parameter matrices for better model performance/efficiency. These methods can be broadly classified into two categories: (1) SVD-based approaches in centralized fine-tuning (CFT) dynamically adjust the ranks by truncating singular values in the form of SVD (Zhang et al.,

2023b; Ding et al., 2023; Zhang et al., 2023a); (2) Rank sampling-based algorithms in both CFT and FFT search for the best rank by sampling a range of ranks and sorting the representations learnt by the model at different ranks during training (Valipour et al., 2023; Rajabzadeh et al., 2024; Xu et al., 2024). They need to fine-tune the model multiple times at different ranks, raising non-trivial cost. Several pioneering rank-adaptive LoRA algorithms for FFT-FM iteratively aggregate local full parameter metrics into a global one and perform the SVD on the latter to find the optimal rank (Chai et al., 2022; Wu et al., 2021; Niu et al., 2023). However, iterative SVD on the high-dimensional full parameter metrics is prohibitive.

A critical challenge of transplanting the SVD-based rank-adaptive LoRA methods from the CFT to the FFT is the client-drift issue (Sun et al., 2024; Wang et al., 2024). Client drift issue describes the discrepancy between independently aggregating client's low rank matrices and aggregating the ideal parameter matrix. To address this, they attempt to resolve the problem by either freezing one of the parameter matrices or using aggregation methods based on matrix stacking and multiplication. However, we addresses a more challenging problem by considering both low-rank parameter matrices $\mathbf{U}^k, \mathbf{V}^k$ and $\mathbf{\Sigma}^k$ to determine the rank. For a detailed analysis, please refer to Appendix 7.8. Here, we introduce an illustrative example with two clients to better explain this issue. An implicit assumption ensuring the global convergence of FFT-FM based on FedAvg McMahan et al. (2017) is $\Delta\mathbf{W} = \frac{1}{2}(\Delta\mathbf{W}^1 + \Delta\mathbf{W}^2)$, where $\Delta\mathbf{W}$ is the global model parameter after the model aggregation on server, $\Delta\mathbf{W}^1$ and $\Delta\mathbf{W}^2$ are the local model parameter on clients 1 and 2. Let the SVDs be $\Delta\mathbf{W}^1 = \mathbf{U}^1\mathbf{\Sigma}^1\mathbf{V}^1$ and $\Delta\mathbf{W}^2 = \mathbf{U}^2\mathbf{\Sigma}^2\mathbf{V}^2$. After using FedAvg to aggregate the low-rank parameter matrices, the server produces

$$\underbrace{\frac{1}{2}\left(\mathbf{U}^1 + \mathbf{U}^2\right) \times \frac{1}{2}\left(\mathbf{\Sigma}^1 + \mathbf{\Sigma}^2\right) \times \frac{1}{2}\left(\mathbf{V}^1 + \mathbf{V}^2\right)}_{\text{Parameter aggregation with SVD-based rank-adaptive LoRA + FedAvg}} \neq \underbrace{\frac{1}{2}\left(\mathbf{U}^1\mathbf{\Sigma}^1\mathbf{V}^1 + \mathbf{U}^2\mathbf{\Sigma}^2\mathbf{V}^2\right) = \frac{1}{2}(\Delta\mathbf{W}^1 + \Delta\mathbf{W}^2) = \Delta\mathbf{W}}_{\text{Ideal parameter aggregation with FedAvg on full parameter matrices}} \quad (1)$$

where the left side denotes the parameter aggregation of FFT-FM with LoRA, while the right side represents the standard parameter aggregation of FFT-FM. As shown in Figure 1, the difference between two sides may become more significant when (1) the number of local update steps between aggregations is large and (2) the local datasets are different across clients. In this case, FFT-FM with LoRA may fail to converge and result in poor model performance.

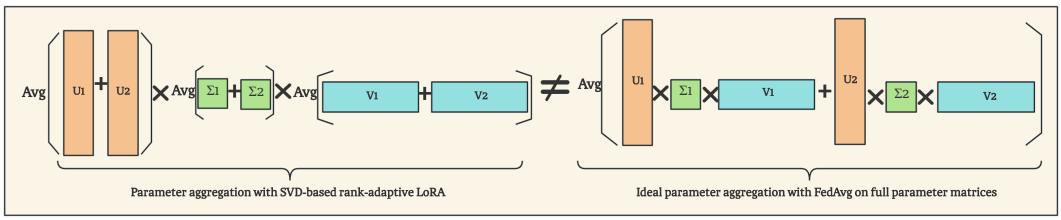

Figure 1: Client Drift in FFT-FM with Rank-Adaptive LoRA

Another significant challenge in FFT-FM with rank-adaptive LoRA is the rank-drift issue, caused by data heterogeneity (McMahan et al., 2017; Smith et al., 2017; Chen et al., 2018; Khodak et al., 2019; Sattler et al., 2019; Liu et al., 2019a; Hsieh et al., 2020), a common problem in federated learning. Non-Independent Identically Distributed (Non-IID) data across clients result in substantial differences between local models and the global model. During training, local models may oscillate across rounds, leading to unstable convergence and suboptimal performance. Similarly, the optimal ranks of local models vary significantly due to data heterogeneity, causing rank-drift. This oscillation further slows convergence and impairs performance. For a detailed analysis, please refer to Appendix 7.8.

To address the client-drift issue, by utilizing Riemannian Procrustes analysis, due to the fact that all local parameter matrices lie on the Riemannian manifold, we propose a Riemannian parameter matching method to match the local parameter matrices $\mathbf{U}^k$ and $\mathbf{V}^k$ on other clients with pivots $\mathbf{U}^1$ and $\mathbf{V}^1$ on client 1, in terms of their lengths and directions. To maintain the consistency between low-rank parameter metrics before and after the Riemannian parameter matching, i.e., $\Delta\mathbf{W}^k = \mathbf{U}^k\mathbf{\Sigma}^k\mathbf{V}^k = \tilde{\mathbf{U}}^k\tilde{\mathbf{\Sigma}}^k\tilde{\mathbf{V}}^k$, for ensuring the effectiveness of FFT-FM with rank-adaptive LoRA, we derive a modified diagonal matrix $\tilde{\mathbf{\Sigma}}^k$ for the other clients by performing the SVD on low-dimensional $r \times r$ matrices $(\mathbf{U}^1)^T\mathbf{U}^k$ and $(\mathbf{V}^1)^T\mathbf{V}^k$. Based on the global diagonal matrix $\frac{1}{K}\left(\mathbf{\Sigma}^1 + \sum_{k=2}^{K}\tilde{\mathbf{\Sigma}}^k\right)$, it is easy to find the optimal rank of the global parameter matrix, with aggre-

gation on only the local low-rank matrices $\mathbf{U}^k$, $\tilde{\mathbf{\Sigma}}^k$, and $\mathbf{V}^k$ (See Eq.(14)). We theoretically derive the equivalence between our RAFFT algorithm with rank-adaptive LoRA for the FFT-FM and the standard FFT-FM on the full parameter matrices based on FedAvg and verify the bounded error introduced by approximation.

For alleviating the rank-drift issue, we propose to extend stochastic gradient descent (SGD) algorithms on a Riemannian manifold and develop a Riemannian gradient descent (RGD) method to guarantee the local full parameter matrices $\Delta\mathbf{W}^k$ on the clients in the form of low-rank ones $\mathbf{U}^k, \mathbf{\Sigma}^k$, and $\mathbf{V}^k$ with fixed rank optimized by the server in each FFT-FM round, to speed up the convergence of RAFFT: $\left((\mathbf{U}^k)^{(t+1)}, (\mathbf{\Sigma}^k)^{(t+1)}, (\mathbf{V}^k)^{(t+1)}\right) = f\left(-\eta_t\left(\left(\Gamma_{\mathbf{U}^k}L^k\right)^{(t)}, \left(\Gamma_{\mathbf{\Sigma}^k}L^k\right)^{(t)}, \left(\Gamma_{\mathbf{V}^k}L^k\right)^{(t)}\right)\right)$, where η_t is a learning rate at round t, $\Delta\mathbf{W}^k$ is a point on a Riemannian manifold M consisting of all matrices with a fixed rank r in $\mathbb{R}^{m\times n}$, $L^k(\Delta\mathbf{W}^k)$ is the loss function L^k at $\Delta\mathbf{W}^k$ in Euclidean space, $\Gamma_{\mathbf{V}^k}L^k$ represent the components of the Riemannian gradient at $\Delta\mathbf{W}^k$, and f is a retraction $f : T_M \to M$ mapping the tangent space at $\Delta\mathbf{W}^k$ to the manifold. We theoretically demonstrate that the RGD optimization on the Riemannian manifold ensures the rank invariance during the local update process and the RGD optimization can converge in the FFT-FM context.

To our best knowledge, this work is the first to offer a rank-adaptive low-rank adaptation solution for FFT-FM with Riemannian theory. Our RAFFT method exhibits three compelling advantages: (1) The proposed Riemannian parameter matching technique based on Riemannian Procrustes analysis is able to solve the client-drift issue when transplanting the centralized LoRA methods to the federated setting. Existing rank-adaptive LoRA methods in the CFT can be plugged into our framework for FFT-FM. Moreover, the model aggregation of FFT-FM is conducted on only local low-rank parameter matrices, without the need of aggregating the global full parameter matrices; (2) Transforming the SVD of high-dimensional full parameter matrices into the SVD of low-dimensional $r \times r$ matrices can significantly improve the efficiency of FFT-FM with low-rank adaption. In addition, this design avoids the expensive cost of training FFT multiple times at different ranks by rank sampling-based algorithms; and (3) The combination of Riemannian gradient descent and Riemannian manifold theory guarantees the local parameter matrices with fixed rank optimized by the server in each FFT-FM round, for alleviating the rank-drift issue to speed up the convergence of RAFFT.

Empirical evaluation on real datasets demonstrates the superior performance of our RAFFT model against several state-of-the-art federated prompt tuning, federated LoRA, and federated rank-adaptive LoRA methods. More experiments, implementation details, and hyperparameter setting are presented in Appendices 7.5-7.6.

2 Background

2.1 Rank-Adaptive Low-Rank Adaptation

AdaLoRA Zhang et al. (2023b) is a parameter-efficient fine-tuning (PEFT) method in centralized setting that parameterizes full parameter metrics as $\Delta\mathbf{W} = \mathbf{U}\mathbf{\Sigma}\mathbf{V}$ and adaptively allocates the rank r for low-rank parameter metrics $\mathbf{U}$, $\mathbf{\Sigma}$, and $\mathbf{V}$ according to their importance in the form of singular value decomposition (SVD) of $\Delta\mathbf{W}$.

$$\mathbf{W} = \mathbf{W}_0 + \Delta\mathbf{W} = \mathbf{W}_0 + \mathbf{U}\mathbf{\Sigma}\mathbf{V} \tag{2}$$

where $\mathbf{W}, \mathbf{W}_0, \Delta\mathbf{W} \in \mathbb{R}^{m\times n}$ are the complete, backbone, and adapter parameter matrices respectively. $\mathbf{U} \in \mathbb{R}^{m\times r}$ and $\mathbf{V} \in \mathbb{R}^{r\times n}$ are matrices representing the left and right singular vectors of full parameter matrices $\Delta\mathbf{W}$ respectively. $\mathbf{\Sigma} \in \mathbb{R}^{r\times r}$ is a diagonal matrix containing the singular values $\{\mathbf{\Sigma}_{ii}\}_{1\le i\le r}$ with rank $r << \min(m, n)$. AdaLoRA is thus able to dynamically adjust the number of the singular values in $\mathbf{\Sigma}$ and assign more/less trainable parameters with higher/lower rank r to the critical/insignificant parameter matrices for better model performance/efficiency.

2.2 Federated Fine-Tuning

First, given a machine learning (ML) task (e.g., image classification), K clients with their local training data $D = \{D_1, \cdots, D_K\}$, and a server, federated learning (FL) based on the FedAvg algorithm McMahan et al. (2017) aims to learn a global ML model on the server by optimizing the problem below.

$$\min_{\mathbf{W}\in\mathbb{R}^{m\times n}} \mathcal{L}(\mathbf{W}) = \sum_{k=1}^{K} \frac{n^k}{n} L^k(\mathbf{W}) \qquad \text{where } L^k(\mathbf{W}) = \frac{1}{n_k} \sum_{\{x_i,y_i\}\in D^k} l_i(\mathbf{W}) \tag{3}$$

where $l_i(\mathbf{W}) = l(x_i, y_i; \mathbf{W})$ denotes the loss function of the prediction on data example $\{x_i, y_i\} \in D_k$ made with a global model parameter $\mathbf{W}$. $n^k = |D_k|$ denotes the size of local dataset D_k. n is the size of total training data D, i.e., $n = n^1 + \cdots + n^K$. In the FL, the global model parameter $\mathbf{W}$ is iteratively updated with the aggregation of all local model parameters $\mathbf{W}^1, \cdot, \mathbf{W}^K$ on K clients in each round, i.e., $\mathbf{W} = \sum_{k=1}^{K} \frac{n^k}{n} \mathbf{W}^k$.

In the context of federated fine-tuning (FFT), in Eq.(2), the backbone parameter matrices $\mathbf{W}_0$ are frozen and only the adapter parameter matrices $\Delta\mathbf{W}$ are adjusted in each round by updating their low-rank versions $\mathbf{U}$, $\mathbf{\Sigma}$, and $\mathbf{V}$ respectively.

$$\min_{\Delta\mathbf{W}\in\mathbb{R}^{m\times n}} \mathcal{L}(\Delta\mathbf{W}) = \sum_{k=1}^{K} \frac{n^k}{n} L^k(\Delta\mathbf{W}) \qquad \text{where } L^k(\Delta\mathbf{W}) = \frac{1}{n_k} \sum_{\{x_i,y_i\}\in D^k} l_i(\Delta\mathbf{W}) \tag{4}$$

3 Riemannian Parameter Matching for Eliminating Client Drift on Server

As discussed in Section 1, among three categories of rank-adaptive low-rank approximation techniques, SVD-based methods in centralized learning Zhang et al. (2023b); Ding et al. (2023); Zhang et al. (2023a) encounter the dilemma of the client drift issue (Sun et al., 2024), rank sampling-based algorithms Valipour et al. (2023); Rajabzadeh et al. (2024); Xu et al. (2024) and federated rank-adaptive LoRA algorithms Chai et al. (2022); Wu et al. (2021); Niu et al. (2023) raise extremely expensive cost. Furthermore, directly using FedAvg McMahan et al. (2017) to aggregate the clients' local matrices $\mathbf{U}^k$, $\mathbf{\Sigma}^k$, $\mathbf{V}^k$ on the server side leads to client-drift issues, as shown in Eq.(1), which negatively impact the convergence and performance of federated learning. To address these challenges, we propose a Riemannian parameter matching method to match the local parameter matrices $\mathbf{U}^k$ and $\mathbf{V}^k$ from other clients with the pivot matrices $\mathbf{U}^1$ and $\mathbf{V}^1$ on client 1, preserving both their lengths and directions. i.e., $\tilde{\mathbf{U}}^k \approx \mathbf{U}^1$ and $\tilde{\mathbf{V}}^k \approx \mathbf{V}^1$. Correspondingly, we adjust the diagonal matrix $\mathbf{\Sigma}^k$ to ensure consistency in the low-rank parameter measurements before and after Riemannian parameter matching, i.e., $\mathbf{U}^k\mathbf{\Sigma}^k\mathbf{V}^k = \tilde{\mathbf{U}}^k\tilde{\mathbf{\Sigma}}^k\tilde{\mathbf{V}}^k \approx \mathbf{U}^1\tilde{\mathbf{\Sigma}}^k\mathbf{V}^1$. This approach allows the server to directly aggregate the aligned local low-rank matrices $\mathbf{U}^k$, $\tilde{\mathbf{\Sigma}}^k$, and $\mathbf{V}^k$ while avoiding client-drift issues. Moreover, the global diagonal matrix enables the server to easily identify the optimal rank for the global parameter matrix, enhancing both efficiency and performance.

Since both $\mathbf{U}^k$ and $\mathbf{V}^k$ are orthogonal matrices, they belong to the Riemann manifold, which is defined as the set of standard orthogonal matrices $S = \{\mathbf{U}^k \in \mathbb{R}^{m\times r} : (\mathbf{U}^K)^T(\mathbf{U}^K) = I\}$ (Chakraborty & Vemuri, 2019; Atiyah & Todd, 1960). Therefore, we can performing the Riemannian parameter matching to ensure that the length and direction of the parameter matrices between clients are as aligned as possible. We adopt the Procrustes distance metric proposed in Kendall et al. (2003) to efficiently compute the parameter matching on the manifold. The procrustes representation S_p on the Riemann manifold S can be defined as follows: an $m \times r$ matrix $\mathbf{U}^k$ on $S_{r,m}$ is identified with the equivalence class of matrices $\mathbf{U}^k\mathbf{R}^k$ in $\mathbf{R}_{m,r}$, for $\mathbf{R} > 0$.

The squared Procrustes distance for each two matrices $\mathbf{U}^k$ and $\mathbf{U}^1$, considering the representation S_p on the Riemann manifold S, is defined as the minimum squared Euclidean distance over all pairs of matrices in the respective equivalence classes.

Therefore, we aim to solve the following Riemann distance optimization problem.

$$\begin{aligned} d^2_{S_P}(\mathbf{U}^1, \mathbf{U}^k) &= \min_{\mathbf{R}^k>0} \operatorname{tr}\left((\mathbf{U}^1 - \mathbf{U}^k\mathbf{R}^k)^T(\mathbf{U}^1 - \mathbf{U}^k\mathbf{R}^k)\right) \\ &= \min_{\mathbf{R}^k>0} \operatorname{tr}\left((\mathbf{R}^k)^T\mathbf{R}^k - 2(\mathbf{U}^1)^T\mathbf{U}^k\mathbf{R}^k + I_r\right) \end{aligned} \tag{5}$$

where $\mathbf{I_r}$ is an identity matrix. Matrix $\mathbf{R}^k$ is a $r \times r$ symmetric positive constraint that ensures the aggregated points remain on the Riemannian manifold.

Notice that $(\mathbf{U}^1)^T\mathbf{U}^k$ is a low-rank matrix with low dimensions $r \times r$. We perform the SVD on $(\mathbf{U}^1)^T\mathbf{U}^k$ to generate $(\mathbf{U}^1)^T\mathbf{U}^k = \mathbf{P}^k\mathbf{\Lambda}^k\mathbf{Q}^k$. According to the properties of the matrix trace and

the symmetry of the Frobenius inner product (Schneider, 2015), the optimization problem in Eq.(5) is further converted to another equivalent optimization problem below.

$$\min_{\mathbf{R}^k} \operatorname{tr}\left((\mathbf{R}^K)^T\mathbf{R}^k - 2(\mathbf{U}^1)^T\mathbf{U}^k\mathbf{R}^k\right) = \min_{\mathbf{R}^k} \|\mathbf{R}^k - \mathbf{P}^k\mathbf{\Lambda}^k\mathbf{Q}^k\|_F^2 = \min_{\mathbf{R}^k} \|(\mathbf{Q}^k)^T\mathbf{R}^k\mathbf{Q}^k - (\mathbf{Q}^k)^T\mathbf{P}^k\mathbf{\Lambda}^k\|_F^2 \tag{6}$$

We introduce two auxiliary variable $\mathbf{Y}^k$, $\mathbf{Z}^k$ and let $\mathbf{Y}^k = (\mathbf{Q}^k)^T\mathbf{R}^k\mathbf{Q}^k$,$\mathbf{Z}^k = (\mathbf{Q}^k)^T\mathbf{P}^k$, then we transform the Riemann Procrustes distance optimization problem into an equivalent optimization problem.

$$d_{S_P}^2(\mathbf{U}^1, \mathbf{U}^k) \iff \min_{\mathbf{R}^k} \|\mathbf{Y}^k - \mathbf{Z}^k\mathbf{\Lambda}^k\|_F^2 = \sum_{i=1}^{r}(\mathbf{Y}_{ii}^k - \mathbf{Z}_{ii}^k\mathbf{\Lambda}_i^k)^2 + \sum_{j>i}\left((\mathbf{Y}_{ij}^k - \mathbf{Z}_{ij}^k\mathbf{\Lambda}_i^k)^2 + (\mathbf{Y}_{ij}^k - \mathbf{Z}_{ji}^k\mathbf{\Lambda}_j^k)^2\right) \tag{7}$$

where $\mathbf{Y}_{ij}^k$, $\mathbf{Z}_{ij}^k$ and $\mathbf{Z}_{ji}^k$ represent the elements of the symmetric matrix $\mathbf{Y}^k$ and matrix $\mathbf{Z}^k$, respectively. Additionally $\mathbf{Y}_{ii}^k$, $\mathbf{\Lambda}_i^k$ and $\mathbf{\Lambda}_j^k$ denote the diagonal elements of the symmetric matrix $\mathbf{Y}^k$ and matrix $\mathbf{\Lambda}^k$.

Given the inherent symmetry of Y, the variables $\mathbf{Y}_{ij}^k$ (where j $\geq$ i) are uncoupled, allowing us to minimize each term separately. Specifically, we minimize $(\mathbf{Y}_{ii}^k - \mathbf{Z}_{ii}^k\mathbf{\Lambda}_i^k)^2$ and $(\mathbf{Y}_{ij}^k - \mathbf{Z}_{ij}^k\mathbf{\Lambda}_i^k)^2 + (\mathbf{Y}_{ij}^k - \mathbf{Z}_{ji}^k\mathbf{\Lambda}_j^k)^2$ for $j > i$. Since Y is a symmetric matrix, it suffices to compute only the upper triangular part. Then we generate the solution of the optimal problem as follows.

$$\mathbf{Y}_{ij}^k = \begin{cases} \mathbf{Z}_{ii}^k\mathbf{\Lambda}_i^k, & i = j \leq \operatorname{rank}((\mathbf{U}^1)^T\mathbf{U}^k), \\ \frac{\mathbf{Z}_{ij}^k\mathbf{\Lambda}_i^k + \mathbf{Z}_{ji}^k\mathbf{\Lambda}_j^k}{2}, & j > i \text{ and } i \leq \operatorname{rank}((\mathbf{U}^1)^T\mathbf{U}^k), \\ 0, & \text{otherwise.} \end{cases} \tag{8}$$

Then we generate optimal $\mathbf{R}^k$ below.

$$\mathbf{R}^k = \mathbf{Q}^k\mathbf{Y}^k(\mathbf{Q}^k)^T \tag{9}$$

By following the same approach, we produce an optimal matrix $\mathbf{S}^k$ for another Riemannian parameter matching problem $\min_{\mathbf{S}^k} d_{S_P}^2(\mathbf{V}^1, \mathbf{V}^k)$s.t. $(\mathbf{S}^k)^T = \mathbf{S}^k$.

Therefore, the low-rank parameter matrices are aligned together. $\tilde{\mathbf{U}}^k$ and $\tilde{\mathbf{V}}^k$ are the aligned parameter matrices for client k.

$$\tilde{\mathbf{U}}^k = \mathbf{U}^k\mathbf{R}^k \approx \mathbf{U}^1, \quad \tilde{\mathbf{V}}^k = \mathbf{S}^k\mathbf{V}^k \approx \mathbf{V}^1 \tag{10}$$

To maintain parameter consistency before and after performing the Riemannian parameter matching, as well as the effectiveness of FFT-FM with rank-adaptive LoRA, i.e., $\tilde{\mathbf{U}}^k\tilde{\mathbf{\Sigma}}^k\tilde{\mathbf{V}}^k = \mathbf{U}^k\mathbf{\Sigma}^k\mathbf{V}^k = \Delta\mathbf{W}^k$, we need to derive a modified version $\tilde{\mathbf{\Sigma}}^k$ of $\mathbf{\Sigma}^k$.

$$\min_{\tilde{\mathbf{\Sigma}}^k} \|\tilde{\mathbf{U}}^k\tilde{\mathbf{\Sigma}}^k\tilde{\mathbf{V}}^k - \mathbf{U}^k\mathbf{\Sigma}^k\mathbf{V}^k\|_F^2 \tag{11}$$

However, it is difficult to directly solve the above optimization problem. We convert it to another equivalent problem below.

$$\min_{\tilde{\mathbf{\Sigma}}^k} \|(\mathbf{U}^k)^T\left(\tilde{\mathbf{U}}^k\tilde{\mathbf{\Sigma}}^k\tilde{\mathbf{V}}^k - \mathbf{U}^k\mathbf{\Sigma}^k\mathbf{V}^k\right)(\mathbf{V}^k)^T\|_F^2 \tag{12}$$

Since $\mathbf{U}^k$ and $\mathbf{V}^k$ are orthogonal matrices, the problem can be further transformed. Notice that $\tilde{\mathbf{U}}^k = \mathbf{U}^k\mathbf{R}^k$, $\tilde{\mathbf{V}}^k = \mathbf{S}^k\mathbf{V}^k$. Additionally, since $\mathbf{R}^k$ and $\mathbf{S}^k$ are non-singular matrices, an invertible matrix must exist.

$$\min_{\tilde{\mathbf{\Sigma}}^k} \|\mathbf{R}^k\tilde{\mathbf{\Sigma}}^k\mathbf{S}^k - \mathbf{\Sigma}^k\|_F^2 = \min_{\tilde{\mathbf{\Sigma}}^k} \|\tilde{\mathbf{\Sigma}}^k - (\mathbf{R}^k)^{-1}\mathbf{\Sigma}^k(\mathbf{S}^k)^{-1}\|_F^2 \tag{13}$$

The optimal solution is obtained when $\tilde{\mathbf{\Sigma}_{\mathbf{ii}}}^k = (\mathbf{R_{ii}}^k)^{-1}\mathbf{\Sigma_{ii}}^k(\mathbf{S_{ii}}^k)^{-1}$. Next, the server can directly perform the aggregation on local low-rank parameter matrices to generate the global ones without the client-drift issue.

$$\begin{aligned} &\frac{1}{K}\left(\mathbf{U}^1 + \sum_{k=2}^{K}\mathbf{U}^k\mathbf{R}^k\right) \times \frac{1}{K}\left(\mathbf{\Sigma}^1 + \sum_{k=2}^{K}\tilde{\mathbf{\Sigma}}^k\right) \times \frac{1}{K}\left(\mathbf{V}^1 + \sum_{k=2}^{K}\mathbf{S}^K\mathbf{V}^K\right) \\ &= \mathbf{U}^1 \times \frac{1}{K}\left(\mathbf{\Sigma}^1 + \sum_{k=2}^{K}\tilde{\mathbf{\Sigma}}^k\right) \times \mathbf{V}^1 \approx \frac{1}{K}\left(\sum_{k=1}^{K}\mathbf{U}^k\mathbf{\Sigma}^k\mathbf{V}^k\right) = \frac{1}{K}\sum_{k=1}^{K}\Delta\mathbf{W}^k \end{aligned} \tag{14}$$

Thus, when searching for the optimal rank on the globally low-rank parameter matrix, there is no need to physically generate full parameter matrix $\Delta\mathbf{W}$ and execute iterative SVD on $\Delta\mathbf{W}$. However, approximation errors may arise during the calculation process. The following theorem derives the bounded error introduced by approximation in Eq.(14).

Theorem 1. *We assume that the Frobenius norm of $\mathbf{R}^k$ is bounded by a constant H, and its eigenvalues lie within the interval $[\lambda_{R_{\min}}, \lambda_{R_{\max}}]$. Similarly, the Frobenius norm of $\mathbf{S}^k$ is bounded by a constant N, with eigenvalues in the range $[\lambda_{S_{\min}}, \lambda_{S_{\max}}]$. Additionally, the matrix ΔW has rank r. Given these conditions, the total approximation error bound in Eq.(14) is derived as follows*

$$\begin{aligned} &\|\mathbf{U}^1 \times \frac{1}{K}\left(\mathbf{\Sigma}^1 + \sum_{k=2}^{K} \tilde{\mathbf{\Sigma}}^k\right) \times \mathbf{V}^1 - \frac{1}{K}\left(\sum_{k=1}^{K} \mathbf{U}^k \mathbf{\Sigma}^k \mathbf{V}^k\right)\|_F^2 \\ &= \sum_{k=2}^{K}\left(2r(1-H-N) + (1+(\frac{\lambda_{R_{\max}}}{\lambda_{R_{\min}}})^2)H^2 + (1+(\frac{\lambda_{S_{\max}}}{\lambda_{S_{\min}}})^2)N^2\right) \end{aligned} \tag{15}$$

Please refer to Appendix 7.2 for detailed proof of Theorem 1.

By following the same idea in existing efforts Falini (2022); Wu et al. (2022), this paper utilizes singular value contribution rate $\Theta(r)$ to determine the rank $\tilde{\mathbf{\Sigma}}^{k'}$ after each round of FFT-FM. $\Theta(r)$ is defined as the cumulative percentage of the first r singular values to all the singular values. We retain the first r singular values such that $\Theta(r)$ is bigger than a threshold value φ.

$$\Theta(r) = \frac{\sum_{i=1}^{r} \tilde{\mathbf{\Sigma}}'_{ii}}{\sum_{i=1}^{r_{max}} \tilde{\mathbf{\Sigma}}'_{ii}} \geq \varphi \tag{16}$$

where r_{max} is a maximum acceptable rank.

4 Riemannian Gradient Descent for Alleviating Rank Drift on Clients

The data heterogeneity issue in the FFT-FM may bring the rank-drift challenges. When the server dispatches the low-rank parameter matrix with the appropriate rank r to the clients, the rank of its local full parameter matrix $\Delta\mathbf{W}^k = \mathbf{U}^k\mathbf{\Sigma}^k\mathbf{V}^k$ on each client may significantly change after local training epoch, and so does the appropriate rank of the global parameter matrix. This may slow down the convergence of FFT-FM and degrade the model performance too. We develop a Riemannian gradient descent (RGD) method to guarantee the local full parameter matrices $\Delta\mathbf{W}^k$ in the form of low-rank ones $\mathbf{U}^k$, $\mathbf{\Sigma}^k$, and $\mathbf{V}^k$ with fixed appropriate rank determined by the server in each iteration of FFT-FM, to speed up the convergence of RAFFT.

By following AdaLoRA (Zhang et al., 2023b), we parameterize full parameter metrics on client k as $\Delta\mathbf{W}^k = \mathbf{U}^k\mathbf{\Sigma}^k\mathbf{V}^k$, in order to avoid the expensive cost of iterative SVD on the large-scale full parameter metrics. We introduce a regularizer into the loss function, defined as $R(\mathbf{U}^k, \mathbf{V}^k)$ to enforce the orthogonality of $\mathbf{U}^k$ and $\mathbf{V}^k$.

$$R(\mathbf{U}^k, \mathbf{V}^k) = \|(\mathbf{U}^k)^T\mathbf{U}^k - \mathbf{I}\|_F^2 + \|\mathbf{V}^k(\mathbf{V}^k)^T - \mathbf{I}\|_F^2 \tag{17}$$

We introduce a Riemannian manifold containing all fixed-rank matrices, i.e., the set M of all matrices with a fixed rank r: $M = \{\Delta\mathbf{W} : \Delta\mathbf{W} \in \mathbb{R}^{m\times n}, \mathrm{rank}(\Delta\mathbf{W}) = r\}$ (do Carmo, 2018; Vandereycken, 2014). This forms a smooth submanifold of $\mathbb{R}^{m\times n}$. This structure ensures that the updated parameter matrices $\mathbf{U}^k\mathbf{\Sigma}^k\mathbf{V}^k$ stay within the manifold, maintaining rank invariance throughout the local update process. In terms of low-rank parameter metrics, the local objective function of FFT-FM on client k is defined below.

$$\min_{\Delta\mathbf{W}^k \in M} L^k(\Delta\mathbf{W}^k) = L^k(\mathbf{U}^k, \mathbf{\Sigma}^k, \mathbf{V}^k) = \frac{1}{n_k}\sum_{\{x_i, y_i\}\in D^k} l_i(\mathbf{U}^k, \mathbf{\Sigma}^k, \mathbf{V}^k) + R(\mathbf{U}^k, \mathbf{V}^k) \tag{18}$$

The tangent space T_M at the point $\Delta\mathbf{W}$ on the manifold M is defined as follows.

$$\begin{aligned} T_M &= \left\{(\mathbf{U}^k \ \mathbf{U}^k_\perp)\begin{bmatrix} \mathbb{R}^{r\times r} & \mathbb{R}^{r\times(n-r)} \\ \mathbb{R}^{(m-r)\times r} & 0^{(m-r)\times(n-r)} \end{bmatrix}(\mathbf{V}^k \ \mathbf{V}^k_\perp)^T\right\} \\ &= \Big\{\mathbf{U}^k\mathbf{G}(\mathbf{V}^k)^T + \mathbf{U}^k_p(\mathbf{V}^k)^T + \mathbf{U}^k(\mathbf{V}^k_p)^T \\ &\quad : \mathbf{G} \in \mathbb{R}^{r\times r}, \mathbf{U}^k_p \in \mathbb{R}^{m\times r}, (\mathbf{U}^k_p)^T\mathbf{U}^k = 0, \mathbf{V}^k_p \in \mathbb{R}^{n\times r}, (\mathbf{V}^k_p)^T\mathbf{V}^k = 0 \quad \Big\} \end{aligned} \tag{19}$$

where $\mathbf{U}^k_\perp$ and $\mathbf{V}^k_\perp$ denote the orthogonal complements of $\mathbf{U}^k$ and $\mathbf{V}^k$ respectively. $\mathbf{G}, \mathbf{U}^k_p, \mathbf{V}^k_p$ represent the tangent vector at ΔW. Please refer to Appendix 7.3 for details of tangent space.

When the data have a manifold structure, traditional gradient descent methods in Euclidean space, such as SGD, often result in updates that stray off the manifold. Thus, we propose to project the gradient $\nabla L^k(\Delta\mathbf{W}^k)$ in Euclidean space onto the tangent space T_M at the point $\Delta\mathbf{W}$ on the manifold M and compute the Riemannian gradient $\Gamma L^k(\Delta\mathbf{W}^k)$. This projection can be accomplished

through orthogonal projection P_{T_M}, ensuring that the optimization trajectory remains confined to the manifold Lee (2012) and is effectively directed towards minimizing the loss function.

$$\begin{aligned}\Gamma L^k(\Delta\mathbf{W}^k) &= (\Gamma_{\mathbf{U}^k}L^k, \Gamma_{\mathbf{\Sigma}^k}L^k, \Gamma_{\mathbf{V}^k}L^k) = P\nabla L^k \in T_M \subseteq \mathbb{R}^{m\times n} \\ &= \mathbf{U}^k((\mathbf{U}^k)^T\nabla L^k\mathbf{V}^k)(\mathbf{V}^k)^T + (\mathbf{I}_m - \mathbf{U}^k(\mathbf{U}^k)^T)\nabla L^k\mathbf{V}^k(\mathbf{V}^k)^T + \\ &\quad \mathbf{U}^k(\mathbf{U}^k)^T\nabla L^k(\mathbf{I}_n - (\mathbf{V}^k)(\mathbf{V}^k)^T)\end{aligned} \tag{20}$$

where $\Gamma_{\mathbf{U}^k}L^k$, $\Gamma_{\mathbf{\Sigma}^k}L^k$, and $\Gamma_{\mathbf{V}^k}L^k$ represent the Riemannian gradients with respect to $\mathbf{U}^k$, $\mathbf{\Sigma}^k$, and $\mathbf{V}^k$ respectively. $\mathbf{I}_m$ and $\mathbf{I}_n$ are the m/n-dimensional identity matrices. Please refer to Appendix 7.3 for derivation details of Riemannian gradient.

Therefore, the gradients of $\mathbf{U}^k$, $\mathbf{\Sigma}^k$, and $\mathbf{V}^k$ in Riemannian space can be derived as follows.

$$\begin{aligned}&\Gamma_{\mathbf{U}^k}L^k = (\mathbf{I}_m - \mathbf{U}^k(\mathbf{U}^k)^T)\nabla_{\mathbf{U}^k}L^k, \qquad \Gamma_{\mathbf{V}^k}L^k = (\mathbf{I}_n - \mathbf{V}^k(\mathbf{V}^k)^T)\nabla_{\mathbf{V}^k}L^k, \\ &\Gamma_{\mathbf{\Sigma}^k}L^k = ((\mathbf{U}^k)^T\nabla_{\mathbf{U}^k}L^k - \nabla_U(L^k)^T\mathbf{U}^k)\mathbf{\Sigma}^k + \mathbf{\Sigma}^k(\mathbf{V}^k\nabla_{\mathbf{V}^k}(L^k)^T - \nabla_{\mathbf{V}^k}L^k(\mathbf{V}^k)^T) + \nabla_{\mathbf{\Sigma}^k}L^k\end{aligned} \tag{21}$$

where $\nabla_{\mathbf{U}^k}L^k$, $\nabla_{\mathbf{V}^k}L^k$, and $\nabla_{\mathbf{\Sigma}^k}L^k$ denote the corresponding Euclidean gradients. They are the conventional derivatives in Euclidean space that are used to compute the gradient descent steps before projection onto the manifold.

We try to find the steepest descent direction $P\nabla L^k$ within the tangent space T_M. Consider the intrinsic geometry of the manifold, we take a gradient step in the direction opposite to $P\nabla L^k$ and apply the learning rate η_t to reach a new point $\Delta\mathbf{W}^k$, which still lies within the tangent space T_M. The retraction maps the tangent vector corresponding to the point $\Delta\mathbf{W}^k$ back to the manifold, ensuring that the rank of the updated point $\Delta\mathbf{W}^k$ remains unchanged. Namely, our RAFFT approach ensures that the local updates of $\mathbf{U}^k$, $\mathbf{\Sigma}^k$, and $\mathbf{V}^k$ preserve a fixed-rank structure. Thus, the approach keeps the rank invariant during the stage of local updates by maintaining the model parameters moving towards the Riemannian manifold.

The following theorem demonstrates that the RGD optimization on the Riemannian manifold ensures the rank invariance during the local update process.

Theorem 2. *Let $\Delta\mathbf{W}^k$ be a point on a Riemannian manifold M consisting of all matrices with a fixed rank r in $\mathbb{R}^{m\times n}$. Suppose $\nabla L^k(\Delta\mathbf{W}^k)$ is the Euclidean gradient of the loss function L^k at $\Delta\mathbf{W}^k$, and $\Gamma_{\mathbf{U}^k}L^k$, $\Gamma_{\mathbf{\Sigma}^k}L^k$, and $\Gamma_{\mathbf{V}^k}L^k$ represent the components of the Riemannian gradient at $\Delta\mathbf{W}^k$. The RGD optimization with a learning rate η_t at round t $(0 \le t \le C)$ ensures that the local update*

$$\left((\mathbf{U}^k)^{(t+1)}, (\mathbf{\Sigma}^k)^{(t+1)}, (\mathbf{V}^k)^{(t+1)}\right) = f\left(-\eta_t\left(\left(\Gamma_{\mathbf{U}^k}L^k\right)^{(t)}, \left(\Gamma_{\mathbf{\Sigma}^k}L^k\right)^{(t)}, \left(\Gamma_{\mathbf{V}^k}L^k\right)^{(t)}\right)\right) \tag{22}$$

preserves the rank r of $\Delta\mathbf{W}^k$, maintaining the structure within the manifold M, where f is a retraction $f : T_M \to M$ mapping the tangent space at $\Delta\mathbf{W}^k$ to the manifold.

Please refer to Appendix 7.3 for the derivation of Riemannian retraction function and the detailed proof of Theorem 2.

We also conduct the convergence analysis of our RAFFT algorithm based on the RGD optimization on the Riemannian manifold.

Theorem 3 (Nonconvex)**.** *Suppose that optimization problem in Eq.(18) satisfies Assumption 1 and 2. We run Algorithm 1, where the selected clients perform gradient descent with a fixed stepsize, and we set $\eta_t \le \frac{1}{c_g}$. Then, the output of Algorithm 1 satisfies the following*

$$\min_{0\le t\le C} \mathbb{E}\left[\| \left(\left(\Gamma_{\mathbf{U}^k}L^k\right)^{(t)}, \left(\Gamma_{\mathbf{\Sigma}^k}L^k\right)^{(t)}, \left(\Gamma_{\mathbf{V}^k}L^k\right)^{(t)}\right) \|^2\right] \le \frac{2c_g}{C}\left(L(\Delta\mathbf{W}^1) - L(\Delta\mathbf{W}^*)\right) \tag{23}$$

where $\Delta\mathbf{W}^*$ denotes the point on the manifold $\mathcal{M}$ that minimizes the function $L(\Delta\mathbf{W}^*) = \arg\min_{\Delta\mathbf{W}\in\mathcal{M}} L(\Delta\mathbf{W})$.

Theorem 4 (Convex)**.** *Suppose that optimization problem in Eq.(18) satisfies Assumptions 1, 2, and 3, where the local functions L are geodesically convex in W (see Definition3). We consider Algorithm 1, where the selected clients perform gradient descent with a fixed stepsize, and the stepsize is set such that $\eta_t \le \frac{1}{2c_g}$. Then, the output of Algorithm 1 satisfies the following*

$$\mathbb{E}\left[L(\Delta\mathbf{W}^{(C)}) - L(\Delta\mathbf{W}^*)\right] \le \frac{\zeta c_g d^2(\Delta\mathbf{W}, \Delta\mathbf{W}^*)}{(\zeta + C - 2)} = \frac{\zeta c_g d^2(\Delta(\mathbf{U_0}, \mathbf{\Sigma_0}, \mathbf{V_0}), \Delta(\mathbf{U}^*, \mathbf{\Sigma}^*, \mathbf{V}^*))}{(\zeta + C - 2)} \tag{24}$$

where $\Delta\mathbf{W}^*$ denotes the point on the manifold $\mathcal{M}$ that minimizes the function $L(\Delta\mathbf{W}^*) = \arg\min_{\Delta\mathbf{W}\in\mathcal{M}} L(\Delta\mathbf{W})$ and ζ is defined in Assumptions 3

Please refer to Appendix 7.4 for detailed proof of Theorems 3 and 4

By assembling different pieces together, we provide the pseudo code of our RAFFT algorithm in Algorithm 1 in Appendix 7.9.

5 Experimental Evaluation

In this section, we present the experimental results over 13 baselines and 3 commonly-used tasks to demonstrate the advantages of our method. We consider an FL environment with 100 devices and a parameter server. In each epoch, we randomly sample 10 devices to perform the local update. We exploit three widely used NLP tasks including SST-2 (Socher et al., 2013), MRPC Dolan & Brockett (2005) and MPQA (Wiebe et al., 2005). We evaluated fix rank method and all other methods on RoBERTa-LARGE (Liu et al., 2019b), which consists of 24 layers of transformers followed by a large language model head and 355M pretrained parameters. To demonstrate the adaptability of our method, we carried out extra experiments with two additional decoder-based models,i.e., LLaMA 3B Touvron et al. (2023) model on MRPC, MPQA, SST-2 dataset, LLaMA 7B model Radford et al. (2019) on MRPC, MPQA, SST-2 dataset. At the same time, we conducted experiments on the image classification data sets CIFAR10 (Krizhevsky et al., 2010), CIFAR100 (Krizhevsky et al., 2010), and Tiny-IamgeNet Le & Yang (2015) of the ViT model. The backbones of these models are frozen for all methods. Please see Appendix 7.5 for details.

	alpha = 5			alpha = 3			alpha = 1		
Method	Accuracy	Loss	Time	Accuracy	Loss	Time	Accuracy	Loss	Time
Cntralized LoRA	80.40	0.3606	5,712	70.30	0.8222	5,762	71.00	0.8047	5,287
AdaLoRA	77.75	0.4070	5,450	78.70	0.3736	5,464	77.75	0.4070	5,421
P-tuning v2	87.25	0.2512	5,717	88.90	0.2510	5,820	87.85	0.2779	5,450
FedPrompt	87.20	0.2556	5,636	88.80	0.2632	5,648	88.30	0.2917	5,450
FedPepTAO	87.60	0.2460	5,639	89.65	0.2526	5,651	88.70	0.2651	5,442
PromptFL	87.35	0.2507	5,670	89.40	0.2507	5,708	86.55	0.3115	5,453
PE_FL	87.00	0.2570	5,682	88.65	0.2643	5,678	87.90	0.2954	5,447
SLoRA	88.75	0.2474	5,296	87.90	0.2451	5,318	86.40	0.2878	5,481
HetLoRA	83.75	0.2964	5,057	86.25	0.2611	5,056	85.95	0.2518	5,038
FedLoRA	78.10	0.4356	4,996	77.50	0.3702	5,033	76.80	0.4629	5,019
FFA-LoRA	87.05	0.2167	5,000	87.45	0.2176	5,318	86.80	0.2249	5,317
Fedkseed	87.81	0.2662	5,641	88.77	0.2698	5,675	88.74	0.3022	5,447
FLoRA	85.60	0.2756	5,306	88.34	0.2594	5,310	87.69	0.2656	5,210
RAFFT	92.00	0.2079	5,010	91.55	0.2293	4,980	90.90	0.1934	4,965
RAFFT-RGD	88.35	0.2365	4,952	89.10	0.2514	4,955	88.90	0.2349	4,961
RAFFT-MR	90.80	0.2602	5,021	90.60	0.2501	4,917	86.05	0.2718	4,886

Table 1: Performance comparison of different methods on LLaMA 7B+MPQA.

Baselines. We take 13 existing approaches as baselines, including 2 stand-alone version lora method,i.e., **LoRA** (Hu et al., 2022), **AdaLoRA** (Zhang et al., 2023b), which significantly reduce the number of trainable parameters by injecting low-rank decomposition matrices into each layer of a Transformer model. We adapt both methods to a federated learning setting for comparison. 1 full parameters tuning method, i.e., **Fedkseed** (Qin et al., 2024), which uses a finite set of random seeds for zeroth-order optimization, reducing the communication overhead between the server and clients. 5 prompt-based tuning method, i.e., **P-Tuning v2** (Liu et al., 2021a), **FedPrompt** (Zhao et al., 2023), **FedPepTAO** (Che et al., 2023), **PromptFL** (Guo et al., 2024), **PE-FL** (Zhao et al., 2024), which integrate lightweight trainable blocks into the frozen foundational models (FMs) and fine-tune additional parameters for localized model adaptation, enhancing computational and communication efficiency while allowing customization based on specific local data characteristics or user preferences and 5 reparameterization-based methods, i.e., **SLoRA** (Babakniya et al., 2023), **HetLoRA** (Cho et al., 2023), **FedLoRA** (Yi et al., 2024), **FFA-LoRA** (Sun et al., 2024),**FLoRA** (Wang et al., 2024), which hypothesize that fine-tuning adaptations can be reparameterized into optimization within low-rank subspaces, addressing performance gaps due to data heterogeneity and optimizing performance across diverse client devices. For detailed descriptions of each baseline, please refer to the appendix 7.1.

Variants of the RAFFT Model. We evaluate two versions of the RAFFT model to showcase the strengths of distinct technical approaches. The first variant, which we term the RAFFT-RGD Model, solely utilizes the Riemannian gradient. This model primarily focuses on the fundamental capability to manage gradient descent within the geometric constraints of the RAFFT manifold, using FedAvg as the aggregation method. The second variant is the RAFFT-MR model, which does not use the Riemannian theory fix rank during training. This means rankings will drop during local updates.

	alpha = 5			alpha = 3			alpha = 1		
Method	Accuracy	Loss	Time	Accuracy	Loss	Time	Accuracy	Loss	Time
Centralized LoRA	71.90	0.7170	3,329	72.16	0.6129	3,395	67.08	0.6977	3,369
AdaLoRA	71.76	0.6936	3,535	71.35	0.6031	3,515	68.11	0.7818	3,529
SLoRA	71.75	0.6843	3,309	71.06	0.7023	3,380	68.14	0.7474	3,316
HetLoRA	71.76	0.6939	3,355	71.26	0.5861	3,331	65.96	0.6800	3,437
FedLoRA	71.56	0.7149	3,282	70.72	0.7149	3,384	68.19	0.6634	3,421
FFA-LoRA	71.47	0.7135	3,321	70.24	0.7369	3,321	65.76	0.6831	3,358
FLoRA	70.95	0.7266	3,401	71.09	0.6335	3,347	65.85	0.6890	3,361
RAFFT	74.54	0.5757	3,304	73.22	0.5765	3,281	70.04	0.6504	3,285
RAFFT-RGD	72.96	0.5945	3,288	72.52	0.6381	3,292	67.14	0.7159	3,299
RAFFT-MR	72.88	0.6070	3,291	72.02	0.6435	3,307	67.24	0.6879	3,311

Table 2: Performance comparison of different methods on ViT+CIFRA10.

Evaluation metrics. In line with protocols established in previous studies on federated learning for large language models (Babakniya et al., 2023; Cho et al., 2023; Sun et al., 2024), we employ three crucial metrics to evaluate the efficacy of parameter efficiency in fine-tuning for classification tasks: Loss, Accuracy, and Time.Loss measures the model's prediction error, providing insight into the effectiveness of the learning process. Accuracy gauges the model's performance on classifying new, unseen data, reflecting the practical applicability of the federated learning model. Time is evaluated to determine the speed of convergence and the overall computational demand, which are critical in federated settings where computational resources and time are often limited.

Accuracy of classification with Riemannian Manifold. Tables 1 and 2 show the classification accuracy of our method, which uses Riemannian parameter matching and a Riemannian optimizer across two datasets. For comparison, the baseline reflects the accuracy of FedPEFT. Our Non-IID dataset was partitioned using a Dirichlet distribution. Our method consistently outperforms 13 other approaches, addressing both "client drift" and "rank drift." Notably, we see accuracy improvements of up to 10.94% on MPQA for LLaMA-3B, 23.21% for LLaMA-7B, and 14.11% on SST-2 for RoBERTa. In image classification, the ViT model sees gains up to 16.61% on CIFAR-100. These results highlight the potential of our approach as a strong alternative to existing FedPEFT methods. For more details, see Appendix 7.5.

Ablation study. Tables 1-2 further compare the accuracy across three datasets with two variants of our RAFFT model, which differ in their aggregation methods and optimizer updates. Our observations reveal that our method consistently achieves optimal precision and minimal error on the SST-2, MRPC, and MPQA datasets, significantly outperforming the two variants. A plausible explanation for this superiority is that our RAFFT approach performs Riemannian parameter matching, effectively addressing "client drift" issues and thereby enhancing the efficacy of rank-adaptive LoRA in federated learning. Additionally, our method leverages the Riemannian Gradient Descent (RGD) technique to ensure that each iteration of federated learning by the server maintains locally updated weight matrices with a fixed optimal rank. This not only mitigates rank drift but also accelerates the aggregation process in RAFFT, enhancing the overall performance.

Execution Time. Tables 1-2 report the total running time for training large models across all clients for both variants of our RAFFT method and all comparison methods on three datasets. Compared to other FedPEFT methods that require operations on the full weight matrix during aggregation, our RAFFT approach achieves higher efficiency. Apart from these methods, our RAFFT method maintains similar efficiency while ensuring higher accuracy rates.

Impact of number of client Figure 2 (c,d) evaluates the performance effects with varying numbers of clients by changing N from 40 to 80. We observe that as N increases, the performance curve of RAFFT generally trends downward. Notably, when the number of clients reaches 80, the accuracy of RAFFT significantly decreases. A plausible explanation for this is that as the number of clients increases, the amount of data allocated to each client decreases, leading to lower quality local model

updates. Additionally, the increase in the number of clients exacerbates the heterogeneity issue. Data distributions may vary significantly across different clients, resulting in substantial differences in the model parameters trained by each client. This increased training complexity ultimately affects the model's performance. As the number of clients increases, the overall training time tends to increase. This is likely due to the higher communication overhead and synchronization delays introduced when coordinating a larger number of clients.

Impact of initial rank Based on Figure 2 (a,b), we evaluate the performance effect when setting the initial ranking value r to 2, 4, 8, and 16. Theoretically, the highest rank should yield the best performance. However, as ovserved in the experiments from the LoRA Hu et al. (2022) and AdaLoRA Zhang et al. (2023b) papers, there is no clear trend between performance and rank. Our results are consistent with this observation, showing that the best rank varies depending on the task. For example, rank 16 performed best for SST-2, MRPC, and MPQA, while rank 8 was optimal for CIFAR-10. Additionally, higher ranks increase training time due to greater computational complexity. When the ranking is higher, the model has more parameters to learn and optimize, which essentially requires more computing resources and time. Thus, different tasks require different ranks, and our approach is adaptive to the rank, allowing it to find the appropriate rank for each specific task.

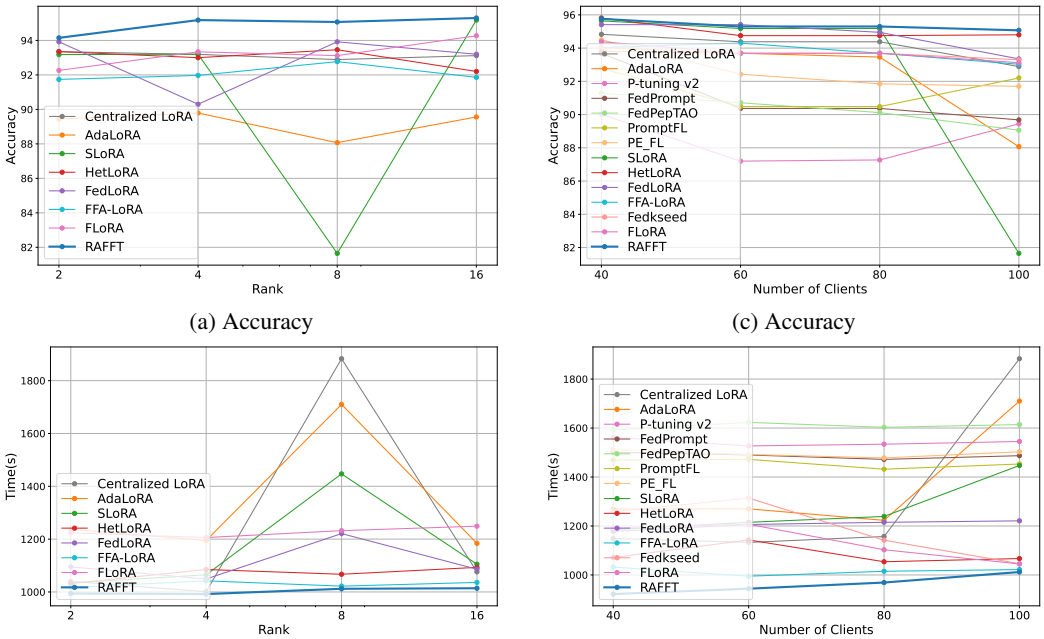

(a) Accuracy (c) Accuracy

(b) Time (d) Time

Figure 2: Accuracy and Time (s) with various LoRA ranks and client numbers on Roberta-SST2

Impact of select rank threshold Based on Figure Appendix 7.6, we evaluate the performance effect of setting the selection ranking threshold to 0.6, 0.7, 0.8, 0.9, and 1. We observe that as the threshold increases, the performance improves slightly initially and performs best at a threshold of 0.9. Beyond this point, performance starts to degrade. This trend suggests that a threshold of 0.9 is optimal, probably because it strikes a balance between filtering out irrelevant information and retaining useful information. When the threshold is set to 1, it means there is no level truncation which may introduce too much noise or redundant information, leading to performance degradation.

6 Conclusions

In this work, we propose rank-adaptive LoRA-based federated fine-tuning algorithm for foundation models. First, we design a novel Riemannian parameter matching method with the SVD on a low-rank matrix to avoid the client-drift issue to enhance the effectiveness of FFT-FM, while further improving its efficiency. Second, we develop a Riemannian gradient descent method on Riemannian manifold to guarantee the local parameter matrices with fixed optimal rank in each iteration, to speed up the convergence.

REFERENCES

P.-A. Absil and Jérôme Malick. Projection-like retractions on matrix manifolds. *SIAM Journal on Optimization*, 22(1):135–158, 2012. doi: 10.1137/100802529. URL https://doi.org/10.1137/100802529.

P.-A. Absil, R. Mahony, and R. Sepulchre. *Optimization Algorithms on Matrix Manifolds*. Princeton University Press, Princeton, NJ, 2008. ISBN 978-0-691-13298-3.

Armen Aghajanyan, Sonal Gupta, and Luke Zettlemoyer. Intrinsic dimensionality explains the effectiveness of language model fine-tuning. In Chengqing Zong, Fei Xia, Wenjie Li, and Roberto Navigli (eds.), *Proceedings of the 59th Annual Meeting of the Association for Computational Linguistics and the 11th International Joint Conference on Natural Language Processing (Volume 1: Long Papers)*, pp. 7319–7328, Online, August 2021. Association for Computational Linguistics. doi: 10.18653/v1/2021.acl-long.568. URL https://aclanthology.org/2021.acl-long.568.

M. F. Atiyah and J. A. Todd. On complex stiefel manifolds. *Mathematical Proceedings of the Cambridge Philosophical Society*, 56(4):342–353, 1960. doi: 10.1017/S0305004100034642.

Sara Babakniya, Ahmed Elkordy, Yahya Ezzeldin, Qingfeng Liu, Kee-Bong Song, MOSTAFA EL-Khamy, and Salman Avestimehr. SLoRA: Federated parameter efficient fine-tuning of language models. In *International Workshop on Federated Learning in the Age of Foundation Models in Conjunction with NeurIPS 2023*, 2023. URL https://openreview.net/forum?id=06quMTmtRV.

Guangji Bai, Zheng Chai, Chen Ling, Shiyu Wang, Jiaying Lu, Nan Zhang, Tingwei Shi, Ziyang Yu, Mengdan Zhu, Yifei Zhang, Carl Yang, Yue Cheng, and Liang Zhao. Beyond efficiency: A systematic survey of resource-efficient large language models, 2024a. URL https://arxiv.org/abs/2401.00625.

Sikai Bai, Jie Zhang, Shuaicheng Li, Song Guo, Jingcai Guo, Jun Hou, Tao Han, and Xiaocheng Lu. Diprompt: Disentangled prompt tuning for multiple latent domain generalization in federated learning. *CoRR*, abs/2403.08506, 2024b. doi: 10.48550/ARXIV.2403.08506. URL https://doi.org/10.48550/arXiv.2403.08506.

Nicolas Boumal. *An Introduction to Optimization on Smooth Manifolds*. École Polytechnique Fédérale de Lausanne, March 2023. ISBN 9781009166157.

Dongqi Cai, Yaozong Wu, Shangguang Wang, Felix Xiaozhu Lin, and Mengwei Xu. Efficient federated learning for modern nlp. In *Proceedings of the 29th Annual International Conference on Mobile Computing and Networking*, ACM MobiCom '23, New York, NY, USA, 2023a. Association for Computing Machinery. ISBN 9781450399906. doi: 10.1145/3570361.3592505. URL https://doi.org/10.1145/3570361.3592505.

Dongqi Cai, Yaozong Wu, Haitao Yuan, Shangguang Wang, Felix Xiaozhu Lin, and Mengwei Xu. Towards practical few-shot federated nlp. In *Proceedings of the 3rd Workshop on Machine Learning and Systems*, EuroMLSys '23. ACM, May 2023b. doi: 10.1145/3578356.3592575. URL http://dx.doi.org/10.1145/3578356.3592575.

Di Chai, Leye Wang, Junxue Zhang, Liu Yang, Shuowei Cai, Kai Chen, and Qiang Yang. Practical lossless federated singular vector decomposition over billion-scale data. In Aidong Zhang and Huzefa Rangwala (eds.), *KDD '22: The 28th ACM SIGKDD Conference on Knowledge Discovery and Data Mining, Washington, DC, USA, August 14 - 18, 2022*, pp. 46–55. ACM, 2022.

Rudrasis Chakraborty and Baba C. Vemuri. Statistics on the Stiefel manifold: Theory and applications. *The Annals of Statistics*, 47(1):415 – 438, 2019. doi: 10.1214/18-AOS1692. URL https://doi.org/10.1214/18-AOS1692.

Tianshi Che, Ji Liu, Yang Zhou, Jiaxiang Ren, Jiwen Zhou, Victor S. Sheng, Huaiyu Dai, and Dejing Dou. Federated learning of large language models with parameter-efficient prompt tuning and adaptive optimization. In Houda Bouamor, Juan Pino, and Kalika Bali (eds.), *Proceedings of the 2023 Conference on Empirical Methods in Natural Language Processing, EMNLP 2023,*

Singapore, December 6-10, 2023, pp. 7871–7888. Association for Computational Linguistics, 2023. doi: 10.18653/V1/2023.EMNLP-MAIN.488. URL https://doi.org/10.18653/v1/2023.emnlp-main.488.

Fei Chen, Mi Luo, Zhenhua Dong, Zhenguo Li, and Xiuqiang He. Federated meta-learning with fast convergence and efficient communication. *CoRR*, abs/1802.07876, 2018.

Haokun Chen, Yao Zhang, Denis Krompass, Jindong Gu, and Volker Tresp. Feddat: An approach for foundation model finetuning in multi-modal heterogeneous federated learning. In Michael J. Wooldridge, Jennifer G. Dy, and Sriraam Natarajan (eds.), *Thirty-Eighth AAAI Conference on Artificial Intelligence, AAAI 2024, Thirty-Sixth Conference on Innovative Applications of Artificial Intelligence, IAAI 2024, Fourteenth Symposium on Educational Advances in Artificial Intelligence, EAAI 2014, February 20-27, 2024, Vancouver, Canada*, pp. 11285–11293. AAAI Press, 2024. doi: 10.1609/AAAI.V38I10.29007. URL https://doi.org/10.1609/aaai.v38i10.29007.

Yae Jee Cho, Luyang Liu, Zheng Xu, Aldi Fahrezi, Matt Barnes, and Gauri Joshi. Heterogeneous loRA for federated fine-tuning of on-device foundation models. In *International Workshop on Federated Learning in the Age of Foundation Models in Conjunction with NeurIPS 2023*, 2023. URL https://openreview.net/forum?id=EmV9sGpZ7q.

Terence Jie Chua, Wenhan Yu, Jun Zhao, and Kwok-Yan Lam. Fedpeat: Convergence of federated learning, parameter-efficient fine tuning, and emulator assisted tuning for artificial intelligence foundation models with mobile edge computing. *CoRR*, abs/2310.17491, 2023. doi: 10.48550/ARXIV.2310.17491. URL https://doi.org/10.48550/arXiv.2310.17491.

Liam Collins, Shanshan Wu, Sewoong Oh, and Khe Chai Sim. Profit: Benchmarking personalization and robustness trade-off in federated prompt tuning. *CoRR*, abs/2310.04627, 2023. doi: 10.48550/ARXIV.2310.04627. URL https://doi.org/10.48550/arXiv.2310.04627.

Wenlong Deng, Christos Thrampoulidis, and Xiaoxiao Li. Unlocking the potential of prompt-tuning in bridging generalized and personalized federated learning, 2024.

Jacob Devlin, Ming-Wei Chang, Kenton Lee, and Kristina Toutanova. BERT: Pre-training of deep bidirectional transformers for language understanding. In Jill Burstein, Christy Doran, and Thamar Solorio (eds.), *Proceedings of the 2019 Conference of the North American Chapter of the Association for Computational Linguistics: Human Language Technologies, Volume 1 (Long and Short Papers)*, pp. 4171–4186, Minneapolis, Minnesota, June 2019. Association for Computational Linguistics. doi: 10.18653/v1/N19-1423. URL https://aclanthology.org/N19-1423.

Ning Ding, Xingtai Lv, Qiaosen Wang, Yulin Chen, Bowen Zhou, Zhiyuan Liu, and Maosong Sun. Sparse low-rank adaptation of pre-trained language models. In *Conference on Empirical Methods in Natural Language Processing*, 2023. URL https://api.semanticscholar.org/CorpusID:265294736.

Manfredo Perdigão do Carmo. *Introduction to Riemannian Manifolds*, volume 176. Springer, 2018. ISBN 978-3-319-91754-2.

William B. Dolan and Chris Brockett. Automatically constructing a corpus of sentential paraphrases. In *Proceedings of the Third International Workshop on Paraphrasing (IWP2005)*, 2005. URL https://aclanthology.org/I05-5002.

Ali Edalati, Marzieh S. Tahaei, Ivan Kobyzev, Vahid Partovi Nia, James J. Clark, and Mehdi Rezagholizadeh. Krona: Parameter efficient tuning with kronecker adapter. *CoRR*, abs/2212.10650, 2022. doi: 10.48550/ARXIV.2212.10650. URL https://doi.org/10.48550/arXiv.2212.10650.

Antonella Falini. A review on the selection criteria for the truncated svd in data science applications. *Journal of Computational Mathematics and Data Science*, 5:100064, 2022. ISSN 2772-4158. doi: https://doi.org/10.1016/j.jcmds.2022.100064. URL https://www.sciencedirect.com/science/article/pii/S2772415822000244.

Zihan Fang, Zheng Lin, Zhe Chen, Xianhao Chen, Yue Gao, and Yuguang Fang. Automated federated pipeline for parameter-efficient fine-tuning of large language models, 2024.

Chun-Mei Feng, Bangjun Li, Xinxing Xu, Yong Liu, Huazhu Fu, and Wangmeng Zuo. Learning federated visual prompt in null space for mri reconstruction. In *2023 IEEE/CVF Conference on Computer Vision and Pattern Recognition (CVPR)*, pp. 8064–8073, 2023. doi: 10.1109/CVPR52729.2023.00779.

Gene H. Golub and Charles F. Van Loan. *Matrix Computations - 4th Edition*. Johns Hopkins University Press, Philadelphia, PA, 2013. doi: 10.1137/1.9781421407944. URL https://epubs.siam.org/doi/abs/10.1137/1.9781421407944.

G.H. Golub, Alan Hoffman, and G.W. Stewart. A generalization of the eckart-young-mirsky matrix approximation theorem. *Linear Algebra and its Applications*, 88-89:317–327, 1987. ISSN 0024-3795. doi: https://doi.org/10.1016/0024-3795(87)90114-5. URL https://www.sciencedirect.com/science/article/pii/0024379587901145.

Tao Guo, Song Guo, Junxiao Wang, Xueyang Tang, and Wenchao Xu. Promptfl: Let federated participants cooperatively learn prompts instead of models - federated learning in age of foundation model. *IEEE Trans. Mob. Comput.*, 23(5):5179–5194, 2024. doi: 10.1109/TMC.2023.3302410. URL https://doi.org/10.1109/TMC.2023.3302410.

Junxian He, Chunting Zhou, Xuezhe Ma, Taylor Berg-Kirkpatrick, and Graham Neubig. Towards a unified view of parameter-efficient transfer learning. In *The Tenth International Conference on Learning Representations, ICLR 2022, Virtual Event, April 25-29, 2022*. OpenReview.net, 2022. URL https://openreview.net/forum?id=0RDcd5Axok.

Roger A. Horn and Charles R. Johnson. *Matrix Analysis*. Cambridge University Press, second edition, 2012. ISBN 1478441518 9781478441519.

Neil Houlsby, Andrei Giurgiu, Stanislaw Jastrzebski, Bruna Morrone, Quentin de Laroussilhe, Andrea Gesmundo, Mona Attariyan, and Sylvain Gelly. Parameter-efficient transfer learning for NLP. In Kamalika Chaudhuri and Ruslan Salakhutdinov (eds.), *Proceedings of the 36th International Conference on Machine Learning, ICML 2019, 9-15 June 2019, Long Beach, California, USA*, volume 97 of *Proceedings of Machine Learning Research*, pp. 2790–2799. PMLR, 2019. URL http://proceedings.mlr.press/v97/houlsby19a.html.

Kevin Hsieh, Amar Phanishayee, Onur Mutlu, and Phillip B. Gibbons. The non-iid data quagmire of decentralized machine learning. In *Proceedings of the 37th International Conference on Machine Learning, ICML 2020, 13-18 July 2020, Virtual Event*, pp. 4387–4398, 2020.

Edward J. Hu, Yelong Shen, Phillip Wallis, Zeyuan Allen-Zhu, Yuanzhi Li, Shean Wang, Lu Wang, and Weizhu Chen. Lora: Low-rank adaptation of large language models. In *The Tenth International Conference on Learning Representations, ICLR 2022, Virtual Event, April 25-29, 2022*. OpenReview.net, 2022. URL https://openreview.net/forum?id=nZeVKeeFYf9.

Yahao Hu, Yifei Xie, Tianfeng Wang, Man Chen, and Zhisong Pan. Structure-aware low-rank adaptation for parameter-efficient fine-tuning. *Mathematics*, 2023. URL https://api.semanticscholar.org/CorpusID:264336659.

Junteng Jia, Ke Li, Mani Malek, Kshitiz Malik, Jay Mahadeokar, Ozlem Kalinli, and Frank Seide. Joint federated learning and personalization for on-device asr. In *2023 IEEE Automatic Speech Recognition and Understanding Workshop (ASRU)*, pp. 1–8, 2023. doi: 10.1109/ASRU57964.2023.10389738.

Jingang Jiang, Xiangyang Liu, and Chenyou Fan. Low-parameter federated learning with large language models. *CoRR*, abs/2307.13896, 2023. doi: 10.48550/ARXIV.2307.13896. URL https://doi.org/10.48550/arXiv.2307.13896.

Wilfrid S. Kendall, Dennis Barden, Timothy K. Carne, and Huiling Le. *Statistics on Special Manifolds*, volume 174. Springer-Verlag, 2003. ISBN 978-0-387-00160-9.

Umar Khalid, Hasan Iqbal, Saeed Vahidian, Jing Hua, and Chen Chen. CEFHRI: A communication efficient federated learning framework for recognizing industrial human-robot interaction. In *IROS*, pp. 10141–10148, 2023. doi: 10.1109/IROS55552.2023.10341467. URL https://doi.org/10.1109/IROS55552.2023.10341467.

Mikhail Khodak, Maria-Florina Balcan, and Ameet S. Talwalkar. Adaptive gradient-based meta-learning methods. In *Advances in Neural Information Processing Systems 32: Annual Conference on Neural Information Processing Systems 2019, NeurIPS 2019, December 8-14, 2019, Vancouver, BC, Canada*, pp. 5915–5926, 2019.

Yeachan Kim, Junho Kim, Wing-Lam Mok, Jun-Hyung Park, and SangKeun Lee. Client-customized adaptation for parameter-efficient federated learning. In Anna Rogers, Jordan Boyd-Graber, and Naoaki Okazaki (eds.), *Findings of the Association for Computational Linguistics: ACL 2023*, pp. 1159–1172, Toronto, Canada, July 2023. Association for Computational Linguistics. doi: 10.18653/v1/2023.findings-acl.75. URL https://aclanthology.org/2023.findings-acl.75.

Alex Krizhevsky, Vinod Nair, and Geoffrey Hinton. Cifar-10 (canadian institute for advanced research). https://www.cs.toronto.edu/~kriz/cifar.html, 2010.

Ya Le and Xuan Yang. Tiny imagenet visual recognition challenge. https://www.kaggle.com/c/tiny-imagenet, 2015.

John M. Lee. *Introduction to Smooth Manifolds*. Springer, 2 edition, 2012. New edition extensively revised and clarified, with topics substantially rearranged. Introduces the rank theorem and the fundamental theorem on flows earlier. Added topics include Sard's theorem, transversality, infinitesimal Lie group actions, first-order partial differential equations, degree theory for smooth maps between compact manifolds, and an introduction to contact structures. Supplementary material available at sn.pub/extras.

Brian Lester, Rami Al-Rfou, and Noah Constant. The power of scale for parameter-efficient prompt tuning. In Marie-Francine Moens, Xuanjing Huang, Lucia Specia, and Scott Wen-tau Yih (eds.), *Proceedings of the 2021 Conference on Empirical Methods in Natural Language Processing, EMNLP 2021, Virtual Event / Punta Cana, Dominican Republic, 7-11 November, 2021*, pp. 3045–3059. Association for Computational Linguistics, 2021. doi: 10.18653/V1/2021.EMNLP-MAIN.243. URL https://doi.org/10.18653/v1/2021.emnlp-main.243.

Guanghao Li, Wansen Wu, Yan Sun, Li Shen, Baoyuan Wu, and Dacheng Tao. Visual prompt based personalized federated learning. *CoRR*, abs/2303.08678, 2023. doi: 10.48550/ARXIV.2303.08678. URL https://doi.org/10.48550/arXiv.2303.08678.

Xiang Lisa Li and Percy Liang. Prefix-tuning: Optimizing continuous prompts for generation. In Chengqing Zong, Fei Xia, Wenjie Li, and Roberto Navigli (eds.), *Proceedings of the 59th Annual Meeting of the Association for Computational Linguistics and the 11th International Joint Conference on Natural Language Processing, ACL/IJCNLP 2021, (Volume 1: Long Papers), Virtual Event, August 1-6, 2021*, pp. 4582–4597. Association for Computational Linguistics, 2021. doi: 10.18653/V1/2021.ACL-LONG.353. URL https://doi.org/10.18653/v1/2021.acl-long.353.

Baohao Liao, Yan Meng, and Christof Monz. Parameter-efficient fine-tuning without introducing new latency. In Anna Rogers, Jordan L. Boyd-Graber, and Naoaki Okazaki (eds.), *Proceedings of the 61st Annual Meeting of the Association for Computational Linguistics (Volume 1: Long Papers), ACL 2023, Toronto, Canada, July 9-14, 2023*, pp. 4242–4260. Association for Computational Linguistics, 2023. doi: 10.18653/V1/2023.ACL-LONG.233. URL https://doi.org/10.18653/v1/2023.acl-long.233.

Zhaojiang Lin, Andrea Madotto, and Pascale Fung. Exploring versatile generative language model via parameter-efficient transfer learning. In Trevor Cohn, Yulan He, and Yang Liu (eds.), *Findings of the Association for Computational Linguistics: EMNLP 2020, Online Event, 16-20 November 2020*, volume EMNLP 2020 of *Findings of ACL*, pp. 441–459. Association for Computational Linguistics, 2020. doi: 10.18653/V1/2020.FINDINGS-EMNLP.41. URL https://doi.org/10.18653/v1/2020.findings-emnlp.41.

Zihao Lin, Yan Sun, Yifan Shi, Xueqian Wang, Lifu Huang, Li Shen, and Dacheng Tao. Efficient federated prompt tuning for black-box large pre-trained models. *CoRR*, abs/2310.03123, 2023. doi: 10.48550/ARXIV.2310.03123. URL https://doi.org/10.48550/arXiv.2310.03123.

Bei Liu, Zekang Ding, Yufei Zhang, Huajun She, and Yiping P. Du. Low-rank tensor subspace decomposition with weighted group sparsity for the acceleration of non-cartesian dynamic mri. *IEEE Transactions on Biomedical Engineering*, 70(2):681–693, 2023a. doi: 10.1109/TBME.2022.3200709.

Lumin Liu, Jun Zhang, Shenghui Song, and Khaled Ben Letaief. Edge-assisted hierarchical federated learning with non-iid data. *CoRR*, abs/1905.06641, 2019a.

Xiao Liu, Kaixuan Ji, Yicheng Fu, Zhengxiao Du, Zhilin Yang, and Jie Tang. P-tuning v2: Prompt tuning can be comparable to fine-tuning universally across scales and tasks. *CoRR*, abs/2110.07602, 2021a. URL https://arxiv.org/abs/2110.07602.

Xiao Liu, Yanan Zheng, Zhengxiao Du, Ming Ding, Yujie Qian, Zhilin Yang, and Jie Tang. GPT understands, too. *CoRR*, abs/2103.10385, 2021b. URL https://arxiv.org/abs/2103.10385.

Xiao Liu, Kaixuan Ji, Yicheng Fu, Weng Tam, Zhengxiao Du, Zhilin Yang, and Jie Tang. P-tuning: Prompt tuning can be comparable to fine-tuning across scales and tasks. In Smaranda Muresan, Preslav Nakov, and Aline Villavicencio (eds.), *Proceedings of the 60th Annual Meeting of the Association for Computational Linguistics (Volume 2: Short Papers)*, pp. 61–68, Dublin, Ireland, May 2022. Association for Computational Linguistics. doi: 10.18653/v1/2022.acl-short.8. URL https://aclanthology.org/2022.acl-short.8.

Xiao-Yang Liu, Rongyi Zhu, Daochen Zha, Jiechao Gao, Shan Zhong, and Meikang Qiu. Differentially private low-rank adaptation of large language model using federated learning. *CoRR*, abs/2312.17493, 2023b. doi: 10.48550/ARXIV.2312.17493. URL https://doi.org/10.48550/arXiv.2312.17493.

Xiaonan Liu, Tharmalingam Ratnarajah, Mathini Sellathurai, and Yonina C. Eldar. Adaptive model pruning and personalization for federated learning over wireless networks, 2024a.

Yi Liu, Xiaohan Bi, Lei Li, Sishuo Chen, Wenkai Yang, and Xu Sun. Communication efficient federated learning for multilingual neural machine translation with adapter. In Anna Rogers, Jordan Boyd-Graber, and Naoaki Okazaki (eds.), *Findings of the Association for Computational Linguistics: ACL 2023*, pp. 5315–5328, Toronto, Canada, July 2023c. Association for Computational Linguistics. doi: 10.18653/v1/2023.findings-acl.327. URL https://aclanthology.org/2023.findings-acl.327.

Yinhan Liu, Myle Ott, Naman Goyal, Jingfei Du, Mandar Joshi, Danqi Chen, Omer Levy, Mike Lewis, Luke Zettlemoyer, and Veselin Stoyanov. Roberta: A robustly optimized BERT pretraining approach. *CoRR*, abs/1907.11692, 2019b. URL http://arxiv.org/abs/1907.11692.

Yixin Liu, Kai Zhang, Yuan Li, Zhiling Yan, Chujie Gao, Ruoxi Chen, Zhengqing Yuan, Yue Huang, Hanchi Sun, Jianfeng Gao, Lifang He, and Lichao Sun. Sora: A review on background, technology, limitations, and opportunities of large vision models. *CoRR*, abs/2402.17177, 2024b. doi: 10.48550/ARXIV.2402.17177. URL https://doi.org/10.48550/arXiv.2402.17177.

Zequan Liu, Jiawen Lyn, Wei Zhu, Xing Tian, and Yvette Graham. Alora: Allocating low-rank adaptation for fine-tuning large language models. *CoRR*, abs/2403.16187, 2024c. doi: 10.48550/ARXIV.2403.16187. URL https://doi.org/10.48550/arXiv.2403.16187.

Wang Lu, Xixu Hu, Jindong Wang, and Xing Xie. Fedclip: Fast generalization and personalization for CLIP in federated learning. *IEEE Data Eng. Bull.*, 46(1):52–66, 2023. URL http://sites.computer.org/debull/A23mar/p52.pdf.

Brendan McMahan, Eider Moore, Daniel Ramage, Seth Hampson, and Blaise Agüera y Arcas. Communication-efficient learning of deep networks from decentralized data. In Aarti Singh and

Xiaojin (Jerry) Zhu (eds.), *Proceedings of the 20th International Conference on Artificial Intelligence and Statistics, AISTATS 2017, 20-22 April 2017, Fort Lauderdale, FL, USA*, volume 54 of *Proceedings of Machine Learning Research*, pp. 1273–1282. PMLR, 2017.

Yue Niu, Saurav Prakash, Souvik Kundu, Sunwoo Lee, and Salman Avestimehr. Overcoming resource constraints in federated learning: Large models can be trained with only weak clients. *Transaction on Machine Learning Research (TMLR)*, 2023.

Jonas Pfeiffer, Aishwarya Kamath, Andreas Rücklé, Kyunghyun Cho, and Iryna Gurevych. Adapterfusion: Non-destructive task composition for transfer learning. In Paola Merlo, Jörg Tiedemann, and Reut Tsarfaty (eds.), *Proceedings of the 16th Conference of the European Chapter of the Association for Computational Linguistics: Main Volume, EACL 2021, Online, April 19 - 23, 2021*, pp. 487–503. Association for Computational Linguistics, 2021. doi: 10.18653/V1/2021.EACL-MAIN.39. URL https://doi.org/10.18653/v1/2021.eacl-main.39.

Zhen Qin, Daoyuan Chen, Bingchen Qian, Bolin Ding, Yaliang Li, and Shuiguang Deng. Federated full-parameter tuning of billion-sized language models with communication cost under 18 kilobytes, 2024. URL https://arxiv.org/abs/2312.06353.

Chen Qiu, Xingyu Li, Chaithanya Kumar Mummadi, Madan Ravi Ganesh, Zhenzhen Li, Lu Peng, and Wan-Yi Lin. Federated text-driven prompt generation for vision-language models. In *The Twelfth International Conference on Learning Representations*, 2024. URL https://openreview.net/forum?id=NW31gAylIm.

Alec Radford, Jeff Wu, Rewon Child, David Luan, Dario Amodei, and Ilya Sutskever. Language models are unsupervised multitask learners. 2019. URL https://api.semanticscholar.org/CorpusID:160025533.

Hossein Rajabzadeh, Mojtaba Valipour, Tianshu Zhu, Marzieh S. Tahaei, Hyock Ju Kwon, Ali Ghodsi, Boxing Chen, and Mehdi Rezagholizadeh. Qdylora: Quantized dynamic low-rank adaptation for efficient large language model tuning. *CoRR*, abs/2402.10462, 2024. doi: 10.48550/ARXIV.2402.10462. URL https://doi.org/10.48550/arXiv.2402.10462.

Andreas Rücklé, Gregor Geigle, Max Glockner, Tilman Beck, Jonas Pfeiffer, Nils Reimers, and Iryna Gurevych. Adapterdrop: On the efficiency of adapters in transformers. In Marie-Francine Moens, Xuanjing Huang, Lucia Specia, and Scott Wen-tau Yih (eds.), *Proceedings of the 2021 Conference on Empirical Methods in Natural Language Processing, EMNLP 2021, Virtual Event / Punta Cana, Dominican Republic, 7-11 November, 2021*, pp. 7930–7946. Association for Computational Linguistics, 2021. doi: 10.18653/V1/2021.EMNLP-MAIN.626. URL https://doi.org/10.18653/v1/2021.emnlp-main.626.

Felix Sattler, Simon Wiedemann, Klaus-Robert Müller, and Wojciech Samek. Robust and communication-efficient federated learning from non-iid data. *CoRR*, abs/1903.02891, 2019.

Andrew Schneider. Investigating traces of matrix products. Ms thesis, University of Minnesota Duluth, Duluth, Minnesota, May 2015. Submitted in partial fulfillment of the requirements for the degree of MS Applied and Computational Mathematics.

Aliaksandra Shysheya, John Bronskill, Massimiliano Patacchiola, Sebastian Nowozin, and Richard E. Turner. Fit: Parameter efficient few-shot transfer learning for personalized and federated image classification. In *The Eleventh International Conference on Learning Representations, ICLR 2023, Kigali, Rwanda, May 1-5, 2023*. OpenReview.net, 2023. URL https://openreview.net/pdf?id=9aokcgBVIj1.

Virginia Smith, Chao-Kai Chiang, Maziar Sanjabi, and Ameet S. Talwalkar. Federated multi-task learning. In *Advances in Neural Information Processing Systems 30: Annual Conference on Neural Information Processing Systems 2017, December 4-9, 2017, Long Beach, CA, USA*, pp. 4424–4434, 2017.

Richard Socher, Alex Perelygin, Jean Wu, Jason Chuang, Christopher D. Manning, Andrew Ng, and Christopher Potts. Recursive deep models for semantic compositionality over a sentiment treebank. In David Yarowsky, Timothy Baldwin, Anna Korhonen, Karen Livescu, and Steven Bethard

(eds.), *Proceedings of the 2013 Conference on Empirical Methods in Natural Language Processing*, pp. 1631–1642, Seattle, Washington, USA, October 2013. Association for Computational Linguistics. URL https://aclanthology.org/D13-1170.

Shangchao Su, Bin Li, and Xiangyang Xue. Fedra: A random allocation strategy for federated tuning to unleash the power of heterogeneous clients. *CoRR*, abs/2311.11227, 2023. doi: 10.48550/ARXIV.2311.11227. URL https://doi.org/10.48550/arXiv.2311.11227.

Guangyu Sun, Matías Mendieta, Jun Luo, Shandong Wu, and Chen Chen. Fedperfix: Towards partial model personalization of vision transformers in federated learning. In *IEEE/CVF International Conference on Computer Vision, ICCV 2023, Paris, France, October 1-6, 2023*, pp. 4965–4975. IEEE, 2023a. doi: 10.1109/ICCV51070.2023.00460. URL https://doi.org/10.1109/ICCV51070.2023.00460.

Jingwei Sun, Ziyue Xu, Hongxu Yin, Dong Yang, Daguang Xu, Yiran Chen, and Holger R. Roth. Fedbpt: Efficient federated black-box prompt tuning for large language models. *CoRR*, abs/2310.01467, 2023b. doi: 10.48550/ARXIV.2310.01467. URL https://doi.org/10.48550/arXiv.2310.01467.

Youbang Sun, Zitao Li, Yaliang Li, and Bolin Ding. Improving loRA in privacy-preserving federated learning. In *The Twelfth International Conference on Learning Representations*, 2024. URL https://openreview.net/forum?id=NLPzL6HWNl.

Marlon Tobaben, Aliaksandra Shysheya, John Bronskill, Andrew Paverd, Shruti Tople, Santiago Zanella Béguelin, Richard E. Turner, and Antti Honkela. On the efficacy of differentially private few-shot image classification. *CoRR*, abs/2302.01190, 2023. doi: 10.48550/ARXIV.2302.01190. URL https://doi.org/10.48550/arXiv.2302.01190.

Hugo Touvron, Thibaut Lavril, Gautier Izacard, Xavier Martinet, Marie-Anne Lachaux, Timothée Lacroix, Baptiste Rozière, Naman Goyal, Eric Hambro, Faisal Azhar, Aurélien Rodriguez, Armand Joulin, Edouard Grave, and Guillaume Lample. Llama: Open and efficient foundation language models. *CoRR*, abs/2302.13971, 2023. doi: 10.48550/ARXIV.2302.13971. URL https://doi.org/10.48550/arXiv.2302.13971.

Lloyd N. Trefethen and David Bau. *Numerical Linear Algebra*. SIAM, 1997. ISBN 0898713617.

Christophe Tribes, Sacha Benarroch-Lelong, Peng Lu, and Ivan Kobyzev. Hyperparameter optimization for large language model instruction-tuning. *CoRR*, abs/2312.00949, 2023. doi: 10.48550/ARXIV.2312.00949. URL https://doi.org/10.48550/arXiv.2312.00949.

Mojtaba Valipour, Mehdi Rezagholizadeh, Ivan Kobyzev, and Ali Ghodsi. Dylora: Parameter-efficient tuning of pre-trained models using dynamic search-free low-rank adaptation. In Andreas Vlachos and Isabelle Augenstein (eds.), *Proceedings of the 17th Conference of the European Chapter of the Association for Computational Linguistics, EACL 2023, Dubrovnik, Croatia, May 2-6, 2023*, pp. 3266–3279. Association for Computational Linguistics, 2023. doi: 10.18653/V1/2023.EACL-MAIN.239. URL https://doi.org/10.18653/v1/2023.eacl-main.239.

Bart Vandereycken. Fixed-rank matrix factorizations and riemannian low-rank optimization. *Computational Statistics*, 29:591–621, Nov 2014. doi: 10.1007/s00180-013-0461-0.

Jiamian Wang, Zongliang Wu, Yulun Zhang, Xin Yuan, Tao Lin, and Zhiqiang Tao. Cooperative hardware-prompt learning for snapshot compressive imaging. *CoRR*, abs/2306.01176, 2023. doi: 10.48550/ARXIV.2306.01176. URL https://doi.org/10.48550/arXiv.2306.01176.

Ziyao Wang, Zheyu Shen, Yexiao He, Guoheng Sun, Hongyi Wang, Lingjuan Lyu, and Ang Li. Flora: Federated fine-tuning large language models with heterogeneous low-rank adaptations, 2024. URL https://arxiv.org/abs/2409.05976.

Janyce Wiebe, Theresa Wilson, and Claire Cardie. Annotating expressions of opinions and emotions in language. *Lang. Resour. Evaluation*, 39(2-3):165–210, 2005. doi: 10.1007/S10579-005-7880-9. URL https://doi.org/10.1007/s10579-005-7880-9.

C. Wu, F. Wu, L. Lyu, et al. Communication-efficient federated learning via knowledge distillation. *Nature Communications*, 13:2032, 2022. doi: 10.1038/s41467-022-29763-x. URL https://doi.org/10.1038/s41467-022-29763-x.

Chuhan Wu, Fangzhao Wu, Ruixuan Liu, Lingjuan Lyu, Yongfeng Huang, and Xing Xie. Fedkd: Communication efficient federated learning via knowledge distillation. *CoRR*, abs/2108.13323, 2021.

Panlong Wu, Kangshuo Li, Ting Wang, and Fangxin Wang. Fedms: Federated learning with mixture of sparsely activated foundations models. *CoRR*, abs/2312.15926, 2023. doi: 10.48550/ARXIV.2312.15926. URL https://doi.org/10.48550/arXiv.2312.15926.

Xinghao Wu, Xuefeng Liu, Jianwei Niu, Haolin Wang, Shaojie Tang, and Guogang Zhu. Fedlora: When personalized federated learning meets low-rank adaptation. In *Submission to the Twelfth International Conference on Learning Representations, ICLR 2024, Vienna, Austria, May 7-11, 2024*, 2024.

Jie Xu, Karthikeyan Saravanan, Rogier C. van Dalen, Haaris Mehmood, David Tuckey, and Mete Ozay. Dp-dylora: Fine-tuning transformer-based models on-device under differentially private federated learning using dynamic low-rank adaptation. 2024. URL https://api.semanticscholar.org/CorpusID:269741226.

Mingbin Xu, Congzheng Song, Ye Tian, Neha Agrawal, Filip Granqvist, Rogier C. van Dalen, Xiao Zhang, Arturo Argueta, Shiyi Han, Yaqiao Deng, Leo Liu, Anmol Walia, and Alex Jin. Training large-vocabulary neural language models by private federated learning for resource-constrained devices. In *IEEE International Conference on Acoustics, Speech and Signal Processing ICASSP 2023, Rhodes Island, Greece, June 4-10, 2023*, pp. 1–5. IEEE, 2023. doi: 10.1109/ICASSP49357.2023.10096570. URL https://doi.org/10.1109/ICASSP49357.2023.10096570.

Jiaming Yan, Jianchun Liu, Shilong Wang, Hongli Xu, Haifeng Liu, and Jianhua Zhou. Heroes: Lightweight federated learning with neural composition and adaptive local update in heterogeneous edge networks. *CoRR*, abs/2312.01617, 2023. doi: 10.48550/ARXIV.2312.01617. URL https://doi.org/10.48550/arXiv.2312.01617.

Yiyuan Yang, Guodong Long, Tao Shen, Jing Jiang, and Michael Blumenstein. Dual-personalizing adapter for federated foundation models. *CoRR*, abs/2403.19211, 2024. doi: 10.48550/ARXIV.2403.19211. URL https://doi.org/10.48550/arXiv.2403.19211.

Liping Yi, Han Yu, Gang Wang, Xiaoguang Liu, and Xiaoxiao Li. pfedlora: Model-heterogeneous personalized federated learning with lora tuning, 2024.

Sixing Yu, J. Pablo Muñoz, and Ali Jannesari. Federated foundation models: Privacy-preserving and collaborative learning for large models. *CoRR*, abs/2305.11414, 2023. doi: 10.48550/ARXIV.2305.11414. URL https://doi.org/10.48550/arXiv.2305.11414.

Feiyu Zhang, Liangzhi Li, Junhao Chen, Zhouqiang Jiang, Bowen Wang, and Yiming Qian. Increlora: Incremental parameter allocation method for parameter-efficient fine-tuning. *CoRR*, abs/2308.12043, 2023a. doi: 10.48550/ARXIV.2308.12043. URL https://doi.org/10.48550/arXiv.2308.12043.

Hongyi Zhang and Suvrit Sra. First-order methods for geodesically convex optimization, 2016. URL https://arxiv.org/abs/1602.06053.

Hongyi Zhang, Sashank J. Reddi, and Suvrit Sra. Riemannian svrg: Fast stochastic optimization on riemannian manifolds, 2017. URL https://arxiv.org/abs/1605.07147.

Qingru Zhang, Minshuo Chen, Alexander Bukharin, Pengcheng He, Yu Cheng, Weizhu Chen, and Tuo Zhao. Adaptive budget allocation for parameter-efficient fine-tuning. In *The Eleventh International Conference on Learning Representations, ICLR 2023, Kigali, Rwanda, May 1-5, 2023*. OpenReview.net, 2023b. URL https://openreview.net/pdf?id=lq62uWRJjiY.

Zhuo Zhang, Yuanhang Yang, Yong Dai, Qifan Wang, Yue Yu, Lizhen Qu, and Zenglin Xu. FedPETuning: When federated learning meets the parameter-efficient tuning methods of pre-trained language models. In Anna Rogers, Jordan Boyd-Graber, and Naoaki Okazaki (eds.), *Findings of the Association for Computational Linguistics: ACL 2023*, pp. 9963–9977, Toronto, Canada, July 2023c. Association for Computational Linguistics. doi: 10.18653/v1/2023.findings-acl.632. URL https://aclanthology.org/2023.findings-acl.632.

Zhuo Zhang, Jingyuan Zhang, Jintao Huang, Lizhen Qu, Hongzhi Zhang, and Zenglin Xu. Fedpit: Towards privacy-preserving and few-shot federated instruction tuning. *CoRR*, abs/2403.06131, 2024. doi: 10.48550/ARXIV.2403.06131. URL https://doi.org/10.48550/arXiv.2403.06131.

Haodong Zhao, Wei Du, Fangqi Li, Peixuan Li, and Gongshen Liu. Fedprompt: Communication-efficient and privacy-preserving prompt tuning in federated learning. In *ICASSP 2023 - 2023 IEEE International Conference on Acoustics, Speech and Signal Processing (ICASSP)*, pp. 1–5, 2023. doi: 10.1109/ICASSP49357.2023.10095356.

Wanru Zhao, Yihong Chen, Royson Lee, Xinchi Qiu, Yan Gao, Hongxiang Fan, and Nicholas Donald Lane. Breaking physical and linguistic borders: Multilingual federated prompt tuning for low-resource languages. In *The Twelfth International Conference on Learning Representations*, 2024. URL https://openreview.net/forum?id=zzqn5G9fjn.

Peiheng Zhou, Ming Hu, Xiaofei Xie, Yihao Huang, Kangjie Chen, and Mingsong Chen. MIP: clip-based image reconstruction from PEFT gradients. *CoRR*, abs/2403.07901, 2024. doi: 10.48550/ARXIV.2403.07901. URL https://doi.org/10.48550/arXiv.2403.07901.

7 Appendix

7.1 Related Work

Parameter Efficient Fine Tuning (PEFT). As the scale of large language models (LLMs) continues to grow, the cost associated with the standard full fine-tuning paradigm has become extremely high. To address this issue, parameter-efficient fine-tuning (PEFT) methods Houlsby et al. (2019) have been proposed. These methods introduce a minimal set of additional trainable parameters to enhance model performance while keeping the majority of the pre-trained parameters frozen. Generally, PEFT approaches can be classified into two main categories based on how they manipulate model parameters. The first category, additive PEFT, involves the incorporation of new trainable modules or parameters to adjust the model architecture, minimizing the parameter count for downstream tasks. This includes Adapter Tuning (Houlsby et al., 2019), where small, trainable adapter modules are inserted within the model architecture to allow for task-specific adaptation without altering the original model weights, and methods such as prefix-tuning (Devlin et al., 2019), P-tuning (Liu et al., 2022), P-tuning v2 (Liu et al., 2021a), and prompt tuning (Lester et al., 2021), which append learnable vectors at the beginning of input sequences. The second category involves reparameterized PEFT techniques that build low-rank representations of original model parameters, incorporating additional trainable parameters during training. This category includes Low-Rank Decomposition, techniques like LoRA Hu et al. (2022) and KronA (Edalati et al., 2022), which decompose original model parameters into low-rank and residual matrices, and LoRA derivatives such as AdaLoRA Zhang et al. (2023b) and SoRA (Liu et al., 2024b), which dynamically select the rank of LoRA to construct adaptable low-rank representations. Collectively, these methods represent the cutting-edge in efficient model training techniques, enabling the deployment of large language models in resource-constrained environments without sacrificing performance.

Additive PEFT Methods in Federated Learning. These methods are specifically designed to minimize computational demands and associated communication overheads. The additive methods integrate lightweight trainable blocks into the frozen foundational models (FMs) and fine-tune additional parameters for localized model adaptation. This approach not only enhances computational and communication efficiency but also allows for the customization of heterogeneous models based on specific local data characteristics or user preferences. Recent work has introduced FedCLIP, a method that leverages lightweight adapters to enhance CLIP's performance in federated

settings, significantly reducing computational and communication costs while ensuring fast generalization and personalization (Lu et al., 2023). Similarly, FedDAT has been developed to fine-tune foundation models in a multi-modal, heterogeneous federated learning environment, utilizing Dual-Adapter Teachers to efficiently handle data heterogeneity and improve knowledge transfer (Chen et al., 2024). The Client-Customized Adaptation approach further tailors federated learning to address client heterogeneity through hypernetworks that generate client-specific adapters, enhancing both the efficiency and efficacy of pre-trained model adaptation (Kim et al., 2023). In addressing the challenges of multilingual neural machine translation, a communication-efficient framework has been proposed that minimizes the need for heavy data transmission by transferring only lightweight adapters, thus maintaining performance despite substantial discrepancies in data distribution (Liu et al., 2023c). A practical approach toward federated learning in NLP, AdaFL1, identifies and configures adapter modules to optimize training efficiency and model performance across various NLP tasks (Cai et al., 2023a). Joint efforts in federated learning and personalization for on-device ASR have shown that integrating personalized adapters with federated training substantially reduces word error rates, demonstrating the effectiveness of combined federated learning and personalization strategies (Jia et al., 2023). Furthermore, the FedPETuning framework explores parameter-efficient tuning methods within federated learning, offering insights into privacy protection, performance efficiency, and resource constraints (Zhang et al., 2023c). Research into image reconstruction from PEFT gradients within federated learning frameworks reveals potential security vulnerabilities, suggesting that even lightweight adapter gradients can be exploited to reconstruct training data (Zhou et al., 2024). The novel concept of Dual-Personalizing Adapter for Federated Foundation Models introduces test-time personalization to address distribution shifts effectively, enhancing both global and local adaptation (Yang et al., 2024). FedPEAT combines emulator-assisted tuning with parameter-efficient fine-tuning within a federated context to tackle the challenges of deploying large foundation models efficiently (Chua et al., 2023). Adaptive model pruning within federated learning frameworks demonstrates a significant reduction in computation and communication latency, enabling efficient learning even over wireless networks (Liu et al., 2024a). The development of a communication-efficient federated learning framework for industrial human-robot interaction addresses data privacy and heterogeneity while reducing communication costs (Khalid et al., 2023). Moreover, new approaches in parameter-efficient fine-tuning aim to reduce latency and storage requirements without compromising the model's performance, indicating a shift towards more sustainable and efficient federated learning methodologies (Liao et al., 2023; Tobaben et al., 2023; Cai et al., 2023a; Shysheya et al., 2023). The other is promt tuning. prompt tuning incorporates trainable task-specific continuous cue vectors at the input layer (Liu et al., 2022). PromptFL Guo et al. (2024) ships an off-the-shelf CLIP, to distributed clients who would cooperatively train shared soft prompts based on very few local data. FedPerfix Sun et al. (2023a) use a local adapter to generate prefixes and aggregate raw self-attention layers.Efforts to mitigate communication overhead in deploying large pre-trained models across decentralized networks have introduced techniques like model split aggregation, which significantly reduce the parameter transmission cost while maintaining robust defenses against adversarial attacks (Zhao et al., 2023). Other studies have emphasized the reduction of communication costs by employing compact, federated visual prompts specifically in contexts like medical imaging, where data heterogeneity often leads to catastrophic forgetting (Feng et al., 2023; Li et al., 2023). The PromptFL framework exemplifies another novel approach, shifting from traditional model training to prompt-based federated learning, leveraging foundational models to improve local training efficiency on limited data (Guo et al., 2024). Concurrently, text-driven prompt generation methods have been developed to adapt vision-language models to federated settings, demonstrating superior generalization capabilities across seen and unseen classes (Qiu et al., 2024). Multilingual and domain-specific adaptations further extend the applicability of prompt tuning in federated learning, offering significant improvements in data efficiency and robustness across various languages, especially in low-resource scenarios (Zhao et al., 2024; Bai et al., 2024b; Deng et al., 2024). Meanwhile, research on personalization and robustness trade-offs in federated systems has explored the implications of localized fine-tuning on model performance, revealing that strategic prompt tuning can significantly enhance both the personalization and robustness of federated models under diverse conditions (Collins et al., 2023; Lin et al., 2023). Innovative methods such as Federated Black-Box Prompt Tuning have also been proposed to address privacy concerns associated with large pre-trained models, emphasizing parameter-efficient strategies that reduce memory and communication requirements without compromising the model effectiveness (Lin et al., 2023; Sun et al., 2023b). The exploration of federated prompt tuning continues to evolve, tackling not only linguistic and domain-specific challenges but also aiming at enhancing the deployment efficiency

and personalization of large-scale models across heterogeneous environments (Wang et al., 2023; Yu et al., 2023; Cai et al., 2023b; Che et al., 2023).

Reparametrization-based PEFT Methods in Federated Learning. The hypothesis behind this class of methods is that fine-tuning adaptions can be reparameterized into optimization within low-rank subspaces (Aghajanyan et al., 2021). Low-Rank Adaptation (LoRA) (Hu et al., 2022), as a popular PEFT method from the area of LLMs, reduces the number of trainable parameters for downstream tasks by representing the weight updates with two smaller matrices (called update matrices) through low-rank decomposition (Liu et al., 2023a). For instance, FedIT Zhang et al. (2024) leverages LoRA to improve the response quality of LLMs by utilizing diverse instructions from different clients. Noticeably, LoRA and its variants have also exhibited considerable potential in addressing the challenges inherent in data heterogeneity among clients in FL. Researchers have developed Heterogeneous LoRA, which introduces a novel approach by employing low-rank approximations with heterogeneous ranks across clients to balance overfitting risks and convergence speed, significantly enhancing federated fine-tuning efficiency and efficacy (Cho et al., 2023). Similarly, the SLoRA method tackles the challenges posed by high data heterogeneity in federated environments by employing a data-driven initialization technique that effectively bridges the performance gap between traditional fine-tuning and parameter-efficient methods (Babakniya et al., 2023). The application of LoRA in privacy-preserving federated settings has also been refined through Federated Freeze A LoRA (FFA-LoRA), which optimizes the stability and efficiency by adjusting the update mechanisms for low-rank matrices (Sun et al., 2024).FedRA introduces a random allocation strategy that leverages heterogeneous client capabilities to optimize federated tuning, highlighting an approach that can dynamically adapt to varying client resources without requiring each to support the full model (Su et al., 2023). The pFedLoRA framework emerges as a solution to model-heterogeneous personalized federated learning by using homogeneous small adapters for efficient knowledge exchange across diverse federated clients, proving to significantly outperform existing methods in terms of computational and communication overheads (Yi et al., 2024). Moreover, the DP-LoRA algorithm has been tailored for differentially private federated learning, enabling secure, efficient large language model fine-tuning across sensitive domains by incorporating a Gaussian noise mechanism for privacy preservation (Liu et al., 2023b). In scenarios with severe resource constraints, Low-Parameter Federated Learning (LP-FL) combines few-shot prompt learning and LoRA techniques to mitigate the high costs associated with large language models, demonstrating robust performance even in limited data environments (Jiang et al., 2023). The automated FedPipe system has also been developed to enhance the parameter-efficient fine-tuning of large language models, employing low-rank adapters and a novel parameter quantization strategy to optimize both training efficiency and memory usage (Fang et al., 2024). Lastly, FedMS introduces a novel two-stage federated learning algorithm that integrates a mixture of sparsely activated foundation models to cater to personalized needs, employing a unique activation strategy to manage computational demands effectively (Wu et al., 2023). Heroes presents a lightweight federated learning framework employing a novel neural composition and adaptive local update mechanism, tailored for heterogeneous edge networks. This method significantly reduces traffic consumption and enhances the speed of federated learning by adaptively configuring neural components and update frequencies according to the capabilities and resources of participating clients (Yan et al., 2023). Meanwhile, efforts to facilitate large-vocabulary neural language model training in resource-constrained environments incorporate Differential Privacy and Partial Embedding Updates. This approach, combined with Low-Rank Adaptation and Noise Contrastive Estimation, allows for effective language model training on compute-constrained devices while ensuring privacy and reducing memory demands (Xu et al., 2023).

Rank-Adaptive Low-Rank Adaption for FFT-FM. This category of algorithms aim to dynamically allocate the rank among low-rank parameter matrices based on their importance score. DyLoRA Valipour et al. (2023) addresses these issues by introducing dynamic, search-free rank adjustment during training, allowing for flexible adaptation across a range of ranks with minimal retraining and significantly accelerates training times across various tasks without substantial sacrifices in performance. QDyLoRA Rajabzadeh et al. (2024) evolves this concept into quantized settings, facilitating dynamic rank adjustments within a single training session on constrained hardware, thus maintaining competitive performance while optimizing hardware utilization efficiently. DP-DyLoRA Xu et al. (2024) integrates dynamic low-rank adaptation with differential privacy under federated learning settings to enhance privacy while mitigating typical performance degradation associated with such measures, making it feasible to deploy large models in privacy-sensitive environments. Structure-Aware Low-Rank Adaptation (SaLoRA) Hu et al. (2023) fine-tunes LLMs

by adapting the rank of updates based on the inherent structural properties of the model's layers, optimizing the allocation of trainable parameters to reflect varying importance across different model components. Sparse Low-rank Adaptation (SoRA) Ding et al. (2023) introduces an innovative method to dynamically adjust the intrinsic rank during the adaptation process using a gating mechanism that optimizes parameter sparsity, effectively balancing the trade-off between parameter efficiency and computational overhead. Hyperparameter Optimization for Large Language Model Instruction-Tuning Tribes et al. (2023)challenges optimizing LoRA's parameters through advanced blackbox optimization techniques to enhance the model's alignment with human-like processing abilities. ALoRA Liu et al. (2024c) pushes boundaries by dynamically allocating ranks during the fine-tuning process based on evaluated importance of different model components, thus allowing for more targeted and efficient adaptation tailored to specific downstream tasks. Lastly, IncreLoRA Zhang et al. (2023a) proposes an incremental parameter allocation method that adaptively adjusts ranks based on real-time assessments of module importance during training, showing great potential particularly in resource-constrained environments by optimizing parameter efficiency and model performance. Several pioneer rank-adaptive LoRA algorithms for FFT-FM iteratively aggregate local full parameter metrics into a global one and perform the SVD on the latter to find the optimal rank (Chai et al., 2022; Wu et al., 2021; Niu et al., 2023).

To our best knowledge, the common characteristics of the above rank-adaptive low-rank adaption methods is to (1) either fail to transplanting from the centralized setting to the federated environment (SVD-based rank-adaptive LoRA methods Zhang et al. (2023b); Ding et al. (2023); Zhang et al. (2023a)) due to the client-drift issue (Sun et al., 2024). (2) or raise extremely expensive cost in centralize learning and federated learning (rank sampling-based algorithms Valipour et al. (2023); Rajabzadeh et al. (2024); Xu et al. (2024) due to multi-time model fine-tuning at different ranks and federated rank-adaptive LoRA algorithms Chai et al. (2022); Wu et al. (2021); Niu et al. (2023) with iterative SVD on large-scale full parameter metrics). This work is the first to offer a rank-adaptive low-rank adaptation solution for FFT-FM with Riemannian manifold theory, by eliminating the client-drift issue and the multi-time model FT, and reducing the SVD of large-scale full parameter matrix to the SVD of a low-rank matrix with low dimensions, for further enhancing both effectiveness and efficiency of FFT-FM.

7.2 Approximation Matrix Upper Bound

Lemma 1 (Orthogonal Matrix and Frobenius Norm Preservation)**.** *Let $U \in \mathbb{R}^{n\times n}$ be an orthogonal matrix, i.e., $U^\top U = I$. For any $A \in \mathbb{R}^{n\times m}$, the Frobenius norm $\|A\|_F$ satisfies:*

$$\|U^\top A\|_F = \|A\|_F. \tag{25}$$

Please refer to Golub & Van Loan (2013) for the detailed proof.

Lemma 2 (Cauchy-Schwarz Inequality for Frobenius Norm)**.** *For any $A, B \in \mathbb{R}^{n\times m}$, the Frobenius norms $\|A\|_F$ and $\|B\|_F$ satisfy:*

$$|tr(A^\top B)| \leq \|A\|_F \|B\|_F. \tag{26}$$

where $tr(\cdot)$ is the trace of a matrix.

Please refer to Horn & Johnson (2012) for the detailed proof.

Lemma 3 (Condition Number and Off-Diagonal Error Amplification)**.** *Let $S \in \mathbb{R}^{n\times n}$ be a symmetric positive definite matrix with condition number $\kappa(S) = \lambda_{\max}(S)/\lambda_{\min}(S)$. Then the Frobenius norm of the off-diagonal part of the inverse matrix is bounded by:*

$$\|S^{-1}_{\text{off-diagonal}}\|_F \leq \kappa(S)\|S_{\text{off-diagonal}}\|_F. \tag{27}$$

where S^{-1} is the inverse of the matrix S.

Please refer to Trefethen & Bau (1997) for the detailed proof.

The following theorems provide upper bounds on the Frobenius norm error for off-diagonal elements after an orthogonal transformation.

Theorem 1. *We assume that the Frobenius norm of $\mathbf{R}^k$ is bounded by a constant H, and its eigenvalues lie within the interval $[\lambda_{R_{\min}}, \lambda_{R_{\max}}]$. Similarly, the Frobenius norm of $\mathbf{S}^k$ is bounded by a constant N, with eigenvalues in the range $[\lambda_{S_{\min}}, \lambda_{S_{\max}}]$. Additionally, the matrix ΔW has rank r. Given these conditions, the total approximation error bound in Equation 14 is derived as follows*

$$\begin{aligned}&\|\mathbf{U}^1 \times \frac{1}{K}\left(\mathbf{\Sigma}^1 + \sum_{k=2}^{K}\tilde{\mathbf{\Sigma}}^k\right) \times \mathbf{V}^1 - \frac{1}{K}\left(\sum_{k=1}^{K}\mathbf{U}^k\mathbf{\Sigma}^k\mathbf{V}^k\right)\|_F^2 \\ &= \sum_{k=2}^{K}\left(2r(1-H-N) + (1+(\frac{\lambda_{R_{\max}}}{\lambda_{R_{\min}}})^2)H^2 + (1+(\frac{\lambda_{S_{\max}}}{\lambda_{S_{\min}}})^2)N^2\right)\end{aligned} \tag{28}$$

Proof. From Equation 14, we observe that the total approximation error consists of three components: the approximation error from the matrices $\mathbf{U^kR^k}$, the approximation error from $\mathbf{V^kS^k}$, and the approximation error due to the diagonal optimal solution of the $\tilde{\mathbf{\Sigma}}^k$ matrix. We calculate the error between the two components by computing the square of the Frobenius norm between them. These components can be expressed as follows:

$$\begin{aligned}&\|\mathbf{U}^1 \times \frac{1}{K}\left(\mathbf{\Sigma}^1 + \sum_{k=2}^{K}\tilde{\mathbf{\Sigma}}^k\right) \times \mathbf{V}^1 - \frac{1}{K}\left(\sum_{k=1}^{K}\mathbf{U}^k\mathbf{\Sigma}^k\mathbf{V}^k\right)\| \\ &= \sum_{k=2}^{K}(\|\mathbf{U}^1 - \mathbf{U}^k\mathbf{R}^k\|_F^2 + \|\mathbf{V}^1 - \mathbf{S}^k\mathbf{V}^k\|_F^2 \\ &+ \|(\mathbf{R_{ii}}^k)^{-1}\mathbf{\Sigma_{ii}}^k(\mathbf{S_{ii}}^k)^{-1} - (\mathbf{R}^k)^{-1}\mathbf{\Sigma}^k(\mathbf{S}^k)^{-1}\|_F^2)\end{aligned} \tag{29}$$

The approximation error analysis for both $\mathbf{U^kR^k}$ and $\mathbf{V^kS^k}$ is similar. Therefore, we focus on $\mathbf{U^kR^k}$ as an example. By expanding the Frobenius norm of the difference, we obtain the following expression:

$$\|\mathbf{U}^1 - \mathbf{U}^k\mathbf{R}^k\|_F^2 = \text{tr}\left((\mathbf{U}^1)^T\mathbf{U}^1\right) - 2\text{tr}\left((\mathbf{U}^1)^T\mathbf{U}^k\mathbf{R}^k\right) + \text{tr}\left((\mathbf{R}^k)^T(\mathbf{U}^k)^T\mathbf{U}^k\mathbf{R}^k\right) \tag{30}$$

For the first term, since $\mathbf{U}^1$ is an orthogonal matrix, we have $(\mathbf{U}^1)^T\mathbf{U}^1 = I$, and thus $\text{tr}(I) = r$. Similarly, since U^k is an orthogonal matrix, the third term can be simplified as $tr(\mathbf{R}^k)^T\mathbf{R}^k)) = \|\mathbf{R}^k\|_F^2 \leq H^2$ For the second term, as shown in Equation (15), we have $-2\text{tr}(\mathbf{P}^k\mathbf{\Lambda}^k(\mathbf{Q}^k)^T\mathbf{R}^k)$. Using the Cauchy-Schwarz inequality, we can further bound this term as follows:

$$\text{tr}(\mathbf{\Lambda}^k(\mathbf{Q}^k)^T\mathbf{R}^k\mathbf{P}^k) \leq \|\mathbf{\Lambda}^k\|_F \cdot \|(\mathbf{Q}^k)^T\mathbf{R}^k\mathbf{P}^k\|_F \leq rH \tag{31}$$

Then we get approximation error between $\mathbf{U^kR^k}$ and $\mathbf{U}^1$

$$\|\mathbf{U}^1 - \mathbf{U}^k\mathbf{R}^k\|_F^2 = r - 2rH + H^2 \tag{32}$$

Similarly, the approximation error between $\mathbf{V^kS^k}$ and $\mathbf{V}^1$ be bounded as follows

$$\|\mathbf{V}^1 - \mathbf{S}^k\mathbf{V}^k\|_F^2 = r - 2rN + N^2 \tag{33}$$

The error between the optimal diagonal solution and the original complete matrix primarily arises from the off-diagonal elements. Since $\mathbf{\Sigma}^k$ is a diagonal matrix, the off-diagonal error is determined solely by the off-diagonal components of $\mathbf{R}^k$ and $\mathbf{S}^k$. Then we have

$$\begin{aligned}&\|(\mathbf{R_{ii}}^k)^{-1}\mathbf{\Sigma_{ii}}^k(\mathbf{S_{ii}}^k)^{-1} - (\mathbf{R}^k)^{-1}\mathbf{\Sigma}^k(\mathbf{S}^k)^{-1}\|_F^2 \\ &= \sum_{i\neq j}((\mathbf{R}^k)_{ij}^{-1}(\mathbf{S}^k)_{ji}^{-1})^2 \leq \|(\mathbf{R}^k)_{ij}^{-1}\|_F^2\|(\mathbf{S}^k)_{ji}^{-1}\|_F^2\end{aligned} \tag{34}$$

Based on the condition number of the matrix, we know that the norm of the off-diagonal part of the inverse matrix can be amplified by at most κ times the norm of the off-diagonal part of the original matrix. Since $\mathbf{R}^k$ and $\mathbf{S}^k$ are symmetric positive definite matrices, the condition number is determined by the ratio of the largest to smallest eigenvalues, then we get

$$\|(\mathbf{R_{ii}}^k)^{-1}\mathbf{\Sigma_{ii}}^k(\mathbf{S_{ii}}^k)^{-1} - (\mathbf{R}^k)^{-1}\mathbf{\Sigma}^k(\mathbf{S}^k)^{-1}\|_F^2 \leq (\frac{\lambda_{R_{\max}}}{\lambda_{R_{\min}}})^2H^2 + (\frac{\lambda_{S_{\max}}}{\lambda_{S_{\min}}})^2N^2 \tag{35}$$

□

7.3 RIEMANN GRADIENT AND RETRACTION

Lemma 4 (Partitioning and Submatrix Inversion). *Let $W \in \mathbb{R}^{m\times n}$ with rank r. If $w_{11} \in \mathbb{R}^{r\times r}$ is an invertible submatrix of W, then W can be partitioned as:*

$$W = \begin{bmatrix} w_{11} & w_{12} \\ w_{21} & w_{22} \end{bmatrix} \tag{36}$$

where w_{12}, w_{21}, and w_{22} are submatrices. The submatrix $X \in \mathbb{R}^{r\times(n-r)}$ satisfies:

$$X = w_{11}^{-1} w_{12}, \quad w_{22} = w_{21} X = w_{21} w_{11}^{-1} w_{12} \tag{37}$$

Please refer to Boumal (2023) for detailed proof.

Lemma 5 (Differentiability of Local Defining Function). *Let $h : \mathbb{R}^{(m-r)\times(n-r)} \to \mathbb{R}^{m\times n}$ be defined as:*

$$h(Y) = Y_{22} - Y_{21} Y_{11}^{-1} Y_{12} \tag{38}$$

where Y_{ij} are submatrices of Y. Then h is smooth and has an inverse mapping h^{-1} such that $ker(Dh(Y))$ is a linear subspace that spans $\mathbb{R}^{m\times n}$.

Please refer to Boumal (2023) for detailed proof.

Lemma 6 (Tangent Space on the Stiefel Manifold). *Let $\mathbf{U}^k \in \mathbb{R}^{m\times r}$ and $\mathbf{V}^k \in \mathbb{R}^{n\times r}$ lie on the Stiefel manifolds $St(m,r)$ and $St(n,r)$, respectively. For any $\Omega \in Skew(r)$ and $B \in \mathbb{R}^{(m-n)\times r}$, the tangent space velocities $\mathbf{U}^{k\prime}(0)$ and $\mathbf{V}^{k\prime}(0)$ are given by:*

$$\mathbf{U}^{k\prime}(0) = \mathbf{U}^k \Omega + \mathbf{U}_\perp^k B, \quad \mathbf{V}^{k\prime}(0) = \mathbf{V}^k \Omega' + \mathbf{V}_\perp^k C \tag{39}$$

where $\mathbf{U}_\perp^k$ and $\mathbf{V}_\perp^k$ are orthogonal complements.

Please refer to Absil et al. (2008) for detailed proof.

Lemma 7 (Orthogonal Projection onto Tangent Space). *Let $\Delta W^k = U^k \Sigma^k (V^k)^\top$ represent a point on M_r. The orthogonal projection of a matrix $Z^k \in \mathbb{R}^{m\times n}$ onto the tangent space T_{M_r} at ΔW^k is given by:*

$$Proj_{\Delta W^k}(Z^k) = U^k G (V^k)^\top + U_\perp^k (V_\perp^k)^\top + U^k (V_\perp^k)^\top \tag{40}$$

where G is a general matrix related to the variation of U^k and V^k along their tangent directions, $U_\perp^k$ and $V_\perp^k$ denote the components of Z^k orthogonal to U^k and V^k, respectively.

Please refer to Absil et al. (2008) for detailed proof.

Lemma 8 (Retraction for Fixed-Rank Matrices). *Let $H \in \mathbb{R}^{m\times n}$ represent the perturbation in the ambient space. The retraction function f maps the tangent space T_M to the manifold M by minimizing the Frobenius norm distance:*

$$f(H) = \arg\min_{\Delta W \in M} \|\Delta W^k + H - \Delta W\|_F^2 \tag{41}$$

Under the constraint of fixed rank r, the retraction is given by the truncated singular value decomposition of $\Delta W^k + H$.

Please refer to Golub & Van Loan (2013) for detailed proof.

We define the set of weight parameter matrices of size $m \times n$ with rank r as:

$$M_r = \{\Delta \mathbf{W}^k \in \mathbb{R}^{m\times n} : \text{rank}(\Delta \mathbf{W}^k) = r\} \tag{42}$$

which is an embedded submanifold of $\mathbb{R}^{m\times n}$. For any $\Delta \mathbf{W}^k \in \mathbb{R}_r^{m\times n}$, we define a continuous, smooth, local defining function. Given that the rank of $\Delta \mathbf{W}^k$ is r, it contains an invertible submatrix of size $r \times r$. Consequently, $\Delta \mathbf{W}^k$ can be partitioned as:

$$\Delta \mathbf{W}^k = \begin{bmatrix} \mathbb{R}^{r\times r} & \mathbb{R}^{r\times(n-r)} \\ \mathbb{R}^{(m-r)\times r} & \mathbb{R}^{(m-r)\times(n-r)} \end{bmatrix} \tag{43}$$

We assume that $w_{11} \in \mathbb{R}^{r\times r}$ is an invertible matrix, $w_{12} \in \mathbb{R}^{r\times(n-r)}$, $w_{21} \in \mathbb{R}^{(m-r)\times r}$, $w_{22} \in \mathbb{R}^{(m-r)\times(n-r)}$ Given a matrix $w \in \mathbb{R}^{m\times n}$ with rank r, its last $n-r$ columns are linear combinations of the first r columns. This implies the existence of a matrix $X \in \mathbb{R}^{r\times(n-r)}$ such that:

$$\begin{bmatrix} w_{12} \\ w_{22} \end{bmatrix} = \begin{bmatrix} w_{11} \\ w_{21} \end{bmatrix} X \tag{44}$$

Here, w_{11} is an invertible $r \times r$ matrix, and w_{12}, w_{21}, w_{22} are submatrices of X partitioned accordingly.

From this relationship, it follows that:

$$X = w_{11}^{-1} w_{12} \tag{45}$$

and consequently,

$$w_{22} = w_{21} X = w_{21} w_{11}^{-1} w_{12} \tag{46}$$

This decomposition shows that under the assumption of w_{11} being invertible, the described relationship between the blocks of w is both necessary and sufficient for w to maintain a rank of r. Consider U to be a subset of $\mathbb{R}^{m\times n}$ where the upper-left $r \times r$ submatrix is invertible. This subset U, being an open set in $\mathbb{R}^{m\times n}$, serves as the domain for the candidate local defining function h given by:

$$h : U \to \mathbb{R}^{(m-r)\times(n-r)}, \quad Y = \begin{bmatrix} Y_{11} & Y_{12} \\ Y_{21} & Y_{22} \end{bmatrix} \mapsto Y_{22} - Y_{21} Y_{11}^{-1} Y_{12} \tag{47}$$

This mapping h is smooth within U and has the inverse mapping $h^{-1}(0) = \mathbb{R}^{m\times n} \cap U$, indicating that the pre-image of zero under h intersects with U. Moreover, the differential of h at any matrix Y in U, for $V \in \mathbb{R}^{m\times n}$, is:

$$Dh(Y)[V] = V_{22} - V_{21} Y_{11}^{-1} Y_{12} + Y_{21} Y_{11}^{-1} V_{11} Y_{11}^{-1} Y_{12} - Y_{21} Y_{11}^{-1} V_{12} \tag{48}$$

utilizing the identity for differentiating a matrix inverse:

$$D(M \mapsto M^{-1})(M)[H] = -M^{-1} H M^{-1} \tag{49}$$

Please refer to the book Boumal (2023) for detailed proof.
The codomain of $Dh(Y)$ spans $\mathbb{R}^{(m-r)\times(n-r)}$, meaning any matrix in this space can be achieved by choosing an appropriate V. Setting V_{11}, V_{12}, V_{21} to zero simplifies $Dh(Y)[V]$ to V_{22}, showing that $Dh(Y)$ is surjective. Thus, h serves as a local defining function for the smooth submanifold around w in $\mathbb{R}^{m\times n}$. If the top-left submatrix of size $r \times r$ is non-invertible, another local defining function can be constructed similarly for different submatrix choices.
These local defining functions collectively establish that $\mathbb{R}_r^{m\times n}$ is an embedded submanifold of $\mathbb{R}^{m\times n}$, endowed with dimension:

$$\dim \mathbb{R}_r^{m\times n} = \dim \mathbb{R}^{m\times n} - \dim \mathbb{R}^{(m-r)\times(n-r)} = mn - (m-r)(n-r) = r(m+n-r) \tag{50}$$

Definition 1 (Tangent Spaces and Embedded Submanifolds)**.** *Boumal (2023) Let M be a subset of $\mathcal{E}$ and $w \in M$. The tangent space at w, denoted $T_w M$, consists of velocity vectors at w of all smooth curves $c : I \to M$ that pass through w at $t = 0$, where I is an open interval containing $t = 0$. Formally,*

$$T_w M = \{c'(0) \mid c : I \to M \text{ is smooth and } c(0) = w\} \tag{51}$$

For an embedded submanifold M of $\mathcal{E}$, $T_w M$ coincides with the subspace defined by $\ker Dh(w)$ *if M is not open within $\mathcal{E}$, otherwise $T_w M = \mathcal{E}$. This structure highlights that $T_w M$ not only captures the linear approximation to M at w but also conforms to the embedding properties of submanifolds within $\mathcal{E}$.*

We recognize that each tangent space possesses a dimension as delineated in equation 50, it is sufficient to exhibit a linear subspace of that dimension which is included in the tangent space. Returning to the 19 of the tangent space , we undertake the explicit construction of smooth curves on $\mathbb{R}_r^{m\times n}$. We have $\Delta\mathbf{W}^k = \mathbf{U}^k \mathbf{\Sigma}^k (\mathbf{V}^k)^T$, define $U(t)$ as a smooth trajectory within $St(m, r)$ initiating at $U(0) = \mathbf{U}^k$, and similarly for $V(t)$ within $St(n, r)$ starting from $V(0) = \mathbf{V}^k$. Additionally, let $S(t)$ describe a trajectory within the invertible $r \times r$ matrices, forming an open submanifold, starting from $S(0) = \mathbf{\Sigma}^k$. Consequently, the curve $c(t) = U(t)S(t)V(t)^T$ forms a smooth trajectory in $\mathbb{R}_r^{m\times n}$ with $c(0) = \Delta\mathbf{W}^k$, where its initial velocity $c'(0)$ represents a tangent vector at w:

$$c'(0) = U'(0)\mathbf{\Sigma}^k(\mathbf{V}^k)^T + \mathbf{U}^k S'(0)(\mathbf{V}^k)^T + \mathbf{U}^k \mathbf{\Sigma}^k V'(0)^T \in T_w \mathbb{R}_r^{m\times n} \tag{52}$$

Given that $U(t)$ traverses smoothly through $\mathbf{U}^k$ on $St(m, r)$, the velocity $U'(0)$ lies within its tangent space at $\mathbf{U}^k$. For any vector within $T_U St(m, r)$, a corresponding smooth curve $U(t)$ can exhibit such velocity at $t = 0$. Referencing the specified relationship for the tangent space at $\Delta\mathbf{W}^k$ in the

Stiefel manifold Absil & Malick (2012) $T_{\Delta \mathbf{W}^k} St(n,p) = \{\Delta \mathbf{W}^k \Omega + \Delta \mathbf{W}^k_\perp B : \Omega \in \text{Skew}(p), B \in \mathbb{R}^{(n-p)\times p}\}$, it implies for any $\Omega \in \text{Skew}(p)$ and $B \in \mathbb{R}^{(n-p)\times p}$ that:

$$U'(0) = \mathbf{U}^k \Omega + \mathbf{U}^k_\perp B \tag{53}$$

where $\mathbf{U}^k_\perp$ ensures orthogonality with $\mathbf{U}^k$. Likewise, for any $\Omega' \in \text{Skew}(r)$ and $C \in \mathbb{R}^{(n-r)\times r}$, the expression for $V'(0)$ becomes:

$$V'(0) = \mathbf{V}^k \Omega' + \mathbf{V}^k_\perp C \tag{54}$$

with $\mathbf{V}^k_\perp$ maintaining orthogonality with $\mathbf{V}^k$. As $S(t)$ evolves smoothly within its manifold, the derivative $S'(0)$ can adopt any matrix configuration within $\mathbb{R}^{r\times r}$. with $\mathbf{V}^k_\perp$ such that $\mathbf{V}^k \mathbf{V}^k_\perp$ is orthogonal. Since $S(t)$ is a smooth curve on an open submanifold of $\mathbb{R}^{r\times r}$, we can choose $S'(0)$ to be any matrix $A \in \mathbb{R}^{r\times r}$. Finally, incorporating the relationships with $\mathbf{U}^k_\perp$ and $\mathbf{V}^k_\perp$, we observe that $U'(0)$ can be represented as $\mathbf{U}^k \Omega + \mathbf{U}^k_\perp B$ and $V'(0)$ as $\mathbf{V}^k \Omega' + \mathbf{V}^k_\perp C$, with $\Omega, \Omega' \in \text{Skew}(r)$ and $B, C \in \mathbb{R}^{(m-r)\times r}$. These adjustments ensure the continuation of $U(t)$ and $V(t)$ as smooth curves, affirming the orthogonality of $\mathbf{U}^k$ and $\mathbf{V}^k$ to their respective complements. Overall, this analysis demonstrates that the following velocities are within the tangent space of $\mathbb{R}^{m\times n}_r$ at w:

$$\begin{aligned} c'(0) &= (\mathbf{U}^k \Omega_2 + \mathbf{U}^k_\perp B)\mathbf{\Sigma}^k (\mathbf{V}^k)^T + \mathbf{U}^k \mathbf{\Sigma}^k ((\mathbf{V}^k)\Omega_2' + \mathbf{V}^k_\perp C)^T \\ &= \mathbf{U}^k (\Omega_2 + A - \mathbf{\Sigma}^k \Omega_2')(\mathbf{V}^k)^T + \mathbf{U}^k_\perp B (\mathbf{V}^k)^T + \mathbf{U}^k (\mathbf{V}^k_\perp C)^T \end{aligned} \tag{55}$$

with $A = \mathbf{\Sigma}^k \Omega_2 - \Omega_2 \mathbf{\Sigma}^k$, where $\Omega_2, \Omega_2' \in \text{Skew}(r)$, $B \in \mathbb{R}^{(m-r)\times r}$, and $C \in \mathbb{R}^{(n-r)\times r}$ are arbitrary matrices. Since $\mathbf{\Sigma}^k$ is invertible, it follows that any matrix of the form

$$\mathbf{U}^k M (\mathbf{V}^k)^T + \mathbf{U}^k_p (\mathbf{V}^k)^T + \mathbf{U}^k (\mathbf{V}^k_p)^T \tag{56}$$

with $M \in \mathbb{R}^{r\times r}$, $\mathbf{U}^k_p \in \mathbb{R}^{m\times r}$, $\mathbf{V}^k_p \in \mathbb{R}^{n\times r}$ such that $(\mathbf{U}^k)^T \mathbf{U}^k_p = (\mathbf{V}^k)^T \mathbf{V}^k_p = 0$ is tangent at $\Delta \mathbf{W}^k$. The conditions on $\mathbf{U}^k_p$ and $\mathbf{V}^k_p$ impose $2r^2$ linear constraints, thereby defining a linear subspace of $T_w \mathbb{R}^{m\times n}_r$ with dimension

$$r^2 + mr + nr - 2r^2 = r(m + n - r) \tag{57}$$

Then the singular value decomposition $(\mathbf{U}^k, \mathbf{\Sigma}^k, \mathbf{V}^k)$ of the matrix $\Delta \mathbf{W}^k$, the tangent space T_{M_r} at the point $\Delta \mathbf{W}^k$ on the manifold M_r can be represented as:

$$\begin{aligned} T_M &= \left\{ (\mathbf{U}^k \ \mathbf{U}^k_\perp) \begin{bmatrix} \mathbb{R}^{r\times r} & \mathbb{R}^{r\times(n-r)} \\ \mathbb{R}^{(m-r)\times r} & 0^{(m-r)\times(n-r)} \end{bmatrix} (\mathbf{V}^k \ \mathbf{V}^k_\perp)^T \right\} \\ &= \{ \mathbf{U}^k \mathbf{G} (\mathbf{V}^k)^T + \mathbf{U}^k_p (\mathbf{V}^k)^T + \mathbf{U}^k (\mathbf{V}^k_p)^T \\ &\quad : \mathbf{G} \in \mathbb{R}^{r\times r}, \mathbf{U}^k_p \in \mathbb{R}^{m\times r}, (\mathbf{U}^k_p)^T \mathbf{U}^k = 0, \mathbf{V}^k_p \in \mathbb{R}^{n\times r}, (\mathbf{V}^k_p)^T \mathbf{V}^k = 0 \quad \} \end{aligned} \tag{58}$$

With $\mathbb{R}^{m\times n}_r$ still endowed with the standard inner product, we now consider the orthogonal projectors of $\mathbb{R}^{m\times n}_r$. From equation 19, the normal space at $\Delta \mathbf{W}^k = \mathbf{U}^k \mathbf{\Sigma}^k (\mathbf{V}^k)^T$ is defined as:

$$\mathbf{N}^k = \{ \mathbf{U}^k \mathbf{\Sigma}^k (\mathbf{V}^k)^T : \Delta \mathbf{W}^k \in \mathbb{R}^{(m-r)\times(n-r)} \} \tag{59}$$

The orthogonal projection of a matrix $\mathbf{Z}^k \in \mathbb{R}^{m\times n}$ onto the tangent space $T_{\Delta \mathbf{W}^k} \mathbb{R}^{m\times n}_r$ can be expressed as:

$$\mathbf{Z}^k - \text{Proj}_{\Delta \mathbf{W}^k}(\mathbf{Z}^k) = \mathbf{U}^k \Delta \mathbf{W}^k_\perp (\mathbf{V}^k)^T \tag{60}$$

for some orthogonal complement $\Delta \mathbf{W}^k_\perp$, and subsequently,

$$\text{Proj}_{\Delta \mathbf{W}^k}(\mathbf{Z}^k) = \mathbf{U}^k \mathbf{G} (\mathbf{V}^k)^T + \mathbf{U}^k_\perp (\mathbf{V}^k_p)^T + \mathbf{U}^k (\mathbf{V}^k_p)^T \tag{61}$$

for matrices $\mathbf{G}$, $\mathbf{U}^k_p$, $\mathbf{V}^k_p$ such that $(\mathbf{U}^k)^T \mathbf{U}^k_p = (\mathbf{V}^k)^T \mathbf{V}^k_p = 0$. These matrices satisfy:

$$\mathbf{Z}^k = \mathbf{U}^k \mathbf{G} (\mathbf{V}^k)^T + \mathbf{U}^k_p (\mathbf{V}^k)^T + \mathbf{U}^k (\mathbf{V}^k_p)^T + \mathbf{U}^k_\perp \Delta \mathbf{W}^k_\perp (\mathbf{V}^k)^T_\perp \tag{62}$$

Define the projectors $P^k_U = \mathbf{U}^k (\mathbf{U}^k)^T$, $P^k_V = \mathbf{V}^k (\mathbf{V}^k)^T$, and their complements $P^k_{U_\perp} = I_m - P^k_U$, $P^k_{V_\perp} = I_n - P^k_V$. Then, we derive:

$$P^k_U P^k_V \mathbf{Z}^k = \mathbf{U}^k \mathbf{G} (\mathbf{V}^k)^T, \quad P^k_{U_\perp} P^k_V \mathbf{Z}^k = U^k_p (\mathbf{V}^k)^T, \quad \text{and} \quad P^k_U P^k_{V_\perp} \mathbf{Z}^k = \mathbf{U}^k (\mathbf{V}^k_p)^T \tag{63}$$

This leads to a reformulated projection:

$$\text{Proj}_{\Delta \mathbf{W}^k}(\mathbf{Z}^k) = P_U^k \mathbf{Z}^k P_V^k + P_{U_\perp}^k \mathbf{Z}^k P_V^k + P_U \mathbf{Z}^k P_{V_\perp}^k \tag{64}$$

yielding the complete orthogonal projection:

$$\text{Proj}_w(\mathbf{Z}^k) = \mathbf{U}^k((\mathbf{U}^k)^T \mathbf{Z}^k \mathbf{V}^k)(\mathbf{V}^k)^T + (I_m - \mathbf{U}^k(\mathbf{U}^k)^T)\mathbf{Z}^k \mathbf{V}^k(\mathbf{V}^k)^T + \mathbf{U}^k(\mathbf{U}^k)^T \mathbf{Z}^k(I_n - \mathbf{V}^k(\mathbf{V}^k)^T) \tag{65}$$

Here, $M = (\mathbf{U}^k)^T \mathbf{Z}^k \mathbf{V}^k$, $U_p^k = \mathbf{Z}^k \mathbf{V}^k - \mathbf{U}^k M$, and $V_p^k = (\mathbf{Z}^k)^T \mathbf{U}^k - \mathbf{V}^k M^T$, indicating that these components form a tangent vector at w represented by the variation $\mathbf{Z}^k$.

Therefore, the gradient of $(\mathbf{U}^k, \mathbf{\Sigma}^k, \mathbf{V}^k)$ in Riemannian space can be expressed as:

$$\begin{aligned} &\Gamma_{\mathbf{U}^k} L^k = (\mathbf{I}_m - \mathbf{U}^k(\mathbf{U}^k)^T)\nabla_{\mathbf{U}^k} L^k, \qquad \Gamma_{\mathbf{V}^k} L^k = (\mathbf{I}_n - \mathbf{V}^k(\mathbf{V}^k)^T)\nabla_{\mathbf{V}^k} L^k, \\ &\Gamma_{\mathbf{\Sigma}^k} L^k = ((\mathbf{U}^k)^T \nabla_{\mathbf{U}^k} L^k - \nabla_U (L^k)^T \mathbf{U}^k)\mathbf{\Sigma}^k + \mathbf{\Sigma}^k(\mathbf{V}^k \nabla_{\mathbf{V}^k}(L^k)^T - \nabla_{\mathbf{V}^k} L^k(\mathbf{V}^k)^T) + \nabla_{\mathbf{\Sigma}^k} L^k \end{aligned} \tag{66}$$

According to the theorem2, we can ensure that the rank remains unchanged during the local training process.

Theorem 2. *Let $\Delta \mathbf{W}^k$ be a point on a Riemannian manifold M consisting of all matrices with a fixed rank r in $\mathbb{R}^{m \times n}$. Suppose $\nabla L^k(\Delta \mathbf{W}^k)$ is the Euclidean gradient of the loss function L^k at $\Delta \mathbf{W}^k$, and $\Gamma_{\mathbf{U}^k} L^k$, $\Gamma_{\mathbf{\Sigma}^k} L^k$, and $\Gamma_{\mathbf{V}^k} L^k$ represent the components of the Riemannian gradient at $\Delta \mathbf{W}^k$. The RGD optimization with a learning rate η_t at round t ensures that the local update*

$$\left((\mathbf{U}^k)^{(t+1)}, (\mathbf{\Sigma}^k)^{(t+1)}, (\mathbf{V}^k)^{(t+1)}\right) = f\left(-\eta_t\left(\left(\Gamma_{\mathbf{U}^k} L^k\right)^{(t)}, \left(\Gamma_{\mathbf{\Sigma}^k} L^k\right)^{(t)}, \left(\Gamma_{\mathbf{V}^k} L^k\right)^{(t)}\right)\right) \tag{67}$$

preserves the rank r of $\Delta \mathbf{W}^k$, maintaining the structure within the manifold M, where f is a retraction $f : T_M \to M$ mapping the tangent space at $\Delta \mathbf{W}^k$ to the manifold.

Proof. To construct a retraction f for updating within a Riemannian manifold, we utilize metric projection. This method involves making a step in the ambient space, denoted by H, and then projecting back to the manifold to minimize the distance in the Frobenius norm, ensuring that the updated matrix retains the same rank as the original. The retraction function is formulated as:

$$f(H) = \arg\min_{\Delta \mathbf{W}^k \in \mathbb{R}^r_{m \times n}} \|\Delta \mathbf{W}^k + H - \Delta \mathbf{W}^k\|_F^2 \tag{68}$$

According to the Eckart-Young-Mirsky theorem Golub et al. (1987), the optimal solution to this optimization problem, under the constraint of rank r, is achieved by the truncated singular value decomposition of $\Delta \mathbf{W}^k + H$. According to quation 19, the $\Delta \mathbf{W}^k + H$ can be represented as:

$$\begin{aligned} \Delta \mathbf{W}^k + H &= (\mathbf{U}^k)^{(t)}((\mathbf{\Sigma}^k)^{(t)} + (-\eta_t \left(\Gamma_{\mathbf{\Sigma}^k} L^k\right)^{(t)}))((\mathbf{V}^k)^{(t)})^T + U_p((\mathbf{V}^k)^{(t)})^T + (\mathbf{U}^k)^{(t)} V_p^T \\ &= \begin{bmatrix}(\mathbf{U}^k)^{(t)} & U_p\end{bmatrix} \begin{bmatrix}((\mathbf{\Sigma}^k)^{(t)} + (-\eta_t \left(\Gamma_{\mathbf{\Sigma}^k} L^k\right)^{(t)})) & I_r \\ I_r & 0\end{bmatrix} \begin{bmatrix}(\mathbf{V}^k)^{(t)} & V_p\end{bmatrix}^T. \end{aligned} \tag{69}$$

Where I_r is the r-dimensional identity matrix. QR factorizations of the augmented matrices $(\mathbf{U}^k)^{(t)}$ and U_p, as well as $(\mathbf{V}^k)^{(t)}$ and V_p, are given by:

$$Q_U R_U = [(\mathbf{U}^k)^{(t)}\ U_p], \quad Q_V R_V = [(\mathbf{V}^k)^{(t)}\ V_p] \tag{70}$$

Here, Q_U and Q_V represent the orthogonal matrices resulting from the QR factorizations of the left and right matrices, ensuring that columns are orthonormal. R_U and R_V are upper triangular matrices which correspond to the R components in the QR factorization process.

Employing the QR factorizations, the perturbed matrix $W + H$ is expressed as:

$$\Delta \mathbf{W}^k + H = Q_U R_U \begin{bmatrix}((\mathbf{\Sigma}^k)^{(t)} + (-\eta_t \left(\Gamma_{\mathbf{\Sigma}^k} L^k\right)^{(t)})) & I_r \\ I_r & 0\end{bmatrix} R_V^T Q_V^T. \tag{71}$$

By performing singular value decomposition on the middle part, we obtain $\tilde{U}\tilde{\Sigma}\tilde{V}^T$, where $\tilde{U}$, $\tilde{V}$, and $\tilde{\Sigma}$ represent the orthogonal matrices and diagonal matrix of singular values, respectively.

The retraction $f(H)$ of the perturbation H at the point $\Delta\mathbf{W}^k$ on the manifold is given by:

$$f(H) = (Q_U\tilde{U})\tilde{\Sigma}(Q_V\tilde{V})^T \tag{72}$$

This expression concludes that the triplet $(Q_U\tilde{U}, \tilde{\Sigma}, Q_V\tilde{V})$ represents the retracted point on the rank-r manifold $\mathbb{R}_r^{m\times n}$. The final outcome of our optimization process on the manifold, representing the updated components for the next iteration, is:

$$\left((\mathbf{U}^k)^{(t+1)}, (\mathbf{\Sigma}^k)^{(t+1)}, (\mathbf{V}^k)^{(t+1)}\right) = (Q_U\tilde{U}, \tilde{\Sigma}, Q_V\tilde{V}) \tag{73}$$

□

7.4 Convergence on Riemannian manifold

Definition 2 (L-smoothness on manifolds)**.** *A function L is said to be Lipschitz smooth on a manifold $\mathcal{M}$ if there exists a constant $c \geq 0$ such that the following inequality holds:*

$$\|grad\, L(y) - P_{y\to x} grad\, L(x)\| \leq cd(x, y), \tag{74}$$

where $P_{y\to x}$ is the parallel transport operator along the geodesic connecting y and x, and $d(x, y)$ is the geodesic distance between x and y.

For a complete Riemannian manifold, the following inequality holds:

$$L(y) \leq L(x) + \langle g_x, Exp_x^{-1}(y)\rangle_x + \frac{L_g}{2}d^2(x, y), \quad \forall x, y \in \mathcal{M} \tag{75}$$

Please refer to the paper Zhang & Sra (2016) for detailed proof.

Definition 3 (Geodesic convexity)**.** *A function $L \in C^1(\mathcal{M})$ is said to be geodesically convex if for all $x, y \in \mathcal{M}$, there exists a geodesic γ such that $\gamma(0) = x$, $\gamma(1) = y$, and:*

$$f(\gamma(t)) \leq (1 - t)L(x) + tL(y), \quad \forall t \in [0, 1] \tag{76}$$

Or equivalently,

$$L(y) \geq L(x) + \langle grad\, L(x), Exp_x^{-1}(y)\rangle_x \tag{77}$$

Please refer to the paper Zhang & Sra (2016) for detailed proof.

Assumption 1. *For all client k, we assume that the function L_i is geodesically c_L-Lipschitz continuous. Therefore, the function l is also geodesically c_L-Lipschitz continuous.*

Assumption 2. *For all client k, we assume that the function L_i is geodesically c_g-smooth, which implies that the function L is geodesically c_g-smooth.*

Assumption 3. *We assume that the manifold under consideration is complete and that there exists a compact subset $\mathcal{W} \subset \mathcal{M}$ with diameter bounded by M, such that all the iterates of Algorithm 1 and the optimal points lie within $\mathcal{W}$. The sectional curvature of $\mathcal{W}$ is bounded within the interval $[\kappa_{\min}, \kappa_{\max}]$. Furthermore, we define the following key geometric constant that captures the impact of the manifold's curvature (Zhang et al., 2017)*

$$\zeta = \begin{cases} \frac{\sqrt{|\kappa_{\min}|}M}{\tanh\left(\sqrt{|\kappa_{\min}|}M\right)} & \text{if } \kappa_{\min} < 0, \\ 1 & \text{if } \kappa_{\min} \geq 0. \end{cases} \tag{78}$$

Theorem 3 (Nonconvex)**.** *Suppose that optimization problem in Eq.(18) satisfies Assumption 1 and 2. We run Algorithm 1, where the selected clients perform gradient descent with a fixed stepsize, and we set $\eta_t \leq \frac{1}{c_g}$. Then, the output of Algorithm 1 satisfies the following*

$$\min_{0\leq t\leq C} \mathbb{E}\left[\| \left(\left(\Gamma_{\mathbf{U}^k} L^k\right)^{(t)}, \left(\Gamma_{\mathbf{\Sigma}^k} L^k\right)^{(t)}, \left(\Gamma_{\mathbf{V}^k} L^k\right)^{(t)}\right) \|^2\right] \leq \frac{2c_g}{C}\left(L((\Delta\mathbf{W})^1) - L((\Delta\mathbf{W}^*))\right) \tag{79}$$

where x^* denotes the point on the manifold $\mathcal{M}$ that minimizes the function f(x)$x^* = \arg\min_{x\in\mathcal{M}} L(x)$.

Proof. According to Equation14, our aggregation method is equivalent to the aggregation of the matrix $\Delta\mathbf{W}$. However, in Euclidean space, it is challenging to accurately measure the distance between two points before and after the update. Therefore, following the approach from [12, 13], we project $\Delta\mathbf{W}$ back to the tangent space using the inverse retraction for aggregation. To measure the distance between the updated point x_{t+1} and the previous point x_t, we use the following distance formula

$$d(x_{t+1}, x_t) = \left\|\mathrm{f}_{x_t}^{-1}(x_{t+1})\right\| = \left\|\frac{1}{k}\sum_{i\in S_t}\mathrm{f}_{x_t}^{-1}(x^{(i)})\right\| \tag{80}$$

According to the update rule of formula 22 we have:

$$\begin{aligned}(\Delta\mathbf{W}^k)^{(t+1)} &= \left((\mathbf{U}^k)^{(t+1)}, (\mathbf{\Sigma}^k)^{(t+1)}, (\mathbf{V}^k)^{(t+1)}\right)\\ &= f\left(-\eta_t\left(\left(\Gamma_{\mathbf{U}^k}L^k\right)^{(t)}, \left(\Gamma_{\mathbf{\Sigma}^k}L^k\right)^{(t)}, \left(\Gamma_{\mathbf{V}^k}L^k\right)^{(t)}\right)\right)\\ f^{-1}_{(\Delta\mathbf{W}^k)^{(t)}}\left((\Delta\mathbf{W}^k)^{(t+1)}\right) &= \left(-\eta_t\left(\left(\Gamma_{\mathbf{U}^k}L^k\right)^{(t)}, \left(\Gamma_{\mathbf{\Sigma}^k}L^k\right), \left(\Gamma_{\mathbf{V}^k}L^k\right)^{(t)}\right)\right)\end{aligned} \tag{81}$$

Using Lipschitz smooth (c_g-smooth) of $\mathbf{L_i}$ based on Definition 2, we have

$$\begin{aligned}L((\Delta\mathbf{W}^k)^{(t+1)}) - L((\Delta\mathbf{W}^k)^{(t)}) &\leq \left\langle f^{-1}_{(\Delta\mathbf{W}^k)^{(t)}}\left((\Delta\mathbf{W}^k)^{(t+1)}\right), \left(\left(\Gamma_{\mathbf{U}^k}L^k\right)^{(t)}, \left(\Gamma_{\mathbf{\Sigma}^k}L^k\right), \left(\Gamma_{\mathbf{V}^k}L^k\right)^{(t)}\right)\right\rangle\\ &+ \frac{c_g}{2}d^2((\Delta\mathbf{W}^k)^{(t+1)}, (\Delta\mathbf{W}^k)^{(t)})\\ &= \left\langle \frac{1}{K}\sum_{k=1}^{K} f^{-1}_{(\Delta\mathbf{W}^k)^{(t)}}\left((\Delta\mathbf{W}^k)^{(t+1)}\right), \left(\left(\Gamma_{\mathbf{U}^k}L^k\right)^{(t)}, \left(\Gamma_{\mathbf{\Sigma}^k}L^k\right), \left(\Gamma_{\mathbf{V}^k}L^k\right)^{(t)}\right)\right\rangle\\ &+ \frac{c_g}{2}\left\|\frac{1}{k}\sum_{k=1}^{K} f^{-1}_{(\Delta\mathbf{W}^k)^{(t)}}\left((\Delta\mathbf{W}^k)^{(t+1)}\right)\right\|^2\\ &= -\eta_t\|\left(\left(\Gamma_{\mathbf{U}^k}L^k\right)^{(t)}, \left(\Gamma_{\mathbf{\Sigma}^k}L^k\right)^{(t)}, \left(\Gamma_{\mathbf{V}^k}L^k\right)^{(t)}\right)\|^2\\ &+ \frac{\eta_t^2 c_g}{2}\|\left(\left(\Gamma_{\mathbf{U}^k}L^k\right)^{(t)}, \left(\Gamma_{\mathbf{\Sigma}^k}L^k\right)^{(t)}, \left(\Gamma_{\mathbf{V}^k}L^k\right)^{(t)}\right)\|^2\end{aligned} \tag{82}$$

Then we have

$$\begin{aligned}\mathbb{E}\left[L((\Delta\mathbf{W}^k)^{(t+1)}) - L((\Delta\mathbf{W}^k)^{(t)})\right] &\leq -\eta_t\mathbb{E}\left[\|\left(\left(\Gamma_{\mathbf{U}^k}L^k\right)^{(t)}, \left(\Gamma_{\mathbf{\Sigma}^k}L^k\right)^{(t)}, \left(\Gamma_{\mathbf{V}^k}L^k\right)^{(t)}\right)\|^2\right]\\ &+ \mathbb{E}\left[\frac{\eta_t^2 c_g}{2}\|\left(\left(\Gamma_{\mathbf{U}^k}L^k\right)^{(t)}, \left(\Gamma_{\mathbf{\Sigma}^k}L^k\right)^{(t)}, \left(\Gamma_{\mathbf{V}^k}L^k\right)^{(t)}\right)\|^2\right]\end{aligned} \tag{83}$$

By taking $\eta_t \leq \frac{1}{c_g}$, then we have

$$\begin{aligned}\mathbb{E}\left[L((\Delta\mathbf{W}^k)^{(t+1)}) - L((\Delta\mathbf{W}^k)^{(t)})\right] &\leq -\frac{1}{c_g}\mathbb{E}\left[\|\left(\left(\Gamma_{\mathbf{U}^k}L^k\right)^{(t)}, \left(\Gamma_{\mathbf{\Sigma}^k}L^k\right)^{(t)}, \left(\Gamma_{\mathbf{V}^k}L^k\right)^{(t)}\right)\|^2\right]\\ &+ \mathbb{E}\left[\frac{(\frac{1}{c_g})^2 c_g}{2}\|\left(\left(\Gamma_{\mathbf{U}^k}L^k\right)^{(t)}, \left(\Gamma_{\mathbf{\Sigma}^k}L^k\right)^{(t)}, \left(\Gamma_{\mathbf{V}^k}L^k\right)^{(t)}\right)\|^2\right]\\ &= -\frac{1}{2c_g}\|\left(\left(\Gamma_{\mathbf{U}^k}L^k\right)^{(t)}, \left(\Gamma_{\mathbf{\Sigma}^k}L^k\right)^{(t)}, \left(\Gamma_{\mathbf{V}^k}L^k\right)^{(t)}\right)\|^2\end{aligned} \tag{84}$$

Summing this inequality over t from 1 to C, we have

$$\begin{aligned}\frac{1}{2c_g}\sum_{t=1}^{C}\|\left(\left(\Gamma_{\mathbf{U}^k}L^k\right)^{(t)}, \left(\Gamma_{\mathbf{\Sigma}^k}L^k\right)^{(t)}, \left(\Gamma_{\mathbf{V}^k}L^k\right)^{(t)}\right)\|^2 &\leq L((\Delta\mathbf{W})^1) - L((\Delta\mathbf{W})^R)\\ &\leq L((\Delta\mathbf{W})^1) - L((\Delta\mathbf{W}^*))\end{aligned} \tag{85}$$

□

Theorem 4 (Convex)**.** *Suppose that optimization problem in Eq.(18) satisfies Assumptions 1, 2, and 3, where the local functions L are geodesically convex in W (see Definition 3). We consider Algorithm 1, where the selected clients perform gradient descent with a fixed stepsize, and the stepsize is set such that $\eta_t \leq \frac{1}{2c_g}$. Then, the output of Algorithm 1 satisfies the following*

$$\mathbb{E}\left[L(\Delta\mathbf{W}^{(C)}) - L(\Delta\mathbf{W}^*)\right] \leq \frac{\zeta c_g d^2(\Delta\mathbf{W}, \Delta\mathbf{W}^*)}{(\zeta + C - 2)} = \frac{\zeta c_g d^2(\Delta(\mathbf{U_0}, \mathbf{\Sigma_0}, \mathbf{v_0}), \Delta(\mathbf{U}^*, \mathbf{\Sigma}^*, \mathbf{v}^*))}{(\zeta + C - 2)} \tag{86}$$

where x^* denotes the point on the manifold $\mathcal{M}$ that minimizes the function f(x)$x^* = \arg\min_{x\in\mathcal{M}} L(x)$ and ζ is defined in Assumptions 3

Proof.

Lemma 9 (Zhang & Sra (2016)[Corollary 8])**.** *For any Riemannian manifold $\mathcal{M}$ where the sectional curvature is lower bounded by $\kappa_{\min}$ and any point $x, x^{(t)} \in \mathcal{M}$, the update $x^{(t+1)} = Exp_{x^{(t)}}(-\alpha g^{(t)})$ with $g^{(t)} \in T_{x^{(t)}}\mathcal{M}$ satisfies*

$$\left\langle -g^{(t)}, Exp^{-1}_{x^{(t)}}(x)\right\rangle \leq \frac{1}{2\alpha}\left(dist^2(x, x^{(t)}) - dist^2(x, x^{(t+1)})\right) + \frac{\zeta(\kappa_{\min}, dist(x, x^{(t)}))\alpha}{2}\|g^{(t)}\|^2, \tag{87}$$

Where $Exp_{x^{(t)}}(x)$ is the exponentail map that projects a tangent vctor x onto the manifold, $Exp^{-1}_{x^{(t)}}(x)$ is the inverse exponential map that maps a point x back to the tangent space, α is the learning rate controlling the magnitude of the update, $dist(x, x^{(t+1)})$ denotes the geodesic distance between points x and $x^{(t+1)}$ on the manifold, and $\zeta(\kappa, c) = \frac{\sqrt{|\kappa|c}}{\tanh\left(\sqrt{|\kappa|c}\right)}$ is the curvature adjustment for distance.

From Lemma 9 we have

$$\begin{aligned}\left\langle \frac{1}{K}\sum_{k=1}^{K} f^{-1}_{(\Delta\mathbf{W})^t}\left((\Delta\mathbf{W}^k)\right), f^{-1}_{(\Delta\mathbf{W})^t}\left((\Delta\mathbf{W})\right)\right\rangle &\leq \frac{1}{2}\left(d^2(\Delta\mathbf{W})^t, \Delta\mathbf{W})) - d^2(\Delta\mathbf{W})^{(t+1)}, \Delta\mathbf{W}))\right) \\ &+ \frac{\zeta}{2}\left\|\frac{1}{k}\sum_{k=1}^{K} f^{-1}_{(\Delta\mathbf{W})^t}\left((\Delta\mathbf{W}^k)\right)\right\|^2\end{aligned} \tag{88}$$

According to the formula 82 we get

$$\begin{aligned}&-\eta_t\left\langle\left(\frac{1}{K}\sum_{k=1}^{K}\left(\left(\Gamma_{\mathbf{U}^k}L^k\right)^{(t)}, \left(\Gamma_{\mathbf{\Sigma}^k}L^k\right)^{(t)}, \left(\Gamma_{\mathbf{V}^k}L^k\right)^{(t)}\right)\right), f^{-1}_{(\Delta\mathbf{W})^t}\left((\Delta\mathbf{W})\right)\right\rangle \\ &\leq \frac{1}{2}\left(d^2(\Delta\mathbf{W})^t, \Delta\mathbf{W})) - d^2(\Delta\mathbf{W})^{(t+1)}, \Delta\mathbf{W}))\right) + \frac{\zeta}{2}\left\|\frac{1}{k}\sum_{k=1}^{K} f^{-1}_{(\Delta\mathbf{W})^t}\left((\Delta\mathbf{W}^k)\right)\right\|^2\end{aligned} \tag{89}$$

Based on the geodesic convexity of L_i and inequality 89, we define $\Delta_t = L(\Delta\mathbf{W})^t) - L(\Delta\mathbf{W}^*)$ and $\Delta_t^k = L_k(\Delta\mathbf{W})^t) - L_k(\Delta\mathbf{W}^*)$, and we have:

$$\Delta_t^k \leq -\langle\left(\left(\Gamma_{\mathbf{U}^k}L^k\right)^{(t)}, \left(\Gamma_{\mathbf{\Sigma}^k}L^k\right)^{(t)}, \left(\Gamma_{\mathbf{V}^k}L^k\right)^{(t)}\right), f^{-1}_{(\Delta\mathbf{W})^t}(\Delta\mathbf{W}^*)\rangle. \tag{90}$$

Summing this inequality over $k = 1, \ldots, K$, we get:

$$\begin{aligned}\Delta_t &\leq -\frac{1}{n}\left\langle\left(\frac{1}{K}\sum_{k=1}^{K}\left(\left(\Gamma_{\mathbf{U}^k}L^k\right)^{(t)}, \left(\Gamma_{\mathbf{\Sigma}^k}L^k\right)^{(t)}, \left(\Gamma_{\mathbf{V}^k}L^k\right)^{(t)}\right)\right), f^{-1}_{(\Delta\mathbf{W})^t}(\Delta\mathbf{W}^*)\right\rangle \\ &\leq \frac{1}{2\eta}\left(d^2((\Delta\mathbf{W})^t, \Delta\mathbf{W}^*)) - d^2((\Delta\mathbf{W})^{(t+1)}, \Delta\mathbf{W}^*))\right) + \frac{\zeta}{2\eta}\left\|\frac{1}{k}\sum_{k=1}^{K} f^{-1}_{(\Delta\mathbf{W})^t}\left((\Delta\mathbf{W}^k)\right)\right\|^2 \\ &\leq \frac{1}{2\eta}\left(d^2((\Delta\mathbf{W})^t, \Delta\mathbf{W}^*)) - d^2((\Delta\mathbf{W})^{(t+1)}, \Delta\mathbf{W}^*))\right) + \frac{\zeta\eta}{2n}\|\left(\left(\Gamma_{\mathbf{U}^k}L^k\right)^{(t)}, \left(\Gamma_{\mathbf{\Sigma}^k}L^k\right)^{(t)}, \left(\Gamma_{\mathbf{V}^k}L^k\right)^{(t)}\right)\|^2.\end{aligned} \tag{91}$$

From Inequality82 we have

$$\Delta_{(t+1)} - \Delta_t \leq (-\eta + \frac{\eta^2 c_g}{2}) \| \left(\left(\Gamma_{\mathbf{U}^k} L^k\right)^{(t)}, \left(\Gamma_{\mathbf{\Sigma}^k} L^k\right)^{(t)}, \left(\Gamma_{\mathbf{V}^k} L^k\right)^{(t)} \right) \|^2 \tag{92}$$

we multiply 92 by ζ and add it into 91, then we get:

$$\begin{aligned} \zeta\Delta_{(t+1)} - (\zeta - 1)\Delta_t \leq \zeta \left(\frac{\eta}{2n} - \eta + \frac{\eta^2 c_g}{2} \right) \| \left(\left(\Gamma_{\mathbf{U}^k} L^k\right)^{(t)}, \left(\Gamma_{\mathbf{\Sigma}^k} L^k\right)^{(t)}, \left(\Gamma_{\mathbf{V}^k} L^k\right)^{(t)} \right) \|^2 \\ + \frac{1}{2\eta} \left(d^2((\Delta\mathbf{W})^t, \Delta\mathbf{W}^*)) - d^2((\Delta\mathbf{W})^{(t+1)}, \Delta\mathbf{W}^*)) \right) \end{aligned} \tag{93}$$

We take $\eta \leq \frac{1}{2c_g}$ and $\left(\frac{\eta}{2n} - \eta + \frac{\eta^2 c_g}{2} \right) \leq 0$, thus

$$\zeta\Delta_{(t+1)} - (\zeta - 1)\Delta_t \leq \frac{1}{2\eta} \left(d^2((\Delta\mathbf{W})^t, \Delta\mathbf{W}^*)) - d^2((\Delta\mathbf{W})^{(t+1)}, \Delta\mathbf{W}^*)) \right) \tag{94}$$

Summing this up over t from 0 to C-1 we get

$$\zeta\Delta_C + \sum_{t=0}^{C-1} \Delta_t \leq (\zeta - 1)\Delta_1 + \frac{d^2(\Delta\mathbf{W}, \Delta\mathbf{W}^*)}{2\eta} \leq \frac{\zeta d^2(\Delta\mathbf{W}, \Delta\mathbf{W}^*)}{2\eta} \tag{95}$$

Where the last inequality follows from $\eta \leq \frac{1}{2c_g}$ and $\Delta^0 \leq c_g dist(\Delta\mathbf{W}, \Delta\mathbf{W}^*)$. Taking expectation for 92 then we get

$$(\zeta + C - 2)\mathbb{E}[\Delta_C] \leq \frac{\zeta d^2(\Delta\mathbf{W}, \Delta\mathbf{W}^*)}{2\eta} \leq \zeta c_g d^2(\Delta\mathbf{W}, \Delta\mathbf{W}^*) \tag{96}$$

thus

$$\Delta_C \leq \frac{\zeta c_g d^2(\Delta\mathbf{W}, \Delta\mathbf{W}^*)}{(\zeta + C - 2)} = \frac{\zeta c_g d^2(\Delta(\mathbf{U_0}, \mathbf{\Sigma_0}, \mathbf{V_0}), \Delta(\mathbf{U}^*, \mathbf{\Sigma}^*, \mathbf{V}^*))}{(\zeta + C - 2)} \tag{97}$$

□

7.5 Experimental Details

Environment. The experiments were conducted on a compute server running on Red Hat Enterprise Linux 7.2 with 2 CPUs of Intel Xeon E5-2650 v4 (at 2.66 GHz) and 8 GPUs of NVIDIA GeForce GTX 2080 Ti (with 11 GB of GDDR6 on a 352-bit memory bus and memory bandwidth in the neighborhood of 620GB/s) and 4 GPUs of NVIDIA H100 (each with 80GB of HBM2e memory on a 5120-bit memory bus, offering a memory bandwidth of approximately 3TB/s),256GB of RAM, and 1TB of HDD. Overall, the experiments took about 10 days in a shared resource setting. We expect that a consumer-grade single-GPU machine could complete the full set of experiments in around 21-23 days, if its full resources were dedicated. The codes were implemented in Python 3.7.10 and PyTorch 1.9.0. Since the datasets used are all public datasets and our methodologies and the hyperparameter settings are explicitly described in section 5 and 7.5, our codes and experiments can be easily reproduced on top of a GPU server.

Training. We study text classification model on three standard text datasets: SST-2 Socher et al. (2013),MRPC Dolan & Brockett (2005) and MPQA (Wiebe et al., 2005). The above three text datasets are all public datasets, which allow researchers to use non-commercial research and educational purposes. We use 7606 examples as training data and 1000 examples as test data for MPQA. We use 3668 examples as training data and 408 as test data for MRPC. We use 20000 examples as training data and 872 examples as test data for SST-2. We train LLaMA-3B,LLaMA-7B and Roberta on this three dataset for text classification. We also train a ViT on CIFAR-10, CIFAR-100 and Tiny-imagnet for image classification. The neural networks are trained with Kaiming initialization using RGD for 50 epochs with an initial learning rate of 4e-4 and batch size 8. In addition, we run each experiment for 3 trials for obtaining more stable results.

Implementation. For 11 state-of-the-art federated large language models of LoRA Hu et al. (2022), AdaLoRA Zhang et al. (2023b), P-Tuningv2 Liu et al. (2021a), FedPrompt Zhao et al. (2023), Fed-PepTAO Che et al. (2023), PromptFL Guo et al. (2024),PE-FL Zhao et al. (2024), SLoRA Babakniya

et al. (2023), HetLoRA Cho et al. (2023), FedLoRA Yi et al. (2024)and FFA-LoRA Sun et al. (2024), we utilized the same model architecture as the official open-source implementation and default parameter settings provided by the original authors for FedPEFT in all experiments. All hyperparameters are standard values from reference codes or prior works. We validate the performance of different FedPEFT methods with a range of rank $\in \{2, 4, 8, 16\}$. All models were trained for 10, 25 and 50 epochs, with a batch size of 8, and a learning rate of 4e-4. We use the Dirichlet distribution with concentration parameters $\alpha \in \{1, 3, 5\}$ to partition the data into non-IID splits. Each device is then assigned a certain number of samples based on the corresponding Dirichlet distribution. The above open-source codes from the GitHub are licensed under the MIT License, which only requires preservation of copyright and license notices and includes the permissions of commercial use, modification, distribution, and private use.

For our RAFFT model, we performed hyperparameter selection by performing a parameter rank $r \in \{2, 4, 8, 16\}$, Dirichlet alpha $\alpha \in \{1, 3, 5\}$, training epochs of the FedPEFT model $\in \{10, 25, 50, 100\}$, select rank and learning rate$\in \{1e^{-4}, 3e^{-4}, 4e^{-4}, 5e^{-5}\}$. We select the best parameters over 50 epochs of training and evaluate the model at test time.

Hyperparameter settings. Unless otherwise explicitly stated, we used the following default parameter settings in the experiments. As shown in Table 37

Parameter	**Value**
Training data on SST-2	20,000
Test data ratio on SST-2	872
Training data on MRPC	3,668
Test data on MRPC	408
Training data on MPQA	7,606
Test data on MPQA	1,000
Training data on CIFRA10	50,000
Test data on CIFRA10	10,000
Training data on CIFRA100	5,000
Test data on CIFRA100	1,000
Training data on Tiny-ImageNet	100,000
Test data on Tiny-ImageNet	10,000
Select rank threshold α	0.9
Training epochs of the FedPEFT model	50
Batch size for training the model	8
Learning rate	4e-4

Table 3: Model parameters and settings

7.6 ADDITIONALEXPERIMENTS

In this section, we present additional experimental results beyond those described in Section 3 to demonstrate the advantages of our proposed method. We considered a Federated Learning (FL) environment with 100 devices and a parameter server, randomly sampling 10 devices in each epoch to perform local updates. We utilized three widely-used NLP tasks, including SST-2 Socher et al. (2013), MRPC Dolan & Brockett (2005), and MPQA (Wiebe et al., 2005). Evaluations were conducted on the RoBERTa-LARGE Liu et al. (2019b) model for the MRPC and SST-2 datasets, the LLaMA 3B Touvron et al. (2023) model for the MRPC and SST-2 datasets, and the LLaMA 7B Radford et al. (2019) model for the MRPC and SST-2 datasets. Additionally, we experimented with the ViT model on image classification datasets CIFAR-10 and CIFAR-100. For all methods, the backbone models remained frozen. These comprehensive evaluations across multiple models and datasets illustrate the robustness and effectiveness of our fixed rank approach compared to 11 baseline methods across three common tasks.

Method	alpha = 5			alpha = 3			alpha = 1		
	Accuracy	Loss	Time	Accuracy	Loss	Time	Accuracy	Loss	Time
Centralized LoRA	89.65	0.2510	1,442	89.85	0.2857	1,419	86.25	0.3776	1,433
AdaLoRA	85.85	0.4134	1,774	82.00	2.2912	1,748	81.95	2.3407	1,763
P-tuning v2	87.45	0.3563	1,581	86.80	0.3256	1,614	86.50	0.3509	1,623
FedPrompt	86.00	0.5352	1,463	85.45	0.4666	1,479	84.80	0.4345	1,537
FedPepTAO	89.20	0.2854	1,608	89.05	0.2545	1,565	88.45	0.2749	1,592
PromptFL	85.75	0.5358	1,696	83.75	0.4847	1,516	83.35	0.4236	1,498
PE_FL	85.50	0.5331	1,663	85.25	0.4669	1,568	83.35	0.4274	1,505
SLoRA	90.05	0.2545	1,473	89.75	0.2546	1,446	86.70	0.2579	1,488
HetLoRA	87.70	0.3377	1,207	87.15	0.3159	1,212	87.25	0.3227	1,239
FedLoRA	89.95	0.2473	1,416	89.95	0.2416	1,517	89.60	0.2492	1,399
FFA-LoRA	87.50	0.3580	1,193	86.95	0.3386	1,168	87.30	0.3443	1,166
Fedkseed	81.90	0.6226	1,193	82.35	0.5921	1,186	82.75	0.5833	1,176
FLoRA	82.25	0.5549	1,216	83.35	0.5286	1,213	84.25	0.5227	1,154
RAFFT	91.45	0.1692	905	91.60	0.1701	902	91.20	0.1602	905
RAFFT-RGD	90.05	0.2311	869	89.85	0.2392	894	89.35	0.2281	890
RAFFT-MR	90.15	0.2299	890	90.10	0.2288	885	89.50	0.2209	884

Table 4: Performance comparison of different methods on Roberta+MPQA.

Method	alpha = 5			alpha = 3			alpha = 1		
	Accuracy	Loss	Time	Accuracy	Loss	Time	Accuracy	Loss	Time
Centralized LoRA	88.40	0.2249	3,351	88.65	0.2203	3,339	88.00	0.2362	3,229
AdaLoRA	83.60	0.3318	3,134	84.85	0.3343	3,136	83.45	0.3179	3,137
P-tuning v2	88.60	0.4830	3,360	86.85	0.3565	3,360	88.50	0.4606	3,358
FedPrompt	86.70	0.4537	3,358	87.70	0.4110	3,387	87.70	0.4110	3,354
FedPepTAO	88.90	0.4001	3,345	87.20	0.3535	3,335	87.70	0.5189	3,354
PromptFL	88.90	0.4000	3,352	88.50	0.2580	3,352	88.85	0.4520	3,360
PE_FL	88.25	0.3837	3,357	88.60	0.2580	3,353	88.60	0.2580	3,356
SLoRA	84.55	0.3028	3,893	81.35	0.3215	3,912	81.73	0.3579	3,851
HetLoRA	88.80	0.2685	2,848	88.95	0.2501	2,842	88.60	0.2310	2,842
FedLoRA	84.55	0.3028	2,792	81.35	0.3215	2,801	81.65	0.3579	2,805
FFA-LoRA	85.25	0.2552	2,789	84.35	0.2745	2,813	84.15	0.2776	2,811
Fedkseed	88.81	0.3979	3,356	88.83	0.2865	3,937	88.55	0.4165	3,356
FLoRA	87.05	0.3469	2,915	84.80	0.3443	2,957	84.84	0.4316	3,105
RAFFT	91.50	0.2769	2,718	91.35	0.2330	2,728	91.00	0.2418	2,754
RAFFT-RGD	90.15	0.3123	2,681	89.50	0.2930	2,678	88.90	0.2741	2,683
RAFFT-MR	89.95	0.2962	2,699	88.90	0.2899	2,701	88.70	0.2775	2,691

Table 5: Performance comparison of different methods on LLaMA 3B+MPQA.

Method	alpha = 5			alpha = 3			alpha = 1		
	Accuracy	Loss	Time	Accuracy	Loss	Time	Accuracy	Loss	Time
Centralized LoRA	81.32	0.4122	1,407	80.77	0.4217	1,411	80.70	0.4519	1,411
AdaLoRA	81.13	0.4309	1,563	80.29	0.4373	1,554	79.16	0.4818	1,570
P-tuning v2	78.48	0.4325	1,049	79.41	0.4116	1,057	77.59	0.3935	1,064
FedPrompt	75.87	0.6784	1,004	75.87	0.6346	979	74.98	3.8650	1,022
FedPepTAO	81.83	0.3691	1,066	80.24	0.3577	1,053	81.21	0.3722	1,066
PromptFL	75.84	0.5917	1,001	75.97	0.7182	977	75.29	0.7722	1,022
PE_FL	76.18	0.5868	1,024	74.98	3.8320	1,052	75.45	0.6071	1,022
SLoRA	80.43	0.4559	1,044	80.81	0.4152	1,052	81.29	0.4075	1,043
HetLoRA	80.52	0.4470	1,086	80.33	0.4404	1,168	79.51	0.3834	1,146
FedLoRA	81.64	0.5644	1,124	82.99	0.4428	1,204	82.21	0.4141	1,193
FFA-LoRA	77.74	0.4846	1,149	78.22	0.4395	1,026	77.02	0.4180	1,070
Fedkseed	81.34	0.7509	1,083	81.29	0.675	1,058	81.40	0.6975	1,036
FLoRA	81.70	0.6994	1,105	82.38	0.6346	1,037	81.29	0.6579	1,175
RAFFT	85.49	0.2758	818	84.09	0.3583	863	83.85	0.3623	890
RAFFT-RGD	82.8	0.4166	802	82.78	0.3928	822	82.12	0.4140	822
RAFFT-MR	82.25	0.4259	798	83.12	0.4039	819	81.95	0.4232	851

Table 6: Performance comparison of different methods on Roberta+MRPC.

Method	alpha = 5			alpha = 3			alpha = 1		
	Accuracy	Loss	Time	Accuracy	Loss	Time	Accuracy	Loss	Time
Centralized LoRA	92.89	0.3394	1,883	93.35	0.3276	1,862	92.89	0.3166	1,877
AdaLoRA	88.07	1.7253	1,710	87.96	1.7722	1,711	87.16	1.6742	1,720
P-tuning v2	89.44	0.6417	1,545	90.36	0.5675	1,504	90.60	0.4632	1,533
FedPrompt	89.68	0.7164	1,487	93.81	0.5829	1,460	89.33	0.5689	1,495
FedPepTAO	91.06	0.4388	1,614	91.74	0.4267	1,620	91.51	0.3499	1,581
PromptFL	92.20	0.5044	1,453	93.12	0.5096	1,444	93.92	0.3634	1,489
PE_FL	93.00	0.4628	1,503	93.00	0.4732	1,498	93.69	0.3523	1,470
SLoRA	92.66	0.2616	1,447	92.88	0.1956	1,473	90.25	0.2588	1,501
HetLoRA	93.46	0.2785	1,067	92.43	0.5086	1,095	93.46	0.2091	1,128
FedLoRA	93.35	0.3002	1,221	93.58	0.2877	1,192	93.69	0.2878	1,248
FFA-LoRA	92.77	0.3048	1,022	91.62	0.8016	1,087	92.43	0.4128	1,065
Fedkseed	93.23	0.3662	1,124	93.23	0.3633	1,251	93.00	0.3636	1,103
FLoRA	93.46	0.3175	1,158	93.46	0.3254	1,186	93.12	0.3307	1,251
RAFFT	95.07	0.1894	1,012	95.41	0.1720	1,012	95.18	0.1605	1,020
RAFFT-RGD	93.12	0.2654	957	92.88	0.3290	952	93.35	0.2026	961
RAFFT-MR	93.00	0.2921	962	92.88	0.3280	951	93.46	0.2337	958

Table 7: Performance comparison of different methods on Roberta+SST2.

Method	alpha = 5			alpha = 3			alpha = 1		
	Accuracy	Loss	Time	Accuracy	Loss	Time	Accuracy	Loss	Time
Centralized LoRA	82.07	0.3670	4,331	81.67	0.4179	4,255	81.36	0.4257	4,291
AdaLoRA	81.22	0.8810	4,086	81.22	0.8473	4,069	81.22	0.7275	4,078
P-tuning v2	81.34	4.1410	4,023	81.34	4.0730	4,103	80.82	4.1940	4,062
FedPrompt	81.18	4.3970	4,120	81.46	0.5310	4,094	81.22	0.4466	4,109
FedPepTAO	81.34	4.1410	3,891	81.34	0.5334	4,093	81.22	0.4460	4,125
PromptFL	79.19	5.7040	4,120	81.34	0.5884	4,093	81.22	0.4490	4,125
PE_FL	73.99	6.8350	4,114	81.34	0.5792	4,101	81.22	0.4447	4,111
SLoRA	81.78	0.3714	4,955	81.89	0.3811	4,952	80.15	0.4276	4,966
HetLoRA	76.80	4.6050	3,994	78.22	6.8990	3,995	78.27	7.0250	4,012
FedLoRA	82.07	0.4880	4,093	82.14	0.4748	4,207	81.97	0.3731	4,017
FFA-LoRA	80.76	3.2140	4,186	79.03	7.0660	4,008	78.78	7.1700	3,991
Fedkseed	74.92	6.5395	4,114	82.00	0.5822	4,100	81.84	0.4495	4,110
FLoRA	81.64	2.0501	4,912	81.83	0.5054	4,985	81.68	0.4092	4,963
RAFFT	82.63	0.4869	3,904	82.41	0.5877	3,915	82.63	0.4738	3,892
RAFFT-RGD	82.07	0.5319	3,971	81.95	0.5170	3,978	81.95	0.5623	3,956
RAFFT-MR	82.20	0.5133	3,956	81.98	0.6992	3,985	81.98	0.6992	3,985

Table 8: Performance comparison of different methods on LLaMA3B+MRPC.

Method	alpha = 5			alpha = 3			alpha = 1		
	Accuracy	Loss	Time	Accuracy	Loss	Time	Accuracy	Loss	Time
Centralized LoRA	94.61	0.1793	3,899	95.41	0.1268	3,897	94.38	0.1752	3,921
AdaLoRA	87.16	0.8543	3,532	88.12	0.9312	3,528	86.47	1.0330	3,548
P-tuning v2	93.23	0.2659	3,891	94.15	0.2156	3,900	92.43	0.2635	3,888
FedPrompt	93.69	0.3066	3,881	94.15	0.2606	3,893	94.04	0.2540	3,894
FedPepTAO	93.12	0.2619	3,778	94.15	0.2162	3,896	94.04	0.2540	3,894
PromptFL	93.92	0.3336	3,906	94.15	0.2606	3,893	92.32	0.2612	3,893
PE_FL	93.92	0.3063	3,924	94.15	0.2588	3,901	93.92	0.2627	3,890
SLoRA	94.04	0.2177	5,878	94.27	0.1750	5,792	93.81	0.1809	5,924
HetLoRA	94.04	0.2637	3,893	93.92	0.2726	3,638	94.50	0.2174	3,634
FedLoRA	94.61	0.2022	3,664	94.72	0.1556	3,723	95.18	0.1804	3,704
FFA-LoRA	93.12	0.2330	3,789	93.12	0.2419	3,593	93.46	0.2061	3,606
Fedkseed	93.92	0.3074	3,918	94.69	0.2604	3,900	94.80	0.2649	3,890
FLoRA	94.36	0.2370	3,853	94.90	0.19	3,904	94.00	0.2198	3,922
RAFFT	95.64	0.2048	3,672	95.53	0.1458	3,733	95.64	0.2029	3,749
RAFFT-RGD	93.81	0.2365	3,596	94.15	0.2314	3,634	93.92	0.2604	3,671
RAFFT-MR	93.80	0.2389	3,604	94.03	0.2353	3,615	93.57	0.2529	3,648

Table 9: Performance comparison of different methods on LLaMA3B+SST2.

Method	alpha = 5			alpha = 3			alpha = 1		
	Accuracy	Loss	Time	Accuracy	Loss	Time	Accuracy	Loss	Time
Centralized LoRA	80.32	0.3386	7,783	80.02	0.3900	7,691	80.09	0.3255	7,722
AdaLoRA	81.18	0.7412	7,522	81.07	0.7650	7,509	81.07	0.6333	7,518
P-tuning v2	81.07	0.9424	7,329	81.05	0.9306	7,261	81.07	0.8343	7,257
FedPrompt	81.34	0.5585	7,735	81.35	0.5322	7,667	81.63	0.4787	7,685
FedPepTAO	81.22	0.8325	7,328	81.11	0.9207	7,270	81.07	0.8174	7,253
PromptFL	81.46	0.5137	7,735	81.34	0.5329	7,673	81.07	0.8174	7,253
PE_FL	81.46	0.5348	7,741	81.35	0.5334	7,666	81.53	0.4791	7,678
SLoRA	81.66	0.5086	7,400	81.93	0.4805	7,314	81.30	0.3968	7,342
HetLoRA	80.88	0.5677	7,400	80.47	0.5675	7,342	80.88	0.4960	7,349
FedLoRA	81.60	0.4918	7,328	81.75	0.4760	7,492	81.60	0.4917	7,303
FFA-LoRA	80.90	0.8238	7,394	80.37	0.8623	7,337	81.26	0.7849	7,331
Fedkseed	81.81	0.5464	7,740	82.06	0.5397	7,666	81.74	0.5715	7,285
FLoRA	81.74	0.6461	7,314	80.98	0.7247	7,311	79.16	0.6914	7,338
RAFFT	83.62	0.4950	7,285	82.58	0.6641	7,216	83.11	0.6454	7,298
RAFFT-RGD	80.85	0.7416	7,291	80.73	0.7416	7,188	80.89	0.8807	7,301
RAFFT-MR	81.55	0.5580	7,295	82.03	0.6274	7,246	81.64	0.7618	7,288

Table 10: Performance comparison of different methods on LLaMA7B+MRPC.

Method	alpha = 5			alpha = 3			alpha = 1		
	Accuracy	Loss	Time	Accuracy	Loss	Time	Accuracy	Loss	Time
Centralized LoRA	94.61	0.1541	7,332	94.84	0.1400	7,442	95.18	0.1677	6,922
AdaLoRA	93.35	0.2736	7,129	93.58	0.2273	7,154	78.89	1.0824	6,811
P-tuning v2	90.02	0.2629	6,790	85.32	0.2731	6,807	94.04	0.2220	6,825
FedPrompt	82.91	0.3996	6,797	85.89	0.2773	6,813	93.92	0.2249	6,810
FedPepTAO	90.14	0.2632	6,719	90.14	0.2215	6,822	94.50	0.2258	6,811
PromptFL	88.42	0.2809	6,827	84.98	0.2677	6,813	93.92	0.2220	6,816
PE_FL	86.93	0.3327	6,797	84.29	0.2869	6,809	93.92	0.2262	6,815
SLoRA	89.22	0.2458	6,770	81.94	0.4805	7,314	81.29	0.3968	7,342
HetLoRA	91.40	0.2757	6,818	90.25	0.2588	6,860	95.18	0.1805	6,818
FedLoRA	94.45	0.1840	6,979	94.38	0.1599	6,498	95.18	0.1805	6,454
FFA-LoRA	94.38	0.2463	6,810	92.66	0.2617	6,838	92.89	0.1956	6,817
Fedkseed	86.77	0.3502	6,799	85.40	0.2927	6,809	94.18	0.2298	6,814
FLoRA	92.66	0.2216	6,610	92.77	0.1940	6,637	93.96	0.2028	6,916
RAFFT	96.33	0.1982	6,681	95.53	0.1949	6,618	95.41	0.2015	6,744
RAFFT-RGD	92.78	0.2951	6,731	93.69	0.2795	6,731	93.12	0.3003	6,738
RAFFT-MR	94.15	0.2758	6,724	93.92	0.2323	6,692	93.69	0.3629	6,819

Table 11: Performance comparison of different methods on LLaMA7B+SST2.

Method	alpha = 5			alpha = 3			alpha = 1		
	Accuracy	Loss	Time	Accuracy	Loss	Time	Accuracy	Loss	Time
Centralized LoRA	46.43	1.7763	3,340	46.32	1.8492	3,394	43.43	2.0657	3,314
AdaLoRA	46.15	1.7674	3,548	46.10	1.8546	3,488	42.81	2.1023	3,454
SLoRA	44.10	1.9510	3,372	43.34	1.9870	3,306	41.39	2.1920	3,362
HetLoRA	46.31	1.8132	3,347	45.68	1.8629	3,321	43.53	2.0552	3,305
FedLoRA	50.08	1.5120	3,404	44.94	1.8940	3,290	42.40	2.1020	3,371
FFA-LoRA	45.99	1.8065	3,363	46.06	1.8210	3,363	43.19	1.9970	3,334
FLoRA	40.39	1.5424	3,288	45.36	1.6339	3,326	41.93	1.811	3,418
RAFFT	48.44	1.3240	3,273	48.36	1.3390	3,295	45.82	1.5210	3,314
RAFFT-RGD	47.11	1.5020	3,308	46.96	1.5480	3,280	43.33	1.6940	3,297
RAFFT-MR	47.21	1.4959	3,625	46.47	1.5746	3,301	43.75	1.7250	3,309

Table 12: Performance comparison of different methods on ViT+CIFRA100.

Method	alpha = 5			alpha = 3			alpha = 1		
	Accuracy	Loss	Time	Accuracy	Loss	Time	Accuracy	Loss	Time
Centralized LoRA	26.92	2.9963	11,497	26.18	3.0743	11,139	24.34	3.2956	11,260
AdaLoRA	27.10	3.0361	12,278	26.72	3.0535	11,820	24.38	3.2249	11,908
SLoRA	26.76	3.2740	11,176	25.76	3.3610	11,755	24.18	3.6510	11,878
HetLoRA	26.78	3.0303	11,487	25.90	3.0713	11,317	24.14	3.2865	11,278
FedLoRA	26.80	3.2570	11,643	26.24	3.3519	11,720	24.32	3.6429	11,960
FFA-LoRA	26.42	3.2642	11,700	26.02	3.3664	11,787	24.06	3.6111	11,797
FLoRA	23.96	3.5034	11,564	23.56	3.5504	11,508	21.82	3.8373	11,755
RAFFT	28.82	2.9140	11,236	27.88	2.9350	11,195	25.12	3.1270	11,225
RAFFT-RGD	27.74	3.0150	11,159	26.90	3.0470	11,598	24.08	3.2850	11,591
RAFFT-MR	27.16	3.0480	10,938	27.18	3.0370	11,245	24.58	3.2260	10,957

Table 13: Performance comparison of different methods on ViT+IamgeNet.

Accuracy of classification using Riemannian manifolds on different numbers of clients. To comprehensively investigate the applicability of our RAFFT method for classification tasks under different client numbers, we evaluated the method with 40, 60, 80, and 100 clients while keeping other settings constant. Tables 14-19 present the classification accuracy on three datasets using Riemannian manifold techniques. We observed consistent results, indicating that the three variants of our RAFFT method achieved the best accuracy in most experiments. This demonstrates the superior performance of RAFFT under varying client numbers. A plausible explanation is that the rigorous mathematical analysis based on Riemannian manifold theory significantly enhances the effectiveness and applicability of our RAFFT method across different scenarios.

Method	N = 40			N = 60			N = 80			N = 100		
	Accuracy	Loss	Time	Accuracy	Loss	Time	Accuracy	Loss	Time	Accuracy	Loss	Time
Centralized LoRA	91.70	0.1511	1,481	90.95	0.1604	1,489	91.40	0.2203	1,472	89.65	0.2510	1,433
AdaLoRA	89.60	0.2471	1,669	89.15	0.2639	1,730	88.05	0.3008	1,710	85.85	0.4136	1,763
P-tuning v2	89.25	0.2481	1,588	88.10	0.2930	1,610	87.60	0.3337	1,631	87.45	0.3563	1,581
FedPrompt	87.90	0.4247	1,485	87.15	0.4846	1,584	85.25	0.5106	1,495	86.00	0.5352	1,463
FedPepTAO	89.95	0.1627	1,586	89.60	0.2348	1,683	89.20	0.2421	1,583	89.20	0.2854	1,608
PromptFL	87.70	0.4394	1,479	86.50	0.4824	1,575	84.90	0.5149	1,499	85.75	0.5358	1,696
PE_FL	88.05	0.3954	1,507	86.15	0.4736	1,489	85.65	0.4727	1,529	85.50	0.5331	1,663
SLoRA	91.15	0.1598	1,410	90.70	0.2509	1,463	91.00	0.2743	1,469	90.05	0.2544	1,488
HetLoRA	88.10	0.3145	1,154	86.80	0.3668	1,221	84.00	0.4775	1,276	87.70	0.3377	1,207
FedLoRA	91.30	0.1522	1,493	90.75	0.2478	1,539	91.10	0.2744	1,571	89.95	0.2473	1,399
FFA-LoRA	87.55	0.3448	1,065	86.00	0.4245	1,098	84.45	0.3580	1,119	87.50	0.3580	1,193
Fedkseed	88.80	0.3138	1,114	86.90	0.4047	1,141	84.95	0.5082	1,168	82.75	0.5833	1,176
FLoRA	89.05	0.2966	1,202	87.75	0.3707	1,151	85.65	0.4662	1,129	84.25	0.5227	1,154
RAFFT	91.80	0.1065	842	92.00	0.1285	905	91.70	0.1469	885	91.45	0.1692	905

Table 14: Performance comparison of different methods on Roberta+MPQA with varying numbers of clients (N).

Method	N = 40			N = 60			N = 80			N = 100		
	Accuracy	Loss	Time	Accuracy	Loss	Time	Accuracy	Loss	Time	Accuracy	Loss	Time
Centralized LoRA	85.21	0.2362	1,416	83.55	0.3623	1,395	83.72	0.3956	1,443	81.32	0.4122	1,407
AdaLoRA	83.37	0.2942	1,545	83.62	0.3217	1,506	83.75	0.3641	1,514	81.13	0.4309	1,563
P-tuning v2	80.63	0.2974	1,037	78.13	0.4139	1,088	79.11	0.4611	1,059	78.48	0.4325	1,049
FedPrompt	76.29	0.5435	1,003	75.29	0.6265	1,003	75.13	0.7028	992	75.87	0.6784	1,004
FedPepTAO	84.98	0.2090	1,042	81.40	0.2732	1,080	81.68	0.3586	1,120	80.85	0.3982	1,049
PromptFL	75.55	0.6329	1,022	74.98	0.6772	1,045	75.34	0.7687	972	75.84	0.5917	1,001
PE_FL	83.26	0.2482	1,045	80.75	0.2792	1,087	81.27	0.3896	1,037	76.18	0.5686	1,024
SLoRA	85.43	0.3257	1,029	83.57	0.3722	1,066	81.39	0.3846	1,021	80.43	0.4559	1,044
HetLoRA	81.68	0.4203	1,035	78.83	0.4678	1,143	76.77	0.5138	1,150	80.52	0.4470	1,086
FedLoRA	85.07	0.4072	1,083	84.11	0.4674	1,114	82.92	0.5052	1,075	81.64	0.5645	1,095
FFA-LoRA	81.06	0.3960	1,116	80.87	0.4550	1,033	78.30	0.5054	1,036	77.74	0.4846	1,060
Fedkseed	81.32	0.6024	1,075	81.28	0.6224	1,084	81.34	0.6945	1,041	81.40	0.6975	1,153
FLoRA	82.38	0.5507	1,153	81.52	0.6001	1,031	81.38	0.6627	1,052	81.29	0.6579	1,188
RAFFT	86.80	0.2629	994	85.55	0.2914	1,005	85.70	0.3949	997	84.75	0.3519	1,097

Table 15: Performance comparison of different methods on Roberta+MRPC with varying numbers of clients (N).

	N = 40			N = 60			N = 80			N = 100		
Method	Accuracy	Loss	Time	Accuracy	Loss	Time	Accuracy	Loss	Time	Accuracy	Loss	Time
Centralized LoRA	94.83	0.2296	1,149	94.38	0.2550	1,133	94.38	0.2523	1,157	92.89	0.3394	1,883
AdaLoRA	93.81	0.2471	1,269	93.69	0.2498	1,270	93.46	0.2424	1,223	88.07	1.7253	1,710
P-tuning v2	90.02	0.6433	1,562	88.07	0.7700	1,527	87.27	0.7822	1,534	89.44	0.6417	1,545
FedPrompt	93.69	0.4831	1,501	90.13	0.6522	1,490	90.37	0.7105	1,472	89.68	0.7164	1,487
FedPepTAO	91.28	0.4281	1,592	90.83	0.5123	1,623	90.71	0.5028	1,603	91.06	0.4388	1,614
PromptFL	92.78	0.4751	1,469	91.86	0.5922	1,472	90.48	0.6318	1,432	92.20	0.5044	1,453
PE_FL	94.50	0.4647	1,512	92.43	0.5441	1,492	91.85	0.5617	1,478	93.00	0.4628	1,503
SLoRA	95.64	0.2084	1,185	95.30	0.2302	1,215	95.18	0.2233	1,239	81.65	3.4859	1,447
HetLoRA	93.69	0.2472	1,071	93.23	0.2734	1,143	93.12	0.3029	1,054	93.46	0.2785	1,067
FedLoRA	95.41	0.2875	1,178	95.05	0.2962	1,206	94.95	0.2701	1,215	93.35	0.3002	1,221
FFA-LoRA	93.00	0.3431	1,032	92.32	0.4621	995	92.77	0.5617	1,015	93.46	0.3048	1,022
Fedkseed	94.03	0.2437	1,258	93.58	0.2739	1,314	93.69	0.2736	1,142	93.00	0.2724	1,046
FLoRA	94.38	0.2389	1,192	93.69	0.2623	1,207	93.69	0.2544	1,103	93.12	0.3307	1,045
RAFFT	95.76	0.1561	922	95.30	0.1665	944	95.30	0.1396	969	95.07	0.1894	1012

Table 16: Performance comparison of different methods on Roberta+SST2 with varying numbers of clients (N).

	N = 40			N = 60			N = 80			N = 100		
Method	Accuracy	Loss	Time	Accuracy	Loss	Time	Accuracy	Loss	Time	Accuracy	Loss	Time
Centralized LoRA	71.95	0.6527	3,278	71.77	0.6565	3,321	71.48	0.6874	3,286	71.90	0.7170	3,329
AdaLoRA	72.34	0.6616	3,518	72.12	0.6467	3,627	71.83	0.6873	3,590	71.76	0.6936	3,535
SLoRA	72.76	0.6372	3,301	72.39	0.6652	3,294	71.77	0.6634	3,330	71.75	0.6843	3,309
HetLoRA	72.22	0.6614	3,310	71.81	0.6831	3,312	71.30	0.7046	3,350	71.76	0.6939	3,355
FedLoRA	72.35	0.6800	3,269	71.64	0.6867	3,343	71.53	0.6873	3,301	71.56	0.7149	3,282
FFA-LoRA	71.79	0.6435	3,269	71.91	0.6848	3,362	71.53	0.6993	3,310	71.47	0.7135	3,321
FLoRA	72.59	0.5949	3,409	72.25	0.6060	3,373	71.03	0.5980	3,350	70.95	0.7266	3,401
RAFFT	75.71	0.5021	3,279	75.67	0.5252	3,286	74.61	0.5232	3,301	74.54	0.5757	3,304

Table 17: Performance comparison of different methods on ViT+CIFRA10 with varying numbers of clients (N).

	N = 40			N = 60			N = 80			N = 100		
Method	Accuracy	Loss	Time	Accuracy	Loss	Time	Accuracy	Loss	Time	Accuracy	Loss	Time
Centralized LoRA	45.69	1.7550	3,267	45.88	1.7610	3,295	45.46	1.8640	3,251	46.43	1.7763	3,340
AdaLoRA	44.28	1.8590	3,535	44.53	1.8950	3,489	43.54	1.9040	3,538	46.15	1.7674	3,548
SLoRA	44.78	1.8630	3,304	45.16	1.8620	3,237	44.52	1.9560	3,311	44.10	1.9510	3,372
HetLoRA	45.80	1.7540	3,278	45.90	1.7990	3,315	45.50	1.8280	3,334	46.31	1.8132	3,347
FedLoRA	46.13	1.7310	3,335	45.72	1.7500	3,286	44.95	1.8430	3,289	45.26	1.5120	3,404
FFA-LoRA	45.75	1.7200	3,331	45.85	1.7780	3,280	45.28	1.8550	3,404	45.99	1.8065	3,363
FLoRA	48.11	1.6190	3,329	48.09	1.6210	3,494	46.76	1.6030	3,344	40.39	1.5424	3,288
RAFFT	48.94	1.1740	3,193	48.85	1.2130	3,122	48.27	1.3310	3,284	48.44	1.3240	3,273

Table 18: Performance comparison of different methods on ViT+CIFRA100 with varying numbers of clients (N).

	N = 40			N = 60			N = 80			N = 100		
Method	Accuracy	Loss	Time	Accuracy	Loss	Time	Accuracy	Loss	Time	Accuracy	Loss	Time
Centralized LoRA	28.46	3.0426	11,604	26.34	3.1904	11,737	26.82	3.2050	11,546	26.92	2.9963	11,497
AdaLoRA	28.86	2.9607	12,264	26.50	3.1529	12,481	26.64	3.1230	12,433	27.10	3.0361	12,278
SLoRA	28.32	3.0342	11,583	26.40	3.2080	11,834	26.92	3.2540	11,734	26.76	3.2740	11,176
HetLoRA	28.50	2.9923	11,838	26.58	3.2077	12,349	27.00	3.2010	12,045	26.78	3.0303	11,487
FedLoRA	28.30	2.9999	11,855	26.48	3.1991	12,008	26.84	3.2300	11,922	26.80	3.2570	11,643
FFA-LoRA	28.44	3.0310	11,789	26.40	3.2059	11,810	26.78	3.2140	11,941	26.42	3.2642	11,700
FLoRA	26.96	3.499	11,586	26.68	3.4914	11,716	25.76	3.5060	11,516	23.96	3.5034	11,564
RAFFT	29.66	2.6210	11,038	27.36	2.9390	11,142	29.24	2.8190	11,349	28.82	2.9140	11,236

Table 19: Performance comparison of different methods on ViT+IamgeNet with varying numbers of clients (N).

Accuracy of classification using Riemannian manifolds on different initial rank values. To comprehensively investigate the applicability of our RAFFT method for classification tasks with different initial rank values, we set the initial ranks to 2, 4, 8, and 16 while keeping other settings constant. Tables 20-25 present the classification accuracy on three datasets using Riemannian manifold techniques. We observed consistent results, indicating that the three variants of our RAFFT method achieved the best accuracy in most experiments. A plausible explanation is that the rigorous mathematical analysis based on Riemannian manifold theory significantly enhances the effectiveness and applicability of our RAFFT method across different scenarios.

	r = 2			r = 4			r = 8			r = 16		
Method	Accuracy	Loss	Time	Accuracy	Loss	Time	Accuracy	Loss	Time	Accuracy	Loss	Time
Centralized LoRA	90.6	0.2157	1,040	90.55	0.2153	1,038	89.65	0.2510	1,442	90.55	0.2075	1,011
AdaLoRA	82.46	0.8709	1,237	81.80	0.8581	1,195	85.85	0.4136	1,774	82.10	0.8887	1,228
SLoRA	90.10	0.2219	1,034	90.10	0.2213	1,065	90.05	0.2545	1,473	90.10	0.2222	1,073
HetLoRA	86.60	0.3707	1,318	83.20	0.5256	1,203	87.70	0.3377	1,207	89.60	0.2552	1,186
FedLoRA	90.20	0.2170	1,095	90.30	0.2175	1,049	89.95	0.2473	1,416	90.20	0.2177	1,140
FFA-LoRA	87.95	0.3290	1,158	88.55	0.3251	1,139	87.50	0.3580	1,193	87.85	0.3413	1,140
FLoRA	84.15	0.5238	1,159	84.10	0.5257	1,180	84.25	0.5227	1,197	84.30	0.5250	1,186
RAFFT	91.00	0.1900	849	91.05	0.1806	848	91.45	0.1692	905	91.55	0.1500	918

Table 20: Performance comparison of different methods on Roberta+MPQA with varying rank values (r).

	r = 2			r = 4			r = 8			r = 16		
Method	Accuracy	Loss	Time	Accuracy	Loss	Time	Accuracy	Loss	Time	Accuracy	Loss	Time
Centralized LoRA	82.27	0.3894	1,417	82.49	0.3853	1,385	81.32	0.4122	1,402	81.86	0.3862	1,401
AdaLoRA	79.98	0.4240	1,516	82.34	0.3992	1,528	81.14	0.4309	1,563	81.66	0.4020	1,572
SLoRA	82.27	0.3864	1,039	82.08	0.3794	1,012	80.43	0.4559	1,044	81.38	0.3824	1,074
HetLoRA	75.40	0.5103	1,045	74.78	0.5767	1,033	80.52	0.4470	1,086	74.78	0.9160	1,082
FedLoRA	81.45	0.5971	1,047	81.37	0.5958	1,022	81.64	0.5645	1,056	81.33	0.5974	1,018
FFA-LoRA	74.81	0.5438	1,003	74.98	0.5441	1,014	77.74	0.4846	1,060	74.91	0.5549	1,048
FLoRA	81.16	0.6580	1,037	81.17	0.6591	1,084	81.29	0.6579	1,010	81.67	0.6592	1,024
RAFFT	85.16	0.3345	813	84.57	0.3000	825	85.39	0.2758	818	86.04	0.3453	830

Table 21: Performance comparison of different methods on Roberta+MRPC with varying rank values (r).

	r = 2			r = 4			r = 8			r = 16		
Method	Accuracy	Loss	Time	Accuracy	Loss	Time	Accuracy	Loss	Time	Accuracy	Loss	Time
Centralized LoRA	93.35	0.2529	1,040	93.19	0.2613	1,001	92.89	0.3394	1,883	93.12	0.2614	1,076
AdaLoRA	89.44	1.5001	1,237	89.79	1.4422	1,195	88.07	1.7253	1,710	89.56	1.5087	1,184
SLoRA	93.18	0.2571	1,034	92.30	0.2595	1,065	81.65	3.4859	1,447	95.18	0.1595	1,105
HetLoRA	93.35	0.2531	1,032	93.00	0.3403	1,085	93.46	0.2785	1,067	92.20	0.7275	1,093
FedLoRA	93.92	0.2559	1,095	90.30	0.2175	1,049	93.92	0.2548	1,221	93.92	0.2559	1,086
FFA-LoRA	91.74	0.6232	1,017	91.97	0.5818	1,042	92.77	0.3048	1,022	91.86	0.7081	1,036
FLoRA	92.26	0.2368	1,224	93.34	0.2369	1,206	93.12	0.3307	1,232	94.27	0.2369	1,249
RAFFT	94.15	0.2316	994	95.18	0.1790	992	95.07	0.1894	1012	95.30	0.2130	1,014

Table 22: Performance comparison of different methods on Roberta+SST2 with varying rank values (r).

	r = 2			r = 4			r = 8			r = 16		
Method	Accuracy	Loss	Time	Accuracy	Loss	Time	Accuracy	Loss	Time	Accuracy	Loss	Time
Centralized LoRA	71.14	0.7078	3,256	72.08	0.6924	3,241	71.90	0.717	3,329	70.69	0.7221	3,318
AdaLoRA	71.06	0.717	3,600	71.62	0.7060	3,510	71.76	0.6936	3,535	71.47	0.7127	3,622
SLoRA	71.54	0.6927	3,269	72.12	0.6871	3,337	71.75	0.6843	3,309	72.03	0.7002	3,357
HetLoRA	71.50	0.7071	3,358	70.66	0.7172	3,333	71.76	0.6939	3,355	70.91	0.7045	3,361
FedLoRA	71.87	0.7133	3,277	71.28	0.7287	3,300	71.56	0.7149	3,282	71.83	0.7111	3,306
FFA-LoRA	71.90	0.6900	3,316	72.10	0.7000	3,291	71.47	0.7135	3,321	71.22	0.7167	3,341
FLoRA	71.75	0.5803	3,840	72.38	0.6042	3,913	70.95	0.7266	3,901	71.34	0.5885	3,970
RAFFT	73.67	0.5615	3,282	74.23	0.5953	3,244	74.54	0.5757	3,304	73.97	0.579	3,301

Table 23: Performance comparison of different methods on ViT+CIFRA10 with varying rank values (r).

	r = 2			r = 4			r = 8			r = 16		
Method	Accuracy	Loss	Time	Accuracy	Loss	Time	Accuracy	Loss	Time	Accuracy	Loss	Time
Centralized LoRA	44.45	1.8870	3,212	44.32	1.9000	3,333	46.43	1.7763	3,340	44.64	1.8830	3,399
AdaLoRA	44.24	1.9410	3,519	43.76	1.9600	3,507	46.15	1.7674	3,548	43.41	1.9920	3,559
SLoRA	43.81	1.9670	3,382	43.42	2.0000	3,317	44.10	1.9510	3,372	43.00	1.9810	3,437
HetLoRA	44.87	1.8690	3,314	44.83	1.8740	3,358	46.31	1.8132	3,347	44.46	1.9110	3,440
FedLoRA	44.41	1.9140	3,365	44.56	1.9090	3,351	45.26	1.8920	3,260	44.53	1.8830	3,337
FFA-LoRA	44.62	1.9000	3,389	44.60	1.9220	3,375	45.99	1.8065	3,363	44.00	1.8880	3,464
FLoRA	45.05	1.6170	3,873	45.23	1.6100	3,813	40.39	1.5424	3,888	46.91	1.6500	3,839
RAFFT	48.76	1.3330	3,305	48.13	1.3220	3,255	48.44	1.3240	3,273	48.94	1.3000	3,296

Table 24: Performance comparison of different methods on ViT+CIFRA100 with varying rank values (r).

Method	r = 2			r = 4			r = 8			r = 16		
	Accuracy	Loss	Time	Accuracy	Loss	Time	Accuracy	Loss	Time	Accuracy	Loss	Time
Centralized LoRA	27.02	3.2640	11,425	27.20	3.2700	11,383	26.92	2.9963	11,497	26.64	3.2910	11,542
AdaLoRA	26.58	3.2550	12,272	26.28	3.2700	12,256	27.10	3.0362	12,278	26.36	3.2980	12,294
SLoRA	26.82	3.2590	11,102	26.84	3.2520	11,145	26.76	3.2740	11,176	26.16	3.2850	11,191
HetLoRA	26.80	3.2540	11,502	27.08	3.2500	11,394	26.78	3.0303	11,487	27.10	3.2540	11,674
FedLoRA	26.56	3.2610	11,523	27.26	3.2190	11,401	26.80	3.2570	11,643	26.28	3.2890	11,723
FFA-LoRA	27.00	3.2530	11,685	26.92	3.2660	11,504	26.42	3.2642	11,700	26.68	3.2630	11,894
FLoRA	24.36	3.477	11,817	24.48	3.4890	11,905	23.96	3.5033	11,564	23.44	3.4843	12,218
RAFFT	29.24	2.9230	11,295	28.40	2.9040	11,012	28.82	2.9140	11,236	28.42	2.9330	11,096

Table 25: Performance comparison of different methods on ViT+IamgeNet with varying rank values (r).

Model	**ACC**				
	$\Theta = 0.6$	$\Theta = 0.7$	$\Theta = 0.8$	$\Theta = 0.9$	$\Theta = 1$
Roberta+SST-2	95.30	95.30	95.41	95.07	93.00
Roberta+MRPC	84.22	83.22	85.67	84.75	82.25
Roberta+MPQA	91.15	91.30	91.55	91.45	90.15
LLaMA 7B+SST-2	95.41	95.53	95.41	95.64	94.15
LLaMA 7B+MRPC	82.77	82.77	82.77	83.62	81.55
LLaMA 7B+MPQA	91.40	91.45	91.70	92.00	90.80
ViT+CIFAR10	74.07	73.53	73.95	73.89	72.88
ViT+CIFAR100	49.16	48.22	47.97	48.44	47.21
ViT+ImageNet	28.92	28.64	28.66	28.82	27.16

Table 26: Performance comparison of different models with varying Theta values (ACC).

Model	**Time (s)**				
	$\Theta = 0.6$	$\Theta = 0.7$	$\Theta = 0.8$	$\Theta = 0.9$	$\Theta = 1$
Roberta+SST-2	976	981	968	1,012	962
Roberta+MRPC	853	850	843	838	798
Roberta+MPQA	865	886	883	905	890
LLaMA 7B+SST-2	6,848	6,848	6,852	6,988	6,961
LLaMA 7B+MRPC	7,595	7,504	7,513	7,558	7,541
LLaMA 7B+MPQA	4,840	5,025	4,916	5,010	5,021
ViT+CIFAR10	3,591	3,611	3,587	3,555	3,687
ViT+CIFAR100	3,553	3,695	3,638	3,585	3,625
ViT+ImageNet	13,260	13,073	13,388	12,706	13,164

Table 27: Performance comparison of different models with varying Theta values (Time).

Model	**ACC**				
	LR=0.0001	LR=0.0005	LR=0.001	LR=0.005	LR=0.01
Roberta+SST-2	86.24	93.81	94.84	95.30	95.64
Roberta+MRPC	74.78	77.33	81.93	84.40	87.04
Roberta+MPQA	79.55	90.10	91.20	91.55	91.70
LLaMA 7B+SST-2	95.18	96.10	96.33	61.70	50.92
LLaMA 7B+MRPC	81.52	82.70	83.62	81.22	81.22
LLaMA 7B+MPQA	91.10	92.00	91.90	67.60	67.70
ViT+CIFAR10	74.54	69.28	54.97	27.90	23.73
ViT+CIFAR100	48.44	44.07	29.38	6.55	6.18
ViT+ImageNet	28.82	16.80	15.40	9.28	2.72

Table 28: Performance comparison of different models with varying Learning Rates (ACC).

Model	Time (s)				
	LR=0.0001	LR=0.0005	LR=0.001	LR=0.005	LR=0.01
Roberta+SST-2	979	981	990	980	967
Roberta+MRPC	862	847	832	826	825
Roberta+MPQA	905	914	920	907	952
LLaMA 7B+SST-2	6,971	6,953	6,988	6,812	6,937
LLaMA 7B+MRPC	7,511	7,508	7,558	7,612	7,545
LLaMA 7B+MPQA	4,886	4,906	4,878	4,988	4,949
ViT+CIFAR10	3,555	3,647	3,783	3,642	3,671
ViT+CIFAR100	3,585	3,704	3,651	3,598	3,543
ViT+ImageNet	12,706	13,041	13,215	13,192	13,264

Table 29: Performance comparison of different models with varying Learning Rates (Time).

Model	ACC				
	Epoch 1	**Epoch 5**	**Epoch 10**	**Epoch 15**	**Epoch 20**
Roberta+SST-2	87.79	93.81	94.72	95.18	95.07
Epoch 10	**Epoch 20**	**Epoch 30**	**Epoch 40**	**Epoch 50**	
Roberta+MRPC	76.60	79.82	81.81	83.40	85.67
Epoch 10	**Epoch 20**	**Epoch 30**	**Epoch 40**	**Epoch 50**	
Roberta+MPQA	88.85	90.15	90.70	91.20	91.45
Epoch 2	**Epoch 4**	**Epoch 6**	**Epoch 8**	**Epoch 10**	
LLaMA 7B+SST-2	89.91	94.84	95.41	95.41	95.64
Epoch 5	**Epoch 10**	**Epoch 15**	**Epoch 20**	**Epoch 25**	
LLaMA 7B+MRPC	81.29	81.29	82.28	82.28	83.62
Epoch 5	**Epoch 10**	**Epoch 15**	**Epoch 20**	**Epoch 25**	
LLaMA 7B+MPQA	89.45	90.90	91.25	91.25	92.00
Epoch 40	**Epoch 80**	**Epoch 120**	**Epoch 160**	**Epoch 200**	
ViT+CIFAR10	57.69	64.74	69.42	71.85	74.54
Epoch 40	**Epoch 80**	**Epoch 120**	**Epoch 160**	**Epoch 200**	
ViT+CIFAR100	29.51	37.72	42.42	45.43	48.44
Epoch 50	**Epoch 100**	**Epoch 200**	**Epoch 300**	**Epoch 400**	
ViT+ImageNet	13.16	17.68	22.48	25.48	28.82

Table 30: Performance comparison of different models with varying Training Epochs (ACC).

Accuracy of classification using Riemannian manifolds on different parameters. As shown in Table 32-33, RAFFT demonstrates superior performance and stability in extreme non-IID data environments across diverse tasks. For instance, in the LLaMA 7B + MPQA task with $\alpha = 0.5$, RAFFT achieves the highest accuracy of 90.80, outperforming all baseline methods. Similarly, in the ViT + CIFAR-10 task with $\alpha = 0.1$, RAFFT achieves the best accuracy of 61.22, surpassing all other methods. These results highlight RAFFT's robustness and effectiveness in handling high data heterogeneity, further supported by its Riemannian framework, which mitigates both client-drift and rank-drift issues and ensures stability across diverse data distributions. As illustrated in Figure 3, the distribution of samples per class for each client in the MPQA dataset reflects the highly heterogeneous nature of the data.

Model	**Time (s)**				
	Epoch 1	**Epoch 5**	**Epoch 10**	**Epoch 15**	**Epoch 20**
Roberta+SST-2	84	324	638	949	1,012
Epoch 10	**Epoch 20**	**Epoch 30**	**Epoch 40**	**Epoch 50**	
Roberta+MRPC	173	341	517	655	843
Epoch 10	**Epoch 20**	**Epoch 30**	**Epoch 40**	**Epoch 50**	
Roberta+MPQA	186	360	528	701	905
Epoch 2	**Epoch 4**	**Epoch 6**	**Epoch 8**	**Epoch 10**	
LLaMA 7B+SST-2	1,380	2,642	4,043	5,462	6,988
Epoch 5	**Epoch 10**	**Epoch 15**	**Epoch 20**	**Epoch 25**	
LLaMA 7B+MRPC	1,547	2,994	4,602	6,012	7,558
Epoch 5	**Epoch 10**	**Epoch 15**	**Epoch 20**	**Epoch 25**	
LLaMA 7B+MPQA	5,071	5,063	5,102	4,972	5,010
Epoch 40	**Epoch 80**	**Epoch 120**	**Epoch 160**	**Epoch 200**	
ViT+CIFAR10	736	1,450	2,143	2,935	3,555
Epoch 40	**Epoch 80**	**Epoch 120**	**Epoch 160**	**Epoch 200**	
ViT+CIFAR100	722	1,460	2,203	2,911	3,585
Epoch 200	**Epoch 250**	**Epoch 300**	**Epoch 350**	**Epoch 400**	
ViT+ImageNet	1,645	3,288	6,728	9,691	12,706

Table 31: Performance comparison of different models with varying Training Epochs (Time).

Method	**Accuracy (%)**	**Loss**	**Time (s)**
Centralized LoRA	82.9000	0.2834	5432
AdaLoRA	32.7500	10.5591	5503
P-tuning v2	85.2000	0.2912	5664
FedPrompt	87.3500	0.2639	5393
FedPepTAO	87.6000	0.2584	5475
PromptFL	87.4000	0.2574	5586
PE_FL	87.2500	0.2661	5263
SLoRA	84.1000	0.3372	5622
HetLoRA	84.2300	0.3035	5229
FedLoRA	87.7400	0.1664	5308
FFA-LoRA	80.0000	0.3496	5358
Fedkseed	82.4500	0.2918	5452
FLoRA	79.1900	0.3016	5293
RAFFT	90.8000	0.2766	5198
RAFFT-RGD	86.2100	0.2947	5151
RAFFT-MR	86.7300	0.3004	5177

Table 32: Performance comparison of methods on LLaMA 7B + MPQA (25 rounds) with $\alpha = 0.5$.

Method	Accuracy (%)	Loss	Time (s)
Centralized LoRA	60.4800	1.0437	3578
AdaLoRA	60.9200	1.1428	3260
SLoRA	58.8900	0.8824	3402
HetLoRA	59.6300	1.0270	3387
FedLoRA	59.1100	0.9824	3310
FFA-LoRA	60.2100	0.9651	3412
FLoRA	59.3100	1.0490	3249
RAFFT	61.2200	0.8544	3222
RAFFT-RGD	60.6200	0.9478	3288
RAFFT-MR	59.9100	1.0032	3265

Table 33: Performance comparison of methods on ViT + CIFAR-10 with $\alpha = 0.1$.

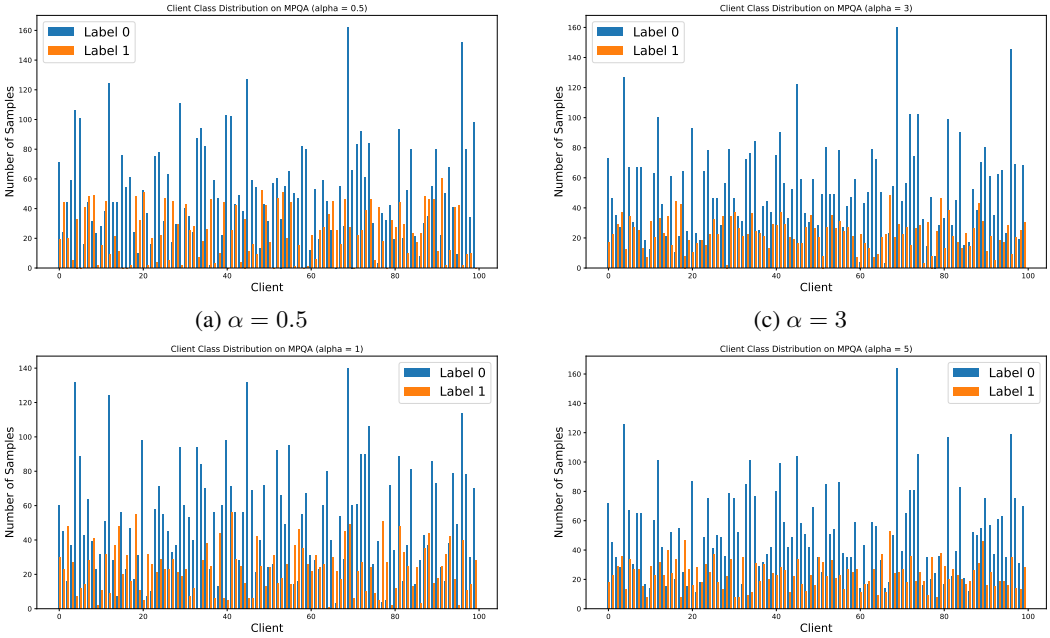

(a) $\alpha = 0.5$ (c) $\alpha = 3$

(b) $\alpha = 1$ (d) $\alpha = 5$

Figure 3: Client class distribution on MPQA dataset for different α values. Each plot shows the number of samples per class across clients, illustrating the heterogeneity in data distribution.

Resource Efficiency Analysis Using Riemannian Optimization. The resource usage of our method is comprehensively quantified across multiple dimensions, including FLOPS (measuring computational complexity), throughput (processing rate), communication volume (data transfer during training), training time, and accuracy, as shown in our experimental results. Definitions of these metrics are provided in Bai et al. (2024a).

As shown in Table 34, the resource usage of 16 federated parameter-efficient fine-tuning methods is evaluated on the LLaMA 7B + MPQA task. Our method, RAFFT, achieves the highest throughput of 6229.19 tokens/sec with lower FLOPS (72.73 GFLOPS) compared to other methods (72.76 GFLOPS). This reduction in FLOPS is achieved because the server selects the optimal rank and sets the remaining ranks and their corresponding parameters to zero, thereby reducing unnecessary computations. Additionally, RAFFT significantly reduces the communication volume to 3146112 bytes, the lowest among LoRA-based methods, and achieves the highest accuracy of 0.908. Similarly, on the ViT + CIFAR-10 task, RAFFT achieves the best accuracy of 61.22, with the shortest training time of 3222 seconds and a communication volume of 98352 bytes. These results highlight RAFFT's ability to balance computational and communication efficiency effectively. A plausible explanation for this superior performance is that the Riemannian parameter matching and Riemannian gradient optimization enable faster convergence and improved accuracy, while the adaptive rank se-

lection reduces redundant computation, making RAFFT a highly practical and efficient approach for real-world federated learning scenarios.

Method	FLOPS (GFLOPS)	Throughput (tokens/sec on H100)	Communication Volume (Bytes)	Training Time (s)	Accuracy (%)
Centralized LoRA	72.7557	5701.2920	4,194,304	5432	82.90
AdaLoRA	72.7557	6052.1700	4,194,816	5503	32.75
P-tuning v2	72.3243	5563.1500	524,288	5664	85.20
FedPrompt	72.3243	5100.2800	524,288	5393	87.35
FedPepTAO	72.3243	5829.5450	524,288	5475	87.60
PromptFL	72.3243	5546.1950	524,288	5586	87.40
PE_FL	72.3243	5710.5881	524,288	5263	87.25
SLoRA	72.7557	6199.1755	4,194,304	5622	84.10
HetLoRA	72.7557	5019.9379	4,194,304	5229	84.23
FedLoRA	72.7557	5100.2800	6,742,618,112	5308	87.74
FFA-LoRA	72.7557	5034.1700	4,194,304	5358	80.00
FLoRA	72.7557	4728.9951	4,194,304	5293	79.19
RAFFT	72.6401	6229.1855	3,146,112	5151	90.80
RAFFT-RGD	72.8020	5525.9890	4,194,816	5198	86.21
RAFFT-MR	72.7557	6392.1002	3,146,112	5177	86.73

Table 34: Performance comparison of methods on LLaMA 7B + MPQA.

Method	FLOPS (GFLOPS)	Throughput (images/sec on 2080Ti)	Communication Volume (Bytes)	Training Time (s)	Accuracy (%)
Centralized LoRA	41.9654	5730.05	98,304	3578	60.48
AdaLoRA	41.9654	4722.30	98,352	3260	60.92
SLoRA	41.9654	5739.46	98,304	3402	58.89
HetLoRA	41.9654	5781.50	98,304	3387	59.63
FedLoRA	41.9654	5663.19	5,322,240	3310	59.11
FFA-LoRA	41.9654	5625.11	98,304	3412	60.21
FLoRA	41.9654	5646.20	98,304	3249	59.31
RAFFT	41.6335	5721.55	78,962	3222	61.22
RAFFT-RGD	41.9927	5315.95	98,304	3288	60.62
RAFFT-MR	41.9654	5681.28	78,962	3265	59.91

Table 35: Performance comparison of methods on ViT + CIFAR-10.

Accuracy of classification using Riemannian manifolds on different parameters. In order to comprehensively study the applicability of our RAFFT method to classification tasks with different parameter values, in addition to the select rank threshold in section 5 we also evaluate the following parameters: training epoch, learning rate (LR), while keeping other settings unchanged. Table 27-31 shows the classification accuracy using Riemannian manifold techniques on data sets for different models. We observe consistent results, showing that the three variants of our RAFFT method achieve the best accuracy in most experiments. A reasonable explanation is that rigorous mathematical analysis based on Riemannian manifold theory significantly enhances the effectiveness and applicability of our RAFFT method in different scenarios.

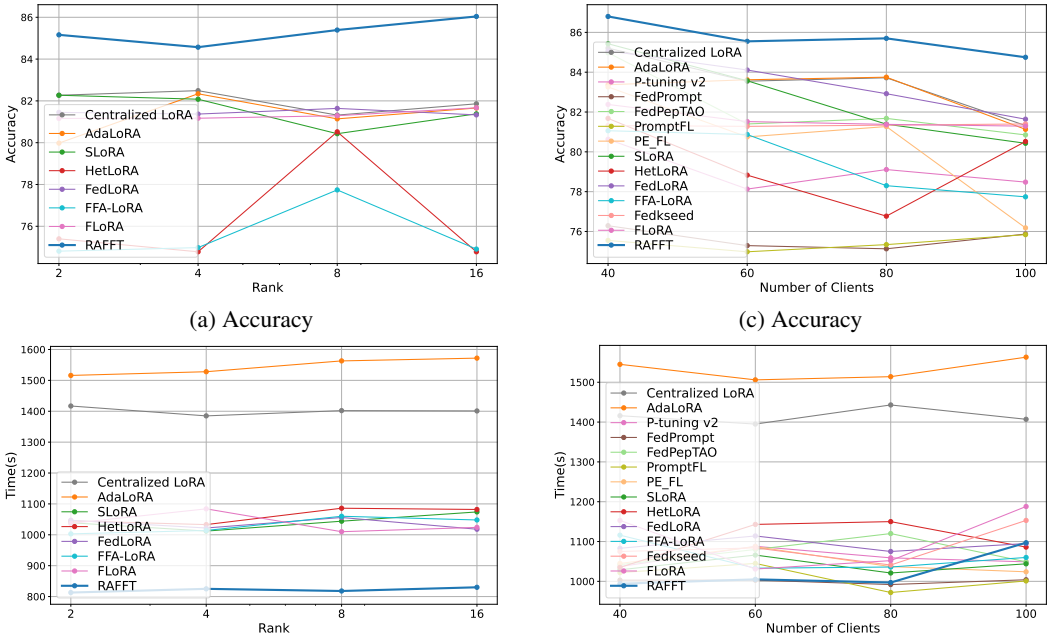

(a) Accuracy (c) Accuracy

(b) Time (d) Time

Figure 4: Accuracy and Time (s) with various LoRA ranks and client numbers on Roberta-MRPC

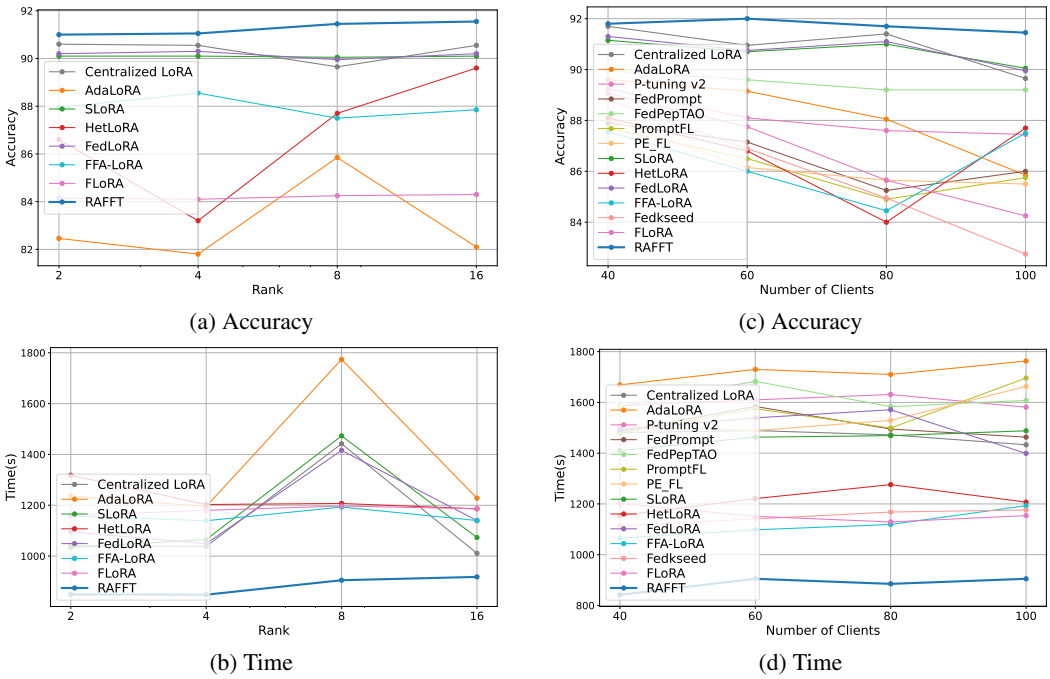

(a) Accuracy (c) Accuracy

(b) Time (d) Time

Figure 5: Accuracy and Time (s) with various LoRA ranks and client numbers on Roberta-MPQA

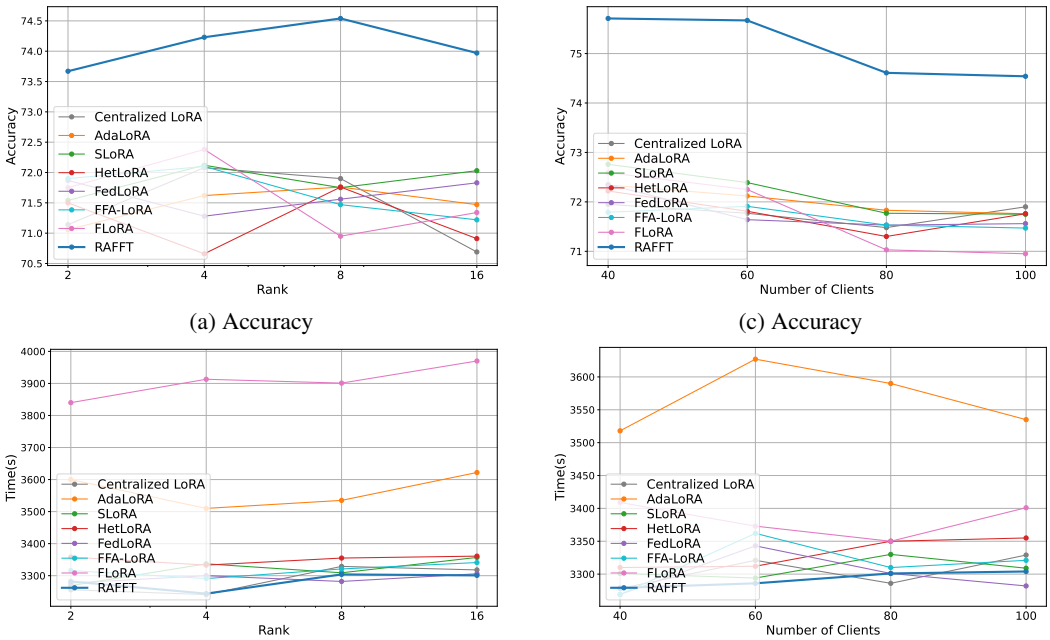

(a) Accuracy (c) Accuracy

(b) Time (d) Time

Figure 6: Accuracy and Time (s) with various LoRA ranks and client numbers on ViT-CIFAR-10

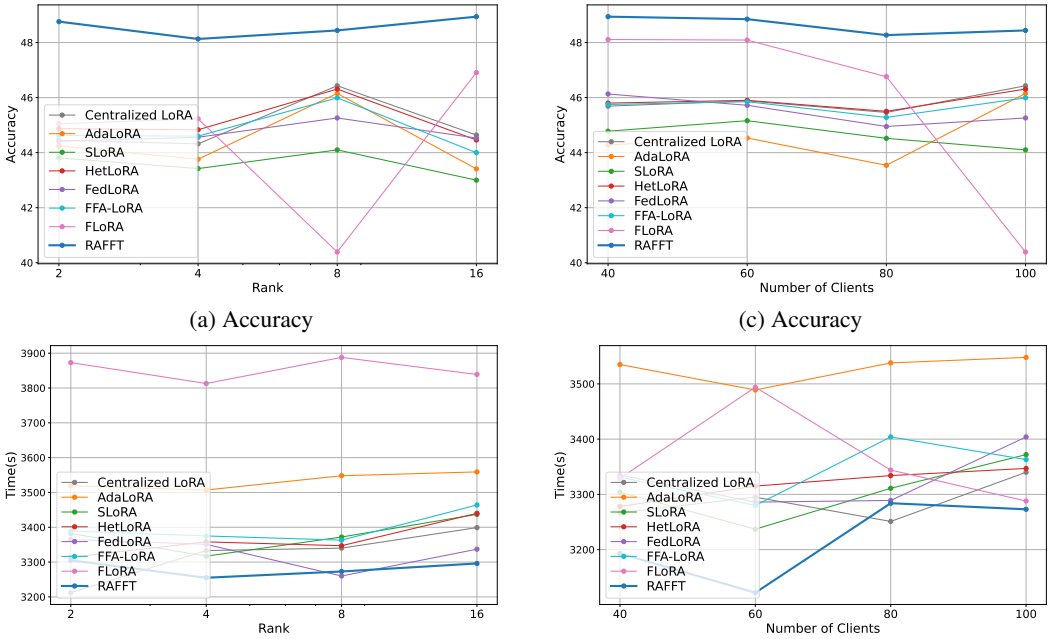

(a) Accuracy (c) Accuracy

(b) Time (d) Time

Figure 7: Accuracy and Time (s) with various LoRA ranks and client numbers on ViT-CIFAR-100

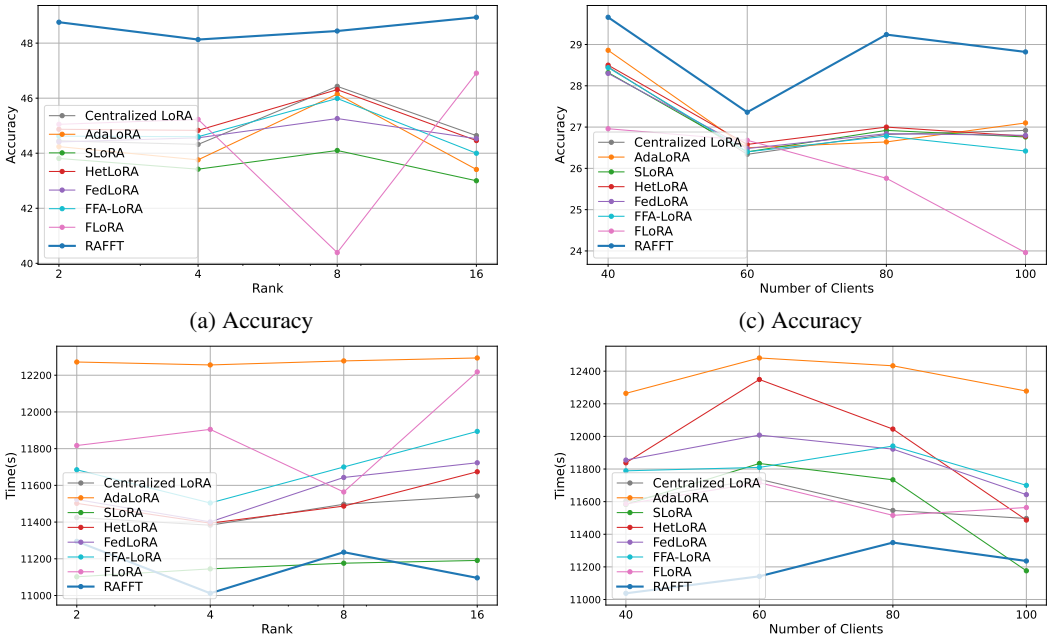

(a) Accuracy (c) Accuracy

(b) Time (d) Time

Figure 8: Accuracy and Time (s) with various LoRA ranks and client numbers on ViT-Tiny-ImageNet

7.7 Potential Negative Societal Impacts and Limitations

In this work, the three large language datasets Socher et al. (2013); Dolan & Brockett (2005); Wiebe et al. (2005) and the three image classification datasets are open-release datasets allowing researchers

to use them for non-commercial research and educational purposes. These three datasets are widely used for training/evaluating text classification. All baseline code is open access from GitHub and is licensed under the MIT License, requiring only that the copyright and license notices be retained, and containing permissions for commercial use, modification, distribution, and private use. To the best of our knowledge, this work is the first to theoretically verify the possibility of solving client drift and ranking drift through Riemannian manifold theory. Compared with existing FedPEFT technology, this work explores the equivalence between the theoretical LoRA-based ranking adaptive federated learning method for base model fine-tuning and the standard federated base model federated fine-tuning method. Our model can be used for various large model fine-tuning tasks that require low latency and energy consumption in resource-intensive scenarios. This paper is primarily of a theoretical nature. We expect our findings to produce positive environmental impact, i.e., significantly improve the efficiency and scalability of federated large model fine-tuning by reducing the time and space requirements of large model fine-tuning in federated learning scenarios during training and testing. To our best knowledge, we do not envision any immediate negative societal impacts of our results, such as security, privacy, and fairness issues. An important product of this paper is the theoretical exploration to verify the feasibility of addressing client drift and rank drift through Riemannian manifold theory. Given the large scale of neural networks in practical scenarios and the limitations of current computational hardware, we employ approximate methods for Riemannian distance. This ensures that the rank-adaptive federated learning method based on LoRA for fine-tuning foundation models is equivalent to the standard federated fine-tuning of foundation models on a fully parameterized FedAvg matrix. Our theoretical framework can inspire further improved development and implementations on FedPEFT with better applicability and efficiency from the academic institutions and industrial research labs.

7.8 Clint-drift and Rank-drift Issue Definition

Client-drift issue: The client-drift issue is due to the aggregation of low-rank matrices in the FFT-FM. Here, we introduce an illustrative example with two clients to better understand the client-drift issue.

Concretely, if the clients locally fine-tune on full parameters and the server aggregates with FedAvg, the new global model parameters can be expressed as follows.

$$\mathbf{W} = \mathbf{W}^0 + \frac{1}{2}(\Delta\mathbf{W}^1 + \Delta\mathbf{W}^2) \tag{98}$$

In our work, the clients locally fine-tune on both low-rank parameter matrices $\mathbf{U}^k$ and $\mathbf{V}^k$ and diagonal matrix $\mathbf{\Sigma}^k$ to determine the rank. The server uses FedAvg to aggregate the low-rank matrices and diagonal matrix.

$$\Delta\mathbf{W}^k = \mathbf{U}^k\mathbf{\Sigma}^k\mathbf{V}^k, \quad k \in 1, 2 \tag{99}$$

The expected global model parameter updates $\Delta\mathbf{W}$ can be expressed as follows.

$$\Delta\mathbf{W} = \frac{1}{2}(\Delta\mathbf{W}^1 + \Delta\mathbf{W}^2) = \frac{1}{2}(\mathbf{U}^1\mathbf{\Sigma}^1\mathbf{V}^1 + \mathbf{U}^2\mathbf{\Sigma}^2\mathbf{V}^2) \tag{100}$$

After using FedAvg to aggregate the local matrices $\mathbf{U}^k, \mathbf{\Sigma}^k, \mathbf{V}^k$, the server produces

$$
\begin{aligned}
\Delta\tilde{\mathbf{W}} &= \frac{1}{2}\left(\mathbf{U}^1+\mathbf{U}^2\right)\times\frac{1}{2}\left(\mathbf{\Sigma}^1+\mathbf{\Sigma}^2\right)\times\frac{1}{2}\left(\mathbf{V}^1+\mathbf{V}^2\right)\\
&= \frac{1}{2}(\mathbf{U}^1\mathbf{\Sigma}^1\mathbf{V}^1+\mathbf{U}^2\mathbf{\Sigma}^2\mathbf{V}^2)\underline{-\frac{3}{8}\mathbf{U}^1\mathbf{\Sigma}^1\mathbf{V}^1-\frac{3}{8}\mathbf{U}^2\mathbf{\Sigma}^2\mathbf{V}^2+\frac{1}{8}\mathbf{U}^1\mathbf{\Sigma}^1\mathbf{V}^2+\frac{1}{8}\mathbf{U}^1\mathbf{\Sigma}^2\mathbf{V}^1}\\
&\quad\underline{+\frac{1}{8}\mathbf{U}^1\mathbf{\Sigma}^2\mathbf{V}^2+\frac{1}{8}\mathbf{U}^2\mathbf{\Sigma}^1\mathbf{V}^1+\frac{1}{8}\mathbf{U}^2\mathbf{\Sigma}^1\mathbf{V}^2+\frac{1}{8}\mathbf{U}^2\mathbf{\Sigma}^2\mathbf{V}^1}\\
&= \Delta\mathbf{W}\underline{-\frac{3}{8}\mathbf{U}^1\mathbf{\Sigma}^1\mathbf{V}^1-\frac{3}{8}\mathbf{U}^2\mathbf{\Sigma}^2\mathbf{V}^2+\frac{1}{8}\mathbf{U}^1\mathbf{\Sigma}^1\mathbf{V}^2+\frac{1}{8}\mathbf{U}^1\mathbf{\Sigma}^2\mathbf{V}^1}\\
&\quad\underline{+\frac{1}{8}\mathbf{U}^1\mathbf{\Sigma}^2\mathbf{V}^2+\frac{1}{8}\mathbf{U}^2\mathbf{\Sigma}^1\mathbf{V}^1+\frac{1}{8}\mathbf{U}^2\mathbf{\Sigma}^1\mathbf{V}^2+\frac{1}{8}\mathbf{U}^2\mathbf{\Sigma}^2\mathbf{V}^1}
\end{aligned}
\tag{101}
$$

where the underlined terms denote the difference between $\Delta\tilde{\mathbf{W}}$ and $\Delta\mathbf{W}$.

It is obvious that $\Delta\tilde{\mathbf{W}} \neq \Delta\mathbf{W}$ when $\mathbf{U}^1 \neq \mathbf{U}^2$, $\mathbf{\Sigma}^1 \neq \mathbf{\Sigma}^2$, and $\mathbf{V}^1 \neq \mathbf{V}^2$ due to the data heterogeneity property of federated learning. Therefore, the client-drift issue is raised.

$$
\underbrace{\tilde{\mathbf{W}} = \mathbf{W}^0 + \Delta\tilde{\mathbf{W}}}_{\text{Parameter aggregation with SVD-based rank-adaptive LoRA + FedAvg}} \neq \underbrace{\mathbf{W}^0 + \Delta\mathbf{W} = \mathbf{W}}_{\text{Ideal parameter aggregation with FedAvg on full parameter matrices}} \tag{102}
$$

The difference between $\Delta\tilde{\mathbf{W}}$ and $\Delta\mathbf{W}$ is mainly due to the noise introduced by the cross-products of LoRA modules from different clients. This difference may become more significant when (1) the number of local update steps between aggregations is large and (2) the local datasets are different across clients.

In the (Sun et al., 2024) paper, when the clients locally fine-tune on low-rank parameters based on LoRA and the server uses FedAvg to aggregate the low-rank matrices, the global model parameters can be expressed as follows.

$$
\underbrace{\tilde{\mathbf{W}} = \mathbf{W}^0 + \frac{1}{2}(\mathbf{B}^1+\mathbf{B}^2)\times\frac{1}{2}(\mathbf{A}^1+\mathbf{A}^2)}_{\text{Parameter aggregation with LoRA + FedAvg}} \neq \underbrace{\mathbf{W}^0 + \frac{1}{2}(\mathbf{B}^1\mathbf{A}^1+\mathbf{B}^2\mathbf{A}^2) = \mathbf{W}_0 + \frac{1}{2}(\Delta\mathbf{W}^1+\Delta\mathbf{W}^2) = \mathbf{W}}_{\text{Ideal parameter aggregation with FedAvg on full parameter matrices}} \tag{103}
$$

When the clients use LoRA locally, we have $\Delta\mathbf{W}^k = \mathbf{B}^k\mathbf{A}^k$ on client k. The data heterogeneity is a common challenging problem in the federated learning. The collected data on different clients are Non-Independent Identically Distributed (NonIID). Thus, the parameters of local models trained on the non-IID data are quite different from each other, i.e., $\mathbf{B}^1 \neq \mathbf{B}^2$ and $\mathbf{A}^1 \neq \mathbf{A}^2$. This leads to the client-drift issue in the (Sun et al., 2024) paper, i.e., the difference between $\mathbf{W}$ and $\tilde{\mathbf{W}}$ is not equal to 0. In order to address the client-drift issue, the (Sun et al., 2024) paper keeps both $\mathbf{W}^0$ and $\mathbf{A}^0$ frozen and makes only $\mathbf{B}$ trainable.

$$
\underbrace{\tilde{\mathbf{W}} = \mathbf{W}^0 + \frac{1}{2}(\mathbf{B}^1+\mathbf{B}^2)\times\mathbf{A}^0}_{\text{Parameter aggregation with LoRA + FedAvg}} = \underbrace{\mathbf{W}^0 + \frac{1}{2}(\mathbf{B}^1\mathbf{A}^0+\mathbf{B}^2\mathbf{A}^0) = \mathbf{W}_0 + \frac{1}{2}(\Delta\mathbf{W}^1+\Delta\mathbf{W}^2) = \mathbf{W}}_{\text{Ideal parameter aggregation with FedAvg on full parameter matrices}} \tag{104}
$$

The magic of the (Sun et al., 2024) paper to handle the client-drift issue is to have only one parameter matrix ($\mathbf{B}$) trainable while freezing other parameter matrices. However, this approach cannot be directly utilized to conduct the client-drift issue in our work. Our work has three trainable parameter matrices $\mathbf{U}^k$, $\mathbf{V}^k$, and $\mathbf{\Sigma}^k$. If updating only the diagonal matrix $\mathbf{\Sigma}^k$ and freezing the parameter matrices $\mathbf{U}^k$ and $\mathbf{V}^k$, then the algorithm fails to update the parameter matrices, resulting in poor model performance. If updating either $\mathbf{U}^k$ or $\mathbf{V}^k$ and freezing $\mathbf{\Sigma}^k$, then the rank cannot be optimized, leading to high computational cost (by higher rank) or poor model performance (by lower rank).

Thus, We propose a Riemannian parameter matching method to match the local parameter matrices $\mathbf{U}^k$ and $\mathbf{V}^k$ on other clients with pivots $\mathbf{U}^1$ and $\mathbf{V}^1$ on client 1, in terms of their lengths

and directions, i.e. $\tilde{\mathbf{U}}^k = \mathbf{U}^k\mathbf{R}^k \approx \mathbf{U}^1$ and $\tilde{\mathbf{V}}^k = \mathbf{S}^k\mathbf{V}^k \approx \mathbf{V}^1$. To maintain the consistency between low-rank parameter metrics before and after the Riemannian parameter matching, i.e., $\mathbf{U}^2\mathbf{\Sigma}^2\mathbf{V}^2 = \tilde{\mathbf{U}}^2\tilde{\mathbf{\Sigma}}^2\tilde{\mathbf{V}}^2 \approx \mathbf{U}^1\tilde{\mathbf{\Sigma}}^2\mathbf{V}^1$, for ensuring the effectiveness of FFT-FM with rank-adaptive LoRA, we derive a modified diagonal matrix $\tilde{\mathbf{\Sigma}}^k$ for the other clients by performing the SVD on low-dimensional $r \times r$ matrices $(\mathbf{U}^1)^T\mathbf{U}^k$ and $(\mathbf{V}^1)^T\mathbf{V}^k$. Thus, the client-drift issue is resolved.

$$\begin{aligned}\Delta\tilde{\mathbf{W}} &= \frac{1}{2}\left(\mathbf{U}^1 + \tilde{\mathbf{U}^2}\right) \times \frac{1}{2}\left(\mathbf{\Sigma}^1 + \tilde{\mathbf{\Sigma}}^2\right) \times \frac{1}{2}\left(\mathbf{V}^1 + \tilde{\mathbf{V}^K}\right) \\ &\approx \mathbf{U}^1 \times \frac{1}{2}\left(\mathbf{\Sigma}^1 + \tilde{\mathbf{\Sigma}}^2\right) \times \mathbf{V}^1 = \frac{1}{2}\left(\mathbf{U}^1\mathbf{\Sigma}^1\mathbf{V}^1 + \mathbf{U}^2\mathbf{\Sigma}^2\mathbf{V}^2\right) = \Delta\mathbf{W}\end{aligned} \tag{105}$$

Based on the global diagonal matrix $\frac{1}{2}\left(\mathbf{\Sigma}^1 + \tilde{\mathbf{\Sigma}}^2\right)$, it is easy to find the optimal rank of the global parameter matrix, with aggregation on only the local low-rank matrices $\mathbf{U}^k$, $\tilde{\mathbf{\Sigma}}^k$, and $\mathbf{V}^k$.

Rank-drift issue: The data heterogeneity is a common challenging problem in the federated learning. The collected data on different clients are Non-Independent Identically Distributed (Non-IID). Thus, the parameters of local models trained on the non-IID data are quite different from each other as well as the parameters of global model. Each local model may oscillate back and forth in different training rounds, leading to unstable and slow convergence and causing suboptimal model performance.

At the same time, due to the heterogeneity of local models, the optimal ranks of local models are quite different from each other as well as the one of global model, raising the rank-drift issue. Similarly, the oscillation of the optimal rank of each local model can slow down the model convergence and degrade the model performance. For example, given two clients 1 and 2, in round 1, the local model on client 1/2 has the optimal rank 5/20. The server aggregates local models from clients to generate a global model based on FedAvg. The global model by model aggregation has the optimal rank 12. In round 2, after the global model are sent back to the clients, the clients begin the training with the global model with the optimal rank 12. Thus, the optimal rank of local models oscillate between 5/20 and 12. The rank oscillation may repeat in each training round, slowing down the model convergence.

The following table 36 presents a case study regarding the rank-drift in federated learning. In round 1, the optimal rank of the global model is 16. In round 2, the optimal rank is changed to 11. In subsequent rounds, the optimal rank continue to oscillate back and forth. The ranks of local models fluctuate around values such as 9.75, 10.17, and 10.53, while the rank of global modelgradually decreases and stabilizes at 8. These results confirm that rank-drift introduces instability into the training process, slowing convergence and degrading performance, which emphasizes the importance of our Riemannian gradient descent optimization approach to stabilize ranks and ensure efficient training.

7.9 Algorithm

In order to solve the client-drift and rank-drift issues and significantly improves the computational cost, we exploit a Riemannian manifold based method as detailed in Algorithm 1. Within each round, every client performs local updates(line 22). The updates are based on the Riemannian gradient and the retraction function (line 11,line 13). After the updates, each client sends the updated parameters back to the server(line 17). The server then performs Riemannian parameter matching between the U and V matrices of all clients and those of the first client to achieve alignment in both length and direction.(line 24-line 28) The singular value matrix is updated according to Formula7, and the aggregated U, V and Σ matrices from all clients are combined.(line 29-line 33) The rank for the next round of training is selected through Formula 16, and the model parameter matrix is updated accordingly.(line 34-line 37)

7.10 Notation Definition

Below, we provide detailed definitions of the notations used in the main text:

Algorithm 1 Federated Learning with Optimal Rank Selection and Alignment

Input: Client datasets $\{\mathcal{D}_k\}_{k=1}^{K}$, Threshold α, The number of local epoch E, The number of global round R
Output: Optimally ranked updated matrices U_R, S_R, V_R
procedure SERVER INITIALIZATION
    Initialize S as zero matrix
    Initialize U, V with random Gaussian values
end procedure
procedure CLIENT UPDATE (K,U,S,V) // RUN ON CLIENT K
    for each local epoch i from 1 to E **do**
        batches $\leftarrow$ ($\mathcal{D}_k$ spilt into batches of size)
        for batch b in batches **do**
            computes the Riemannian gradient $P\nabla L^k$ based on Eq.(21)
            $(\mathbf{U}^k L^k, \mathbf{\Sigma}^k L^k, \mathbf{V}^k L^k)$
            computes $(\mathbf{U}^k)^{(t+1)}, (\mathbf{\Sigma}^k)^{(t+1)}, (\mathbf{V}^k)^{(t+1)}$ based on Eq.(22)
            $\left((\mathbf{U}^k)^{(t+1)}, (\mathbf{\Sigma}^k)^{(t+1)}, (\mathbf{V}^k)^{(t+1)}\right) = f\left(-\eta_t\left(\left(\Gamma_{\mathbf{U}^k} L^k\right)^{(t)}, \left(\Gamma_{\mathbf{\Sigma}^k} L^k\right)^{(t)}, \left(\Gamma_{\mathbf{V}^k} L^k\right)^{(t)}\right)\right)$
        end for
    end for
    return $(\mathbf{U}^k)^{(t+1)}, (\mathbf{\Sigma}^k)^{(t+1)}, (\mathbf{V}^k)^{(t+1)}$ to the server
end procedure
procedure SERVER ALIGNMENT AND AGGREGATION
    for each round t from 1 to C **do**
        for each client k in K clients **do**
            $(\mathbf{U}^k)^{(t+1)}, (\mathbf{\Sigma}^k)^{(t+1)}, (\mathbf{V}^k)^{(t+1)} \leftarrow$ Client Update (k,$(\mathbf{U}^k)^{(t)}, (\mathbf{\Sigma}^k)^{(t)}, (\mathbf{V}^k)^{(t)}$)
        end for
        Compute alignment matrix $\mathbf{S}^k, \mathbf{R}^k$ using $(\mathbf{U}^1)^{(t+1)}, (\mathbf{V}^1)^{(t+1)}$ as reference based on Eq.(9)
        for $k = 1$ to K **do**
            Align $(\mathbf{U}^k)^{(t+1)}$ to $(\mathbf{U}^1)^{(t+1)}$: $(\tilde{\mathbf{U}}^k)^{(t+1)} = (\mathbf{U}^k)^{(t+1)}\mathbf{R}^k$
            Align $(\mathbf{V}^k)^{(t+1)}$ to $(\mathbf{V}^1)^{(t+1)}$: $(\tilde{\mathbf{V}}^k)^{(t+1)} = \mathbf{S}^k(\mathbf{V}^k)^{(t+1)}$
        end for
        Update $(\mathbf{\Sigma}^k)^{(t+1)}$ based on Eq.(13)
        Aggregate updates:
        $\tilde{\mathbf{U}}' = \sum_{k=1}^{K} \frac{n_k}{n} \tilde{\mathbf{U}}^k$
        $\tilde{\mathbf{\Sigma}}' = \sum_{k=1}^{K} \frac{n_k}{n} \tilde{\mathbf{\Sigma}}^k$
        $\tilde{\mathbf{V}}' = \sum_{k=1}^{K} \frac{n_k}{n} \tilde{\mathbf{V}}^k$
        Determine rank r based on Eq.(16):
        $\Theta(r) = \frac{\sum_{i=1}^{r} \tilde{\mathbf{\Sigma}}'_{ii}}{\sum_{i=1}^{r_{max}} \tilde{\mathbf{\Sigma}}'_{ii}} \geq \varphi$
        Update $\tilde{\mathbf{\Sigma}}'$ to only include top r singular values
        Update $\tilde{\mathbf{U}}', \tilde{\mathbf{V}}'$ accordingly
    end for
end procedure

Round (1-25)	Client Rank	Server Rank
1	16.000000	16
2	9.206250	11
3	9.153125	10
4	9.750000	10
5	10.165625	9
6	10.004688	9
7	9.881250	9
8	9.951563	9
9	10.168750	9
10	10.392188	8
11	10.467188	8
12	10.526563	8
13	10.506250	8
14	10.518750	8
15	10.507813	8
16	10.454688	8
17	10.393750	8
18	10.295313	8
19	10.212500	8
20	10.175000	8
21	10.110938	8
22	10.029688	8
23	9.981250	8
24	9.932813	8
25	9.903125	8

Table 36: Client and Server Ranks for LLaMA 7B + MPQA across 25 Rounds

Notation	Explanation
$\mathbf{W} \in \mathbb{R}^{m \times n}$	Full parameter matrix of the foundation model
$\mathbf{W}^k \in \mathbb{R}^{m \times n}$	Local model parameter matrix for client K.
$\mathbf{W}_0 \in \mathbb{R}^{m \times n}$	Pre-trained foundation model parameters
$\Delta\mathbf{W} \in \mathbb{R}^{m \times n}$	Adapter parameters, used for fine-tuning
$\Delta\mathbf{W}^k \in \mathbb{R}^{m \times n}$	Adapter parameter matrix for client K
$\mathbf{U}^k \in \mathbb{R}^{m \times r}$,$\mathbf{V}^k \in \mathbb{R}^{r \times n}$	Matrices representing the left and right singular vectors of $\Delta\mathbf{W}^k$
$\mathbf{\Sigma}^k \in \mathbb{R}^{r \times r}$	Diagonal matrix containing the singular values of $\Delta\mathbf{W}^k$
$\mathbf{B} \in \mathbb{R}^{r \times n}$,$\mathbf{A} \in \mathbb{R}^{m \times r}$	Low-rank matrices representing adapter parameters$\Delta\mathbf{W} = \mathbf{BA}$
$r \in \mathbb{R}^{r \times r}$	Rank of decomposition, much smaller than m and n
$D = \{D_1, \cdots, D_K\}$	The set of local training data from K clients
K	The total number of clients involved in federated learning
n^k	The size of the local dataset D_k, i.e., $n^k = \|D_k\|$.
n	The size of the total training data $\mathbf{D}$, i.e., $n = n_1 + \cdots + n_K$.
$\mathcal{L}(\mathbf{W})$	The global loss function to be minimized, aggregated over all clients.
$L^k(\mathbf{W})$	The loss function for client K.
$l_i(\mathbf{W})$	The loss function for a single data sample $\{x_i, y_i\}$
S	The set of orthogonal matrices on Riemann manifold
S_p	The procrustes representation space on manifold S
$\mathbf{R}^k \in \mathbb{R}^{r \times r}$,$\mathbf{S}^k \in \mathbb{R}^{r \times r}$	The symmetric positive matrix for Riemannian parameter matching.
$\mathbf{P}^k \in \mathbb{R}^{m \times r}$,$\mathbf{\Lambda}^k \in \mathbb{R}^{r \times r}$, $\mathbf{Q}^k \in \mathbb{R}^{r \times n}$	Matrices obtained from the SVD of $(\mathbf{U}^1)^T\mathbf{U}^k$
$\mathbf{Y}^k$, $\mathbf{Z}^k$	Auxiliary variables introduced to reformulate the Riemann problem.
$\tilde{\mathbf{U}}^k \in \mathbb{R}^{m \times r}$,$\tilde{\mathbf{V}}^k \in \mathbb{R}^{r \times n}$	Matrices representing the aligned parameters after Riemannian matching
$\tilde{\mathbf{\Sigma}}^k$	Modified version of diagonal matrix $\mathbf{\Sigma}^k$ for ensuring consistency
$\lambda_{R_{\min}}, \lambda_{R_{\max}}$	Minimum and maximum eigenvalues of the matrix $\mathbf{R}^k$
$\lambda_{S_{\min}}, \lambda_{S_{\max}}$	Minimum and maximum eigenvalues of the matrix$\mathbf{S}^k$
H, N	Constants bounding the Frobenius norms of matrices $\lambda_{R_{\min}}$ and $\lambda_{S_{\min}}$
$\Theta(r)$	Singular value contribution rate
φ	Threshold value for determining rank
$R(\mathbf{U}^k, \mathbf{V}^k)$	Regularization term to enforce orthogonality of $\mathbf{U}^k$ and $\mathbf{V}^k$
M	The set of fixed rank matrices on Riemann manifold
T_M	Tangent space of the Riemannian manifold M at the point $\Delta\mathbf{W}$
$\mathbf{G} \in \mathbb{R}^{r \times r}$, $\mathbf{U}_p^k \in \mathbb{R}^{m \times r}$, $\mathbf{V}_p^k \in \mathbb{R}^{n \times r}$	The tangent vector at $\Delta\mathbf{W}$
$\mathbf{U}_\perp^k$,$\mathbf{V}_\perp^k$	The orthogonal complements of $\mathbf{U}^k$ and $\mathbf{V}^k$
$\nabla L^k(\Delta\mathbf{W}^k)$	Gradient of the local objective function L^k in Eucliean space
$\Gamma L^k(\Delta\mathbf{W}^k)$	Riemannian gradient of the local objective function L^k
P	Orthogonal projection
$\Gamma_{\mathbf{U}^k} L^k$, $\Gamma_{\mathbf{\Sigma}^k} L^k$, $\Gamma_{\mathbf{V}^k} L^k$	The components of the Riemannian gradient at$\Delta\mathbf{W}^k$
η_t	Learning rate
$f()$	Retraction function
$t\ (0 \leq t \leq C)$	Federated learning round
c_g	Geodesic smoothness constant for the function L^k
ζ	Key geometric constant that captures the impact of the manifold's curvature

Table 37: Definitions of Notations